

GAS TRANSPORT AND WATER VAPOURIZATION IN OUT-OF-AUTOCLAVE PREPREG LAMINATES

by

Kevin Hsiao

B.A.Sc., The University of British Columbia, 2009

A THESIS SUBMITTED IN PARTIAL FULFILLMENT OF THE REQUIREMENTS
FOR THE DEGREE OF

MASTER OF APPLIED SCIENCE

in

The Faculty of Graduate Studies
(Materials Engineering)

THE UNIVERSITY OF BRITISH COLUMBIA
(Vancouver)

July 2012

© Kevin Hsiao, 2012

ABSTRACT

Primary load-bearing aerospace structures have traditionally been manufactured using autoclave processing. However, recent advances in material technology have led to the development of pre-impregnated (prepreg) composites that are designed to be cured out-of-autoclave (OOA) and can potentially reduce the costs of processing.

In OOA processing, voids are removed by vacuum evacuation through gas pathways in the prepreg. The availability and interconnectivity of these pathways determine the prepreg's gas transport ability. Voids enter into the prepreg via moisture absorption during storage and physical air entrapment during manufacturing and material handling. Environmental effects, such as relative humidity, can alter the moisture content of prepregs and lead to significant vapour generation during cure. This study examines the gas transport and water vapourization characteristics of OOA prepreg CYCOM 5320/T650 (epoxy/carbon). Gas permeabilities in the in-plane and through-thickness directions are measured, and the effects of processing history (debulk time, temperature etc.) on gas transport are examined. The relationships between relative humidity, moisture content, and vapour generation are analyzed, and the use of mass flow sensors for water vapour quantification is validated.

Gas transport is shown to be highly anisotropic in CYCOM 5320/T650, with in-plane gas permeability being three orders of magnitude greater than through-

thickness. Processing history has a significant effect on permeability, with extended debulking sessions reducing in-plane permeability by 50%. Increasing temperature causes in-plane and through-thickness permeabilities to fall. Microscopy analyses reveal that permeability change is a result of collapsing voids and resin flow during heating. Moisture content is relatively unaffected by relative humidity until reaching 30% RH, after which increases in moisture content become more apparent. Vapourization of absorbed moisture between 0 %RH and ambient conditioned vacuum bagged laminates are similar, suggesting that under typical process conditions moisture vapourization mainly comes from the vacuum bag consumables. During vacuum bag processing, vapourization of absorbed moisture occurs immediately upon heating, peaks around 40 to 60°C, and then dissipates as heating reaches the hold temperature. The mass flow sensors are demonstrated to be capable of detecting the onset and termination of moisture vapourization and quantifying the total mass of water vapourized to within 10% error.

TABLE CONTENTS

ABSTRACT.....	ii
TABLE CONTENTS.....	iv
LIST OF TABLES.....	vii
LIST OF FIGURES	viii
ACKNOWLEDGEMENTS.....	xv
1 INTRODUCTION.....	1
1.1 COMPOSITES PROCESSING	2
1.1.1 Autoclave and VBO Processing	5
1.2 OUT-OF-AUTOCLAVE PREPREG: CYCOM 5320/T650.....	9
1.3 OBJECTIVES.....	10
2 LITERATURE REVIEW	13
2.1 GAS TRANSPORT	13
2.2 PERMEABILITY	16
2.2.1 Application of Darcy's Law	20
2.3 MICROSCOPY.....	25
2.4 WATER VAPOURIZATION	29
2.4.1 Application of Kardos' Solubility Model.....	31
2.4.2 Application of Clausius-Clapeyron Equation	32
2.4.3 Application of Langmuir Evaporation Equation.....	34

3	PERMEABILITY TESTING	36
3.1	METHODS	36
3.1.1	In-Plane Setup	38
3.1.2	Long Debulk Setup.....	44
3.1.3	Through-Thickness.....	45
3.1.4	Microscopy	48
3.2	RESULTS.....	54
3.2.1	In-Plane Results	54
3.2.2	Long Debulk Results	56
3.2.3	Through-Thickness Results.....	58
3.2.4	Microscopy Results	61
4	WATER VAPOURIZATION TESTING.....	70
4.1	METHODS	70
4.1.1	Humidity Conditioning Test	73
4.1.2	Water Vapourization Test.....	75
4.1.3	Vacuum Bagged Water Vapourization Test	78
4.2	RESULTS.....	81
4.2.1	Humidity Conditioning Results	81
4.2.2	Water Vapourization Results.....	85
4.2.3	Vacuum Bagged Water Vapourization Results	92

5	DISCUSSION	96
5.1	Anisotropy of Gas Transport	96
5.2	Evolution of Gas Transport with Process History	99
5.3	Effect of Humidity on Moisture Content.....	102
5.4	Water Vapour Flow Measurements with Mass Flow Sensors	104
5.5	Timescales for Moisture Removal.....	105
5.6	Water Vapourization During VBO Processing.....	107
6	CONCLUSION.....	112
6.1	Future Work	116
	REFERENCES	119
	APPENDICES.....	131
A)	Derivation of Modified Darcy’s Law	131
B)	Verification of Laminar Flow	133
C)	Total System Leak Test.....	135
D)	Inter-Chamber Leak Test, Transverse Gas Flow, and Air-Channel Bridging.....	136
E)	Procedure for Initial Moisture Conditioning Trial.....	138
F)	Flow Calibration Calculation.....	141
G)	Vacuum Bagged Water Vapourization Leak Test.....	142

LIST OF TABLES

Table 1.1. Bagging material consumables	5
Table 3.1. Permeability test matrix for 5320/T650.	38
Table 4.1. Moisture vapourization test matrix for 5320/T650 and MTM45- 1/CF2426A.....	72
Table 4.2. Water vapourization test matrix for bagging consumables.....	73

LIST OF FIGURES

Figure 1.1. Prepreg vacuum bag processing setup.....	4
Figure 1.2. Prepreg processing methods. A) Autoclave processing; B) VBO processing.	7
Figure 2.1. In-plane and through-thickness gas transport through prepreg laminates	14
Figure 2.2. Difficulty in forming interconnected pathways for through-thickness gas transport.....	15
Figure 2.3. 1-D fluid flow pipe analogy using the steady-state approach and Darcy's law.	21
Figure 2.4. Pipe analogy translated into in-plane and through-thickness gas flow for a prepreg laminate. A) In-plane gas flow; B) Through-thickness gas flow.....	22
Figure 2.5. Rolling and transverse laminate orientations.	25
Figure 2.6. Void categorization during microscopy of OOA prepreg. Interlaminar voids are located between prepreg plies, and are represented by a green highlight. Fibre tow voids are located within individual fibre bundles, and are represented by a yellow highlight. Resin voids are isolated by the matrix, and are represented by a red highlight.....	28
Figure 3.1. In-plane permeability test setup. A) Chamber configuration and test equipment layout; B) Lay-up order of consumables, and direction of in-plane gas flow.	40

Figure 3.2. Isolated 1D gas flow in the in-plane direction. Effective length refers to the section of specimen truly subjected to 1-D in-plane gas flow (2”) which is used in determining permeability.41

Figure 3.3. Heated in-plane permeability setup. A) Lay-up order of consumables, and direction of in-plane gas flow; B) Setup within heating enclosure; C) Setup during heated permeability testing.43

Figure 3.4. Through-thickness permeability test setup. A) Chamber configuration and test equipment layout; B) Lay-up order of consumables, and direction of through-thickness gas flow.46

Figure 3.5. Isolated 1D gas flow in the through-thickness direction. Effective length refers to the section of specimen truly subjected to 1-D through-thickness gas flow (16.0 mm) which is used in determining permeability.47

Figure 3.6. 5320/T650 microscopy specimens.50

Figure 3.7. Microscopy mount preparation. A) Top view; B) Side view.
Microscopy specimens were elevated to allow mount resin infiltration from both top and bottom directions.....52

Figure 3.8. Ambient in-plane gas permeability. 5320/T650 four ply specimens with three repeats.54

Figure 3.9. Heated in-plane gas permeability. 5320/T650 four ply specimens with three repeats. Critical “opening-up” temperature occurred at approximately 90°C.....55

Figure 3.10. Close-up of heated in-plane gas permeability. 5320/T650 four ply specimens with three repeats. Critical “opening-up” temperature occurred at approximately 90°C.....56

Figure 3.11. Long debulk permeability. 5320/T650 four ply specimens with three repeats. Half of total permeability loss occurred within the first half hour of testing.57

Figure 3.12. Normalized long debulk permeability. 5320/T650 four ply specimens with three repeats. Half of total permeability loss occurred within the first half hour of testing.....58

Figure 3.13. Ambient through-thickness gas permeability. 5320/T650 eight ply specimens with three repeats.59

Figure 3.14. Heated through-thickness gas permeability. 5320/T650 eight ply specimens with three repeats. Critical “opening-up” temperature occurred at approximately 80°C.....60

Figure 3.15. Close-up of heated through-thickness gas permeability. 5320/T650 eight ply specimens with three repeats. Critical “opening-up” temperature occurred at approximately 80°C.....61

Figure 3.16. Micrograph of 1 Ply Uncured (As Laid-Up) 5320/T650 laminate specimen. Fibre tows in the in-plane rolling direction are indicated by a light blue highlight. Fibre tows in the transverse in-plane direction are indicated by a dark blue highlight.....62

Figure 3.17. Micrograph of 4 Ply Uncured (As Laid-Up) 5320/T650 laminate specimen. A) Laminate cross-section. Interlaminar voids are

indicated by a green highlight; B) Close-up image of fibre tow cross-section. Fibre tow voids are indicated by a yellow highlight	63
Figure 3.18. Micrograph of 4 Ply Uncured (Debulk) 5320/T650 laminate specimen. A) Laminate cross-section with no observable interlaminar voids; B) Close-up image of fibre tow cross-section. Fibre tow voids are indicated by a yellow highlight.	65
Figure 3.19. Micrograph of 4 Ply Cured (Vent Closed) 5320/T650 laminate specimen. A) Laminate cross-section with no observable interlaminar voids except for a void filled with polishing media (highlighted in red); B) Close-up image of fibre tow cross-section with no observable fibre tow voids.	67
Figure 3.20. Micrograph of 4 Ply Cured (Vent Open) 5320/T650 laminate specimen. A) Laminate cross-section. Interlaminar voids filled with polishing media are indicated by a red highlight. Interlaminar voids filled with mounting resin are indicated by a green highlight; B) Close-up image of fibre tow cross-section with no observable fibre tow voids.	69
Figure 4.1. Humidity conditioning test setup. Four different mediums are used to achieve four separate relative humidity levels. Lab air humidity varies from 20 %RH in the winter to 50 %RH in the summer. Brine consists of a saturated solution of salt water in equilibrium with solid salt.	75
Figure 4.2. Water vapourization test setup and equipment layout.	76

Figure 4.3. Vacuum bag water vapourization test setup. A) Specimen Lay-up; B) Vacuum bagged setup in heating enclosure; C) Vacuum bagged setup and equipment layout.....80

Figure 4.4. Humidity conditioning results for 5320/T650. Experimental results follow Kardos' solubility model (Kardos et al., 1980) up until 100 %RH, where large scatter in the results are observed.....83

Figure 4.5. Humidity conditioning results for MTM45-1/CF2426A. Experimental results follow Kardos' solubility model (Kardos et al., 1980) up until 100 %RH, where large scatter in the results are observed.....84

Figure 4.6. Humidity conditioning results for bagging consumables. The nylon vacuum bag consumable shows the greatest level of moisture content at a given relative humidity.....85

Figure 4.7. Water vapourization results from beaker tests. The baseline curve represents an empty beaker. The limited water curve represents a beaker containing a single gram of water. The infinite water curve represents a beaker containing over a hundred grams of water. The pressure curve represents falling pressure inside the metal chamber during testing.87

Figure 4.8. Water vapourization results from the beaker tests. The baseline (empty beaker) setup is compared against the known volume of the metal chamber to verify the accuracy of air flow measurements. The limited water (1 g) and infinite water (> 100 g) setups are compared

against measured mass changes in the beakers to verify the accuracy of water vapour flow measurements.....	88
Figure 4.9. Modeling of water vapourization flow rate from the limited water test. Modeling was conducted using a finite difference model using Langmuir's evaporation equation.....	89
Figure 4.10. Water vapourization results from composite tests. The dry composite curve represents a 0 %RH conditioned specimen. The wet composite curve represents a 100 %RH conditioned specimen. The limited water setup is included for comparison.	91
Figure 4.11. Water vapourization results from the composite tests. The dry composite (0 %RH) setup is compared against the known volume of the metal chamber. The moist composite (100 %RH) setup is compared against measured mass changes in the composite.	92
Figure 4.12. Water vapourization results of vacuum bagged 5320/T650 4 ply specimens conditioned at 100 %RH, ambient, and 0 %RH. Results of the consumables conditioned at ambient humidity are also included.	94
Figure 4.13. Water vapourization results of vacuum bagged MTM45-1/CF2426A 4 ply specimens conditioned at 100 %RH, ambient, and 0 %RH. Results of the consumables conditioned at ambient humidity are also included.	94
Figure 4.14. Water vapourization results of vacuum bagged 5320/T650 and MTM45-1/CF2426A 4 ply specimens conditioned at 100 %RH,	

ambient, and 0 %RH. Results of the consumables conditioned at ambient humidity are also included.....	95
Figure 5.1. Illustration of partial impregnation and gas transport anisotropy.....	98
Figure 5.2. Photos of prepreg weave pattern (single ply). A) 5320/T650; B) MTM45-1/CF2426A	99
Figure 5.3. 5320/T650 matrix viscosity evolution with temperature. Plot is reproduced from Cyttec datasheet (CYTEC, 2009)	101
Figure 5.4. Determination of water vapourization in the laminate. A) Ideal scenario with unchanging lab relative humidity; B) Actual scenario with fluctuating lab relative humidity; C) Using Kardos' model to approximate actual consumable moisture contents	110
Figure C.1. Total system leak test setup.....	135
Figure D.1. Inter-chamber leak test setup for transverse gas flow.....	137
Figure D.2. Inter-chamber leak test setup for air-channel bridging.	137

ACKNOWLEDGEMENTS

First and foremost, I would like to thank my supervisor, Dr. Goran Fernlund, for his invaluable support and guidance during my M.A.Sc. research.

I would like to thank current and past members of the UBC Composites Group, especially Bryan Louis, Leyla Farhang, James Kay, and Ryan Thorpe, for the insightful discussions and wisdom they have shared with me over the course of my studies. I would also like to extend my gratitude to the Department of Materials Engineering for their administrative and facilities support.

For his assistance in the design and construction of test apparatuses, I would like to thank Roger Bennett, Senior Technician of the UBC Composites Group. Additionally, I wish to thank both Dr. Abdul Arafath and Malcolm Lane of Convergent Materials Technologies for lending me the mass flow sensor equipment and sharing with me their technical expertise.

I would like to acknowledge all of our academic and industrial partners involved in this project, especially Bell Helicopter and Bombardier for supplying the material used in this work (CYCOM 5320/T650 and MTM45-1/CF2426A).

Lastly, thank you to all my family and friends for the unconditional love, encouragement, and support.

1 INTRODUCTION

Advanced composite materials have been gaining wider acceptance in the aerospace industry since their first introduction during the 1970's (Nutt & Boyd). For commercial aircraft applications, these materials were mostly used in manufacturing non-structural components such as rotor blades, wing spars, and vertical stabilizers (tail fins) (Louis, 2010). However, continued improvements in both material and process technologies have increased industry confidence in advanced composites. In recent years, major commercial aircraft manufacturers have begun utilizing advanced composites to build primary load-bearing structures (fuselage, wings, wing box etc.). Prime examples of the growing trend of advanced composites use can be seen in the Boeing 787 Dreamliner (50% composites), the Airbus A380 and A350XWB (>20% composites), and Bombardier's Learjet85 and C Series aircrafts (Boeing, 2012; Bombardier, 2012; K. Campbell, 2009; Marks, 2005; Price, Dalley, McCullough, & Choquette, 1997; K. Wood, 2010).

The term "advanced composites" is generally used to describe high-strength fibre-resin systems containing fibre volume fractions of greater than fifty percent (Price et al., 1997). Reinforcement materials often used are carbon, graphite, or aramid fibres. Matrix materials can consist of thermosets (epoxies, polyesters, bismaleimides, polyimides, phenolics etc.), thermoplastics (polyether-ether-ketone, polypropylene, polyethyleneimine, polyphenylene sulfide etc.), or a

combination of the two. The most prevalent fibre-matrix composite currently found in aerospace applications is carbon-fibre with epoxy-resin due to the combination of carbon fibre's superior mechanical, fatigue, and corrosion resistance properties with epoxy resins' strength, adhesion, and versatility (F. C. Campbell, 2004). As this is the material combination of interest in this thesis work, all further discussions concerning composites will refer to carbon-fibre/epoxy-resin unless specified.

1.1 COMPOSITES PROCESSING

In composites processing, the goal is to maximize the material's glass transition temperature (T_g) while minimizing its void content (Boey & Lye, 1992). The composite's T_g determines the maximum working temperature that it can withstand without a significant reduction in mechanical properties (F. C. Campbell, 2004). Porosity and voids tend to inhibit mechanical performance and lead to early part failure (Costa, Almeida, & Rezende, 2001; Liu, Zhang, Wang, & Wu, 2006). Voids are defined as individual empty spaces containing no fibre or resin, whereas porosity or void content is the volume fraction of voids within the composite (Farhang & Fernlund, 2011a).

Composite structures are created by stacking layers of laminates together to form required part thicknesses. The composite can be supplied separately as dry reinforcement and resin, or as pre-impregnated (prepreg) material. Dry fibre forms require resin application either through wet lay-up as dry fibre sheets or by

resin transfer as preforms. Wet lay-up processing methods are low cost and can be performed manually by applying resin to each individual layer of dry fibres. However, high porosity and lack of tight control over resin and fibre volume fractions mean that they are limited to recreational and low performance applications (recreational marine equipment, sporting goods, commercial products etc.) (Nutt & Boyd). Preforms are often used in liquid composite moulding (LCM) methods such as resin transfer moulding (RTM and vacuum-assisted RTM) and resin film infusion (RFI). The preforms are laid up between matching moulds (or an open mould with a vacuum bag), and resin is injected and “transferred” to the laminate structure under applied pressure and temperature. These methods are very efficient for high volume part production. However, the injection pressure, resin viscosity, and resin temperature must be carefully controlled to ensure that preform wet out is complete before resin gelation sets in (Kang, Jung, & Lee, 2000). Furthermore, complex curvatures make controlling resin flow very challenging. If these process parameters are not taken into careful consideration, high porosity may result in the final part.

Prepreg materials are often selected for manufacturing high performance parts in aerospace applications. These materials can be supplied as unidirectional tapes or as various types of weaves (plain, twill, or satin), and are typically shipped out to part manufacturers in the form of large rolls. With prepregs, risk of excess resin is minimized as the fibres are pre-impregnated to a target fibre volume fraction with negligible resin loss during cure (net-resin systems) (Nutt & Boyd).

This also allows for tailoring the properties of the final structure by controlling the fibre volume fraction through the impregnation process (Louis, 2010). Prepreg processing can be carried out using autoclave and vacuum-bag only (VBO) methods (Louis, 2010). Both methods often utilize open moulds where one mould half is replaced by a vacuum bag as shown in Figure 1.1. The prepreg layers are laid onto a mould along with several types of consumables, and then vacuum bagged and cured within an autoclave (or an oven in VBO processing). Table 1.1 lists the consumable materials and their purposes. Before curing, the prepreg lay-up can be subjected to a “debulking” (vacuum hold) step. Debulking involves applying vacuum pressure to help improve material consolidation and conformation against the mould prior to heating.

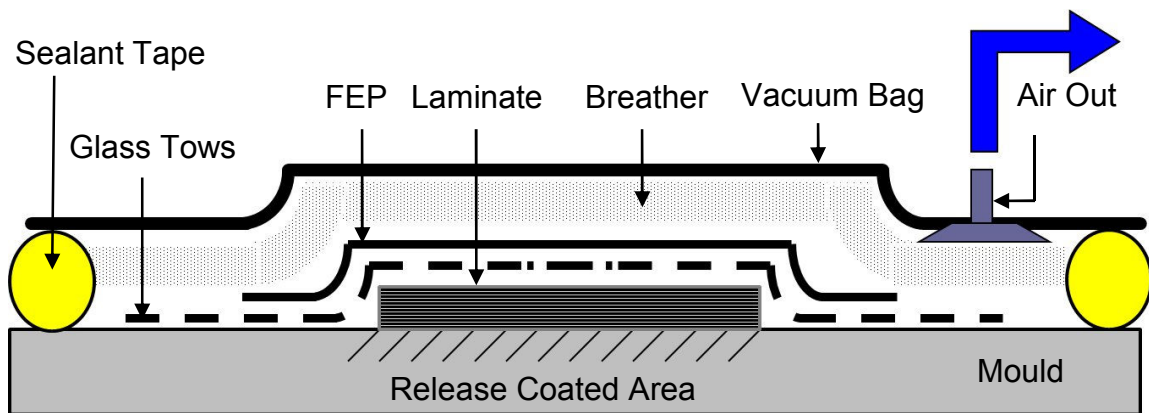


Figure 1.1. Prepreg vacuum bag processing setup

Table 1.1. Bagging material consumables

Consumables	Purpose
Non-stick layer (i.e. fluorinated ethylene polyethylene or FEP)	Prevents consumables from adhering to the cured laminate structure after processing
Bleeder/breather	Provides pathways for gas extraction, promotes even pressure distribution, and absorbs excess resin (bleeding)
String (i.e. glass fibre tows)	Provides incompressible pathways for gas extraction (in contact with bleeder/breather)
Release coat	Prevents cured laminate structure from adhering to the mould
Vacuum bag	Covers the lay-up and provides compaction pressure during vacuum application
Sealant tape	Seals the vacuum bag to the mould surface, preventing gas from leaking into the lay-up

1.1.1 Autoclave and VBO Processing

Autoclave processing has been demonstrated to be a robust and reliable method of consistently producing low porosity laminate structures (Grunenfelder & Nutt, 2010; Louis, 2010; Repecka & Boyd, 2002; Thomas, 2009). The key advantage in autoclave processing is the ability to generate high compaction pressures

(upwards of seven to ten times atmospheric pressure) to force entrapped gases into solution in the resin and prevent void growth (Figure 1.2) (F. C. Campbell, 2004; Grunenfelder & Nutt, 2010). The major benefits of VBO processing include the low cost of equipment and consumables, and the ability to perform rapid prototyping. However, VBO methods do not have access to the autoclave's high compaction pressures and have traditionally been unable to achieve the same level of part quality and performance due to high void content (Bond, Griffith, Han, Bongiovanni, & Boyd, 2008). Thus, the use of VBO-processed parts has been precluded from primary structural applications in aerospace until very recently (Ridgard, 2009). Additionally, autoclave cure temperatures can easily reach up to 180°C or more whereas VBO cure temperatures usually remain between 80 – 120°C due to the thermal limitations of the consumables. Although the use of lower process temperatures in VBO processing allows manufacturers to lower energy costs, the trade-off is that longer cycle times are required to fully cure the structure.

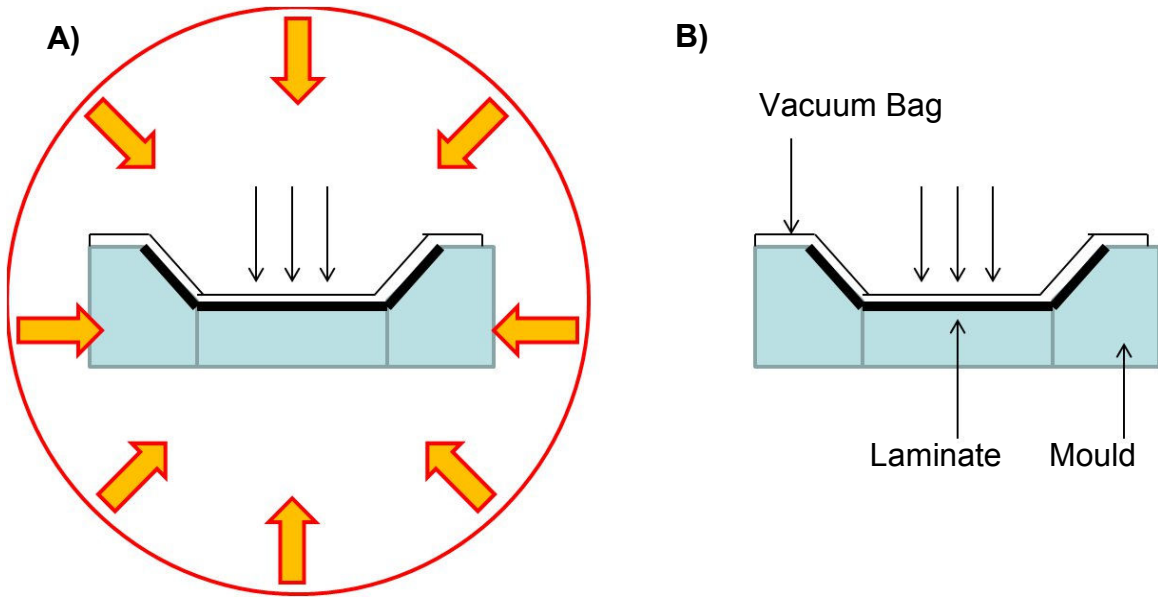


Figure 1.2. Prepreg processing methods. A) Autoclave processing; B) VBO processing.

The success of prepreg processing can be explained through the concept of void management (Arafath, Fernlund, & Poursartip, 2009). Void management is the balance of “void sources” with “void sinks” as shown:

Void Sources

- Physical entrapment of air between plies
- Dissolution of air into the resin during mixing
- Moisture absorption into the resin during storage and processing
- Generation of cure-reaction by-products
- Vacuum bag leaks

Void Sinks

- Compaction pressure (applied pressure must be > vapour pressure of volatiles in order to force gases into resin solution)
- Gas transport by vacuum evacuation (through interconnected void spaces)

In void management, low porosity is only achievable if the effectiveness of the void sinks is greater than the impact of the void sources. For autoclave processing, both high compaction pressure and vacuum evacuation are available avenues for void removal. VBO processing only has access to one atmosphere of pressure which may be insufficient for keeping volatiles contained in solution (Kardos, Dudukovic, & Dave, 1980). Therefore, removal of entrapped gases and volatiles in VBO processing is heavily reliant on gas transport mechanisms. However, autoclave processing also poses a number of significant drawbacks:

- Autoclave equipment requires high initial investment
- Many expenses associated with upkeep of consumables and equipment (i.e. nitrogen gas for positive pressure, high temperature/pressure resistant tooling)
- Part-size limitation imposed by maximum inner autoclave dimensions

- Operation requires user knowledge and training due to complexity of autoclave equipment

Because of the high costs associated with autoclave processing, the aerospace industry has had a continued interest in the development of improved VBO technology.

1.2 OUT-OF-AUTOCLAVE PREPREG: CYCOM 5320/T650

Recent advancements in prepreg technology have led to the development of a new class of materials called out-of-autoclave (OOA) prepregs. As indicated by their name, OOA prepregs are designed to produce autoclave quality parts (in terms of performance and void content) using VBO methods. Since removal of entrapped gases in VBO processing is mainly achieved through gas transport mechanisms, OOA prepregs are designed to maximize the prepreg's ability to "breathe" (Nutt & Boyd; Ridgard, 2009). Ch. 2.1 will delve into further discussion on the strategies employed by OOA prepregs for facilitating gas transport.

The primary OOA prepreg material used in this study is CYCOM 5320/T650 developed by Cytec Engineered Materials (Cytec). It consists of T650 3k carbon tows woven into a plain weave material and partially impregnated with CYCOM 5320 toughened epoxy resin. The CYCOM 5320/T650 OOA prepreg is designed to be curable at a range of temperatures (80 – 120°C), and can be post cured at 177°C to further increase T_g (CYTEC, 2009). Cytec claims that the OOA prepreg

can be vacuum-bag processed to produce autoclave quality primary structures (equivalent mechanical properties and porosity levels). A second OOA prepreg material, Advanced Composite Group's (ACG) MTM45-1/CF2426A, is used to provide comparisons to Cytec's 5320/T650. MTM45-1/CF2426A consists of CF2426A 6k carbon tows woven into a five harness satin weave material and partially impregnated with MTM45-1 toughened epoxy resin (ACG, 2007). A number of studies have previously investigated the gas transport characteristics of MTM45-1/CF2426A, and the findings from these studies will be included for comparison with 5320/T650 in Ch. 5.

1.3 OBJECTIVES

The scope of this thesis work was to measure the gas transport and water vapourization characteristics of Cytec's CYCOM 5320/T650 3k PW OOA prepreg (from here on referred to simply as 5320/T650). A portion of this study examined the effects of debulk time and temperature on gas transport in the prepreg. The experimental results were correlated with observations from microscopy image analyses to describe how gas transport characteristics evolve during the process cycle. The remainder of this study examined the effects of relative humidity on the moisture content of the prepreg, and quantified how much water vapour this translated into. Additional experiments were performed to measure moisture vapourization duration under vacuum conditions, as well as to determine when vapourization occurred during the process cycle. The findings from this study

were used to examine if the gas transport mechanisms in 5320/T650 can facilitate complete gas removal under typical processing conditions.

The justification for this study is described by Thorfinnson and Biermann in their research on void formation. They determined that high porosity was due to the resin impregnation process, which effectively closed off all of the gas transport pathways within the prepreg (Thorfinnson & Biermann, 1986). Work done by Repecka and Boyd supported this theory and hypothesized that lack of gas permeability in the prepreg was a major factor that led to high porosity (Repecka & Boyd, 2002). The relationship between moisture content and voids in prepreg structures has been demonstrated by Kardos et al, Vanlandingham et al, Kay et al's, and Hsiao et al's work, where experimental evidence strongly suggested that absorbed moisture had a significant contribution to void content (Hsiao, Kay, & Fernlund, 2011; Kardos et al., 1980; Kay, Farhang, Hsiao, & Fernlund, 2011; Vanlandingham, Eduljee, & Gillespie, 1999).

Objectives:

- Characterize gas transport in the in-plane and through-thickness laminate directions
- Investigate the effect of debulk time and temperature
- Observe laminate microstructure evolution over the cure cycle
- Determine the relationship between humidity and moisture content of the laminate

- Determine when vapourization of absorbed moisture occurs during VBO processing and quantify how much moisture is vapourized from laminates

2 LITERATURE REVIEW

2.1 GAS TRANSPORT

Gas transport in porous media takes place through a combination of advective and diffusive transport (Ho & Webb, 2006). In prepreg laminates, advection transport can occur through macro pores (void channels) and is driven by a pressure differential, whereas diffusion transport can occur within the matrix resin and is driven by a concentration gradient. Previous studies have theorized that the effects of diffusion transport in prepregs are negligible due to the timescales involved for gas diffusion (Louis, 2010; Tavares, Michaud, & Manson, 2009). For instance, Tavares et al reported that the diffusion length of nitrogen gas in epoxy resin is roughly 0.8 mm over 5 hours, which corresponds to typical cure cycle times for prepreg materials (Tavares et al., 2009). For actual prepreg structures (i.e. honeycomb skins) which can be several millimetres thick, very long process cycles (on the order of days) are required before gas removal by diffusion becomes relevant. Considering that gas diffusion lengths over the cure cycle are shorter than typical part thicknesses, modeling of gas transport in prepregs assuming only advection transport is usually sufficient. As advection is the transport mechanism of interest in this thesis work, all further discussions regarding gas transport in prepregs will refer to gas advection unless specified.

In VBO processing, evacuation of entrapped gases and volatiles is dependent on available gas transport pathways. Gas transport in prepregs can occur in the in-plane and through-thickness directions as shown in Figure 2.1. In-plane gas

transport can be further divided into interlaminar (between plies) and intralaminar (within plies) regions (K. J. Ahn, Seferis, Price, & Berg, 1991). To facilitate gas transport, “engineered vacuum channels” (EVCs) are often designed into the prepreg to provide pathways for gas removal (Boyd, 2003; Nutt & Boyd). These EVCs can be created through selective resin impregnation, such as using resin strips, porous resin films, and other partial impregnation techniques (Boyd, 2003; Louis, 2010). In many procedures, the resin is only applied to the surface of the fibres, leaving the empty spaces within the fibre tows un-wetted (Boyd, 2003).

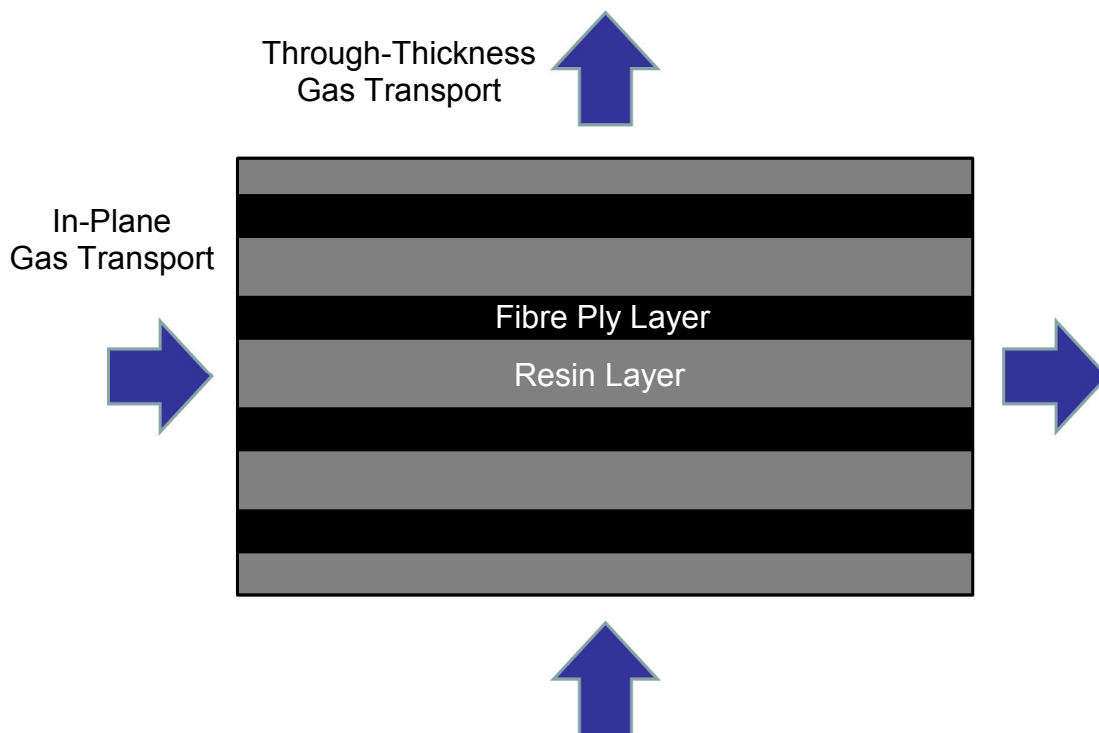


Figure 2.1. In-plane and through-thickness gas transport through prepreg laminates

Studies performed by Kratz, Louis et al, and Farhang et al have shown that gas transport in prepregs is highly anisotropic, with in-plane gas transport being more dominant (Farhang & Fernlund, 2011a; Farhang & Fernlund, 2011b; Kratz, 2009; Louis et al., 2010; Louis, 2010). They theorized that gas can flow through the empty spaces between dry fibre tows much more easily than traversing through multiple layers of fibre and resin. For gas to travel through the prepreg layers, void regions in the fibre and resin layers must line up to form interconnected pathways (Figure 2.2) (Kardos et al., 1980; Louis, 2010). Various prepreg manufacturers and research groups have continually stressed the importance of edge breathing for gas evacuation, suggesting that in-plane gas transport is more dominant by design (ACG, 2007; Boyd, 2003; CYTEC, 2009; Nutt & Boyd; Ridgard, 2009).

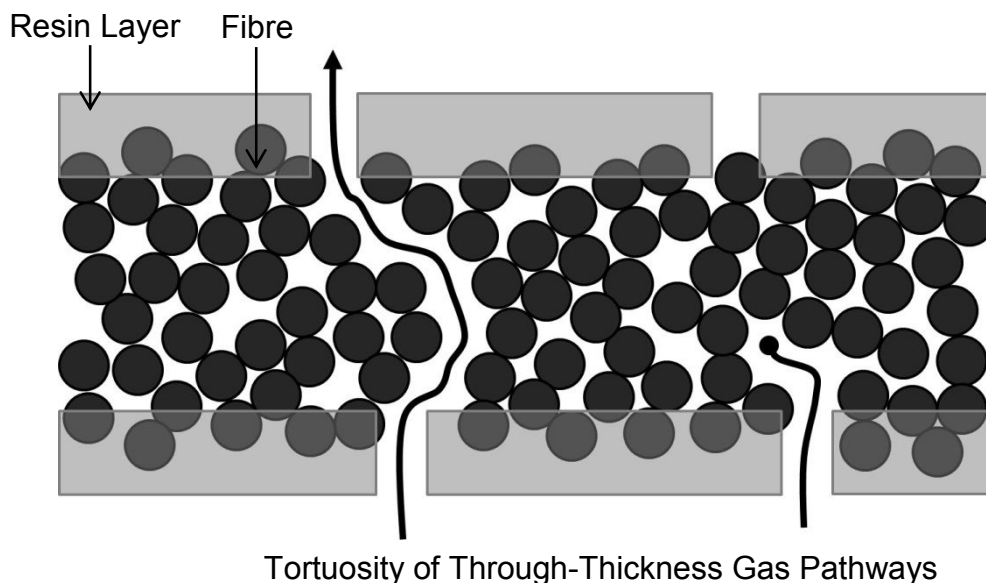


Figure 2.2. Difficulty in forming interconnected pathways for through-thickness gas transport.

For OOA prepregs, the key to low porosity is removal of entrapped air and volatiles before resin gelation and cure. Chris Ridgard, Vice President of Technology at Advanced Composites Group (ACG), believes that the principal difference between traditional autoclave prepregs and OOA prepregs lies in the resin properties (i.e. resin rheology and reactivity) (Ridgard, 2010). According to Ridgard, early iterations of ACG's OOA prepreg systems utilized low viscosity resins which would flow prematurely and close off escape pathways before air was adequately removed (J. R. Wood & Bader, 1995). In order to improve gas evacuation, subsequent ACG OOA prepreg systems, such as their MTM45-1/CF2426A 5-harness satin (5HS), incorporated modified resins that were tailored to have higher initial viscosities and increased gelation time (compared to autoclave prepregs) in order to extend the duration that the EVaCs remain open (Ridgard, 2010). Once sufficient time has passed, the viscosities of these resins were designed to fall quickly to allow resin flow into the EVaCs and other voids before gelation takes place. By controlling parameters like the degree of impregnation, and the resin rheology and reactivity, the gas transport characteristics of the OOA prepreg can be optimized.

2.2 PERMEABILITY

Permeability is a measure of a porous material's ability to facilitate fluid flow. Permeability studies are often carried out in the fields of hydrogeology (ground water flow in aquifers), petroleum engineering (oil and natural gas extraction from

reservoirs), and filtration/separation technologies (membranes for drug delivery, water purification, and fuel cell applications) (Gode, Lindbergh, & Sundholm, 2002; Sakhaee-Pour & Bryant, 2011; Sobera & Klejin, 2006; Zhu, Jiang, Teng-Man, & Kin-Kai, 2002).

For composites processing, liquid permeability (resin flow in dry preforms and prepregs) represents the bulk of the more recent permeability studies (Gebart & Lidstrom, 1996; Gutowski et al., 1987; Lam & Kardos, 1989; Loos & Springer, 1983; Michaud & Mortensen, 2007; Shim, Ahn, Seferis, Berg, & Hudson, 1994; Thomas, Bongiovanni, & Nutt, 2008; Thomas & Nutt, 2009). Gas permeability has not been receiving much attention until the last decade (Louis, 2010). For prepreg processing, gas permeability is significant because it provides an indication of how readily entrapped gases and volatiles can be removed. Several groups have previously done work on testing and measuring air permeation of prepregs and have found that higher permeability prepregs consistently produced lower porosity parts (K. J. Ahn et al., 1991; Nam, Seferis, Kim, & Lee, 1995; Putnam & Seferis, 1995; Shim & Seferis, 1997; Thorfinnson & Biermann, 1986). For instance, Thorfinnson and Biermann's investigation into the cause of voids in unitape prepreg structures highlighted the importance of gas permeation as a function of degree of resin impregnation (Thorfinnson & Biermann, 1986). Their findings determined that simply altering the impregnation process from full to partial impregnation resulted in the production of void-free parts. Through partial impregnation, empty pathways and channels within the prepreg remained open

to allow entrapped gases and volatiles to escape. These void channels were eventually filled in once applied temperatures and pressures allowed resin flow. However, with fully impregnated prepregs, the movement of entrapped gases and volatiles becomes severely restricted, increasing the likelihood of high porosity.

Gas permeability studies led by Seferis' research group showed that both interlaminar and intralaminar permeabilities were critical for void removal in prepreg processing (K. J. Ahn et al., 1991; Nam et al., 1995; Putnam & Seferis, 1995; Shim & Seferis, 1997). Interlaminar permeability was one to two orders of magnitude higher than intralaminar, and was strongly affected by prepreg form (woven fabric > unitape) as well as surface quality (rough > smooth). Intralaminar permeability was highly dependent on the presence of open pores within the prepreg, and was limited to the direction of the fibres. However, it should be noted that permeability contributions from interlaminar and intralaminar regions will vary across material systems depending on the fibre architecture and resin impregnation process (Louis, 2010). Recent prepreg permeability studies have revealed that both in-plane and through-thickness permeabilities change during processing due to evolving resin viscosity. As mentioned earlier, work done on MTM45-1/CF2426A 5HS OOA prepregs by Kratz, Louis et al, and Farhang et al all showed that measured in-plane and through-thickness permeabilities varied from one to two orders of magnitude throughout their cure cycles, with in-plane permeability decreasing with temperature and through-

thickness permeability increasing with temperature (Farhang & Fernlund, 2011a; Farhang & Fernlund, 2011b; Kratz, 2009; Louis et al., 2010; Louis, 2010). These findings seem to indicate that opportunities for advection gas removal may be limited to a small processing window.

Two common approaches for measuring permeability are a pressure-decay method and a steady-state method (Ho & Webb, 2006; Louis, 2010). Both approaches utilize Darcy's law, which relates fluid discharge rate in a porous medium to the pressure drop, the fluid viscosity, and the permeability of the medium. In the pressure-decay method, a prepreg laminate specimen is prepared such that one end is exposed to atmosphere while the other is placed under vacuum (i.e. in a vacuum bag) (K. J. Ahn et al., 1991; Putnam & Seferis, 1995; Tavares et al., 2009). Once full vacuum is achieved, the vacuum source is disconnected, allowing pressure to return under the vacuum bag. The rate of pressure change is proportional to the gas flow rate, which can be described using Darcy's Law to calculate for the permeability of the prepreg (K. J. Ahn, Seferis, & Berg, 1991; Scheidegger, 1974). In the steady-state method, the prepreg laminate is prepared in much the same way except the vacuum source is not removed. A constant pressure differential develops across the laminate specimen which leads to steady-state gas flow. Darcy's Law can then be used to describe the relationship between pressure differential and steady-state gas flow in order to calculate prepreg permeability (Nam et al., 1995; Shim & Seferis, 1997). In this thesis work, the more direct steady-state approach was chosen for

quantifying in-plane and through-thickness permeabilities of CYCOM 5320/T650 PW prepreg laminates.

2.2.1 Application of Darcy's Law

The use of Darcy's law has become a standard approach for characterizing porous materials (Chen & Penumadu, 2008). Although originally used to describe the flow of incompressible fluids through packed beds, Darcy's law can be modified to describe slow, viscous gas flow in porous mediums (laminar regime, characterized by small Reynold's number ($RE < 1$)) (Noman & Zubair Kalam, 1990). To account for additional factors such as turbulent flow or boundary shear effects (friction), the Forchheimer and Brinkman extensions can be applied to Darcy's law, respectively (Ho & Webb, 2006). However, gas flow in porous media has been determined to be generally non-turbulent and the effects of boundary shear to be insignificant (Ho & Webb, 2006). Therefore, these extensions to Darcy's law are not considered in the present study.

Darcy's law can be used to determine prepreg permeability through the steady-state approach by considering a simple pipe analogy illustrated in Figure 2.3. The Darcy's law relation for an incompressible fluid is provided in Equation 1.

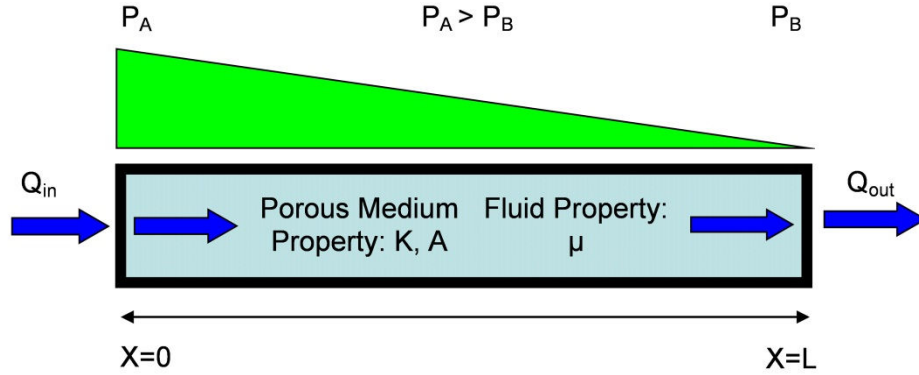


Figure 2.3. 1-D fluid flow pipe analogy using the steady-state approach and Darcy's law.

$$Q = \frac{AK}{\mu} \left(\frac{P_A - P_B}{L} \right) \quad (\text{Equation 1})$$

For an incompressible fluid, Darcy's law states that the rate of flow is governed by the pressure change ($P_A - P_B$) across the total pipe length (L), pipe cross-sectional area (A), permeability of the porous material (K), and dynamic viscosity of the fluid (μ). When a fixed pressure gradient is induced along the pipe length, a steady-state fluid flow (Q) is established. If the steady-state flow rate, fluid dynamic viscosity, pressure gradient, and dimensions of the porous medium are known, Equation 1 can be solved for permeability.

For the present permeability study, this pipe analogy was extended to describe gas flow in prepreg laminates in the in-plane and through-thickness directions as shown in Figure 2.4. Here, the prepreg laminate was considered a homogeneous medium, and gas flow in the in-plane and through-thickness

directions were considered to be independent of one another. The evaluation of gas flow was also restricted to a 1-D analysis for simplicity.

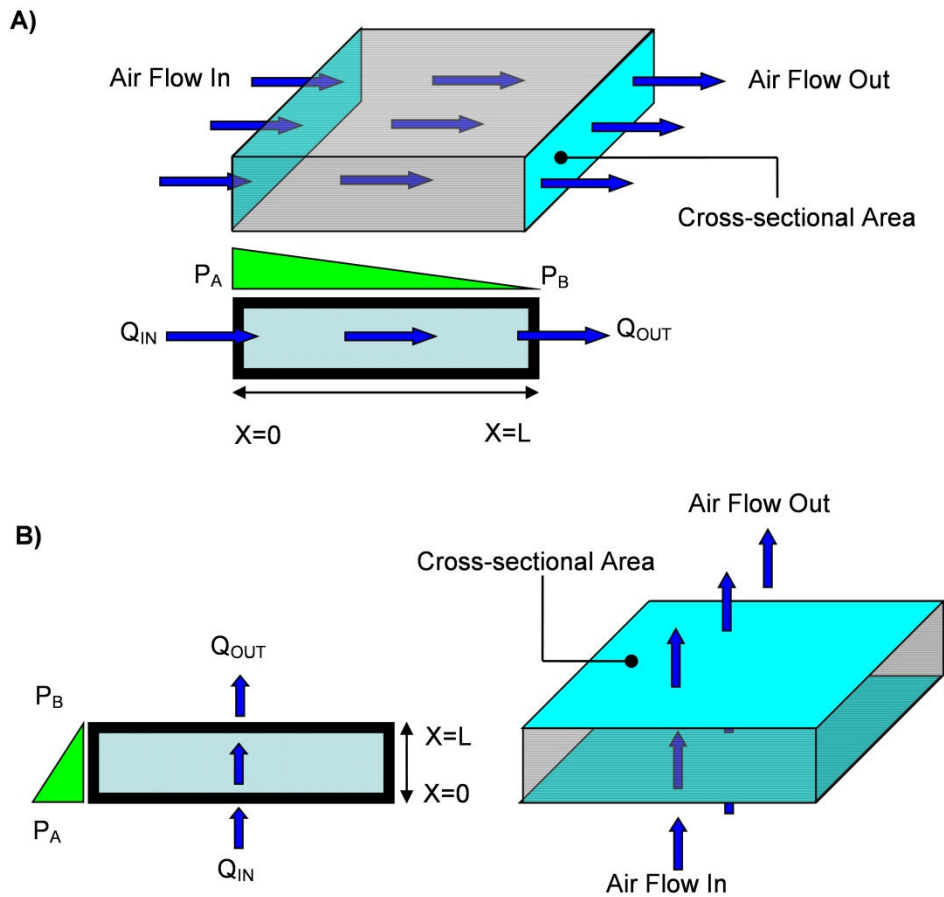


Figure 2.4. Pipe analogy translated into in-plane and through-thickness gas flow for a prepreg laminate. A) In-plane gas flow; B) Through-thickness gas flow.

As Darcy's Law was originally intended for use on incompressible fluids, a modified expression that accounted for the compressibility of gases was needed. An expression for 1-D fluid flow of a compressible fluid through a porous medium based on Darcy's Law and the Ideal Gas Law was derived by Arafath et al

(Arafath et al., 2009). This expression was used in the permeability study presented in this work, and is provided in Equation 2. The complete derivation of this modified Darcy's Law expression for compressible fluids is provided in the Appendix A.

$$Q = \frac{AK}{2\mu L} \left(\frac{P_A^2 - P_B^2}{P_A} \right) \quad (\text{Equation 2})$$

Where:

- Q [m^3/s] is steady-state volumetric flow
- A [m^2] is cross-sectional area
- K [m^2] is permeability
- μ [$Pa \cdot s$] is fluid dynamic viscosity
- L [m] is length
- P_A [Pa] is pressure state at point "A"
- P_B [Pa] is pressure state at point "B"

Air dynamic viscosity at ambient conditions was taken to be $1.98E-05$ Pa*s (The Engineering ToolBox, 2011). In reality, the air dynamic viscosity varies slightly with temperature. However, to simplify the problem, actual air flow temperatures were assumed to be close to ambient levels. To determine steady-state flow rate under standard conditions, the Ideal Gas Law can be invoked again to obtain Equation 3.

$$Q_s = \left(\frac{T_s}{T}\right) \left(\frac{P}{P_s}\right) Q \quad (\text{Equation 3})$$

The actual flow rate (Q) can be related to the standard condition flow (Q_s) using actual and standard condition temperatures and pressures (T, P, T_s, P_s). In this thesis work, the old IUPAC standard of 273.15K and 101325 Pa were used (The Engineering ToolBox, 2009).

The calculation of permeability using Equation 2 or Equation 3 is based on several simplifying assumptions:

- The cross-sectional area and the volume of open pathways within the laminate remain constant during gas flow measurement
- The fluid obeys Darcy's law, the Ideal Gas law, and flows in the laminar regime (verification of laminar flow is shown in Appendix B)
- Moisture vapourization and other off-gassing related effects are negligible compared to the induced steady-state gas flow
- In-plane and through-thickness gas flow are independent of one another
- Gas flow in the in-plane transverse direction is equivalent to the rolling direction due to weave ($0^\circ/90^\circ$) symmetry

In reality, the thickness (and therefore cross-section) of the laminate and the volume of open pathways is constantly changing during the cure cycle because of resin flow and compaction. To simplify the challenge of measuring an evolving cross-section, the cured ply thickness (CPT) can be used to determine the cross-

sectional area for permeability calculations (F. C. Campbell, 2004). The rolling and transverse directions mentioned in the final assumption are illustrated in Figure 2.5 for clarity.

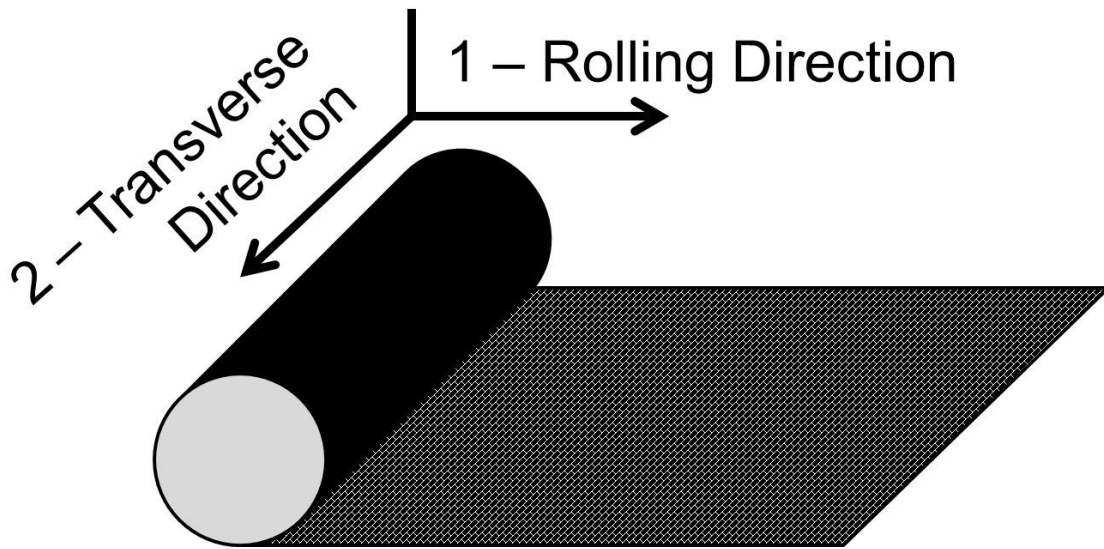


Figure 2.5. Rolling and transverse laminate orientations.

2.3 MICROSCOPY

Void analysis is a significant part of the material & process evaluation and quality assurance step in composites manufacturing. For aerospace applications, material T_g and final void content are usually the two most important physical properties to be optimized (Boey & Lye, 1992). Proper thermal management (through well-designed cure cycles and tooling/bagging arrangements) facilitates uniform and controlled heating of the composite structure, thereby allowing material T_g to be maximized (Scheidegger, 1974). Likewise, void management

is crucial in minimizing the occurrence of voids. As discussed in Ch. 1, void management involves the balance of void sources with void sinks (Arafath et al., 2009). Voids can be formed from physical entrapment of air during prepreg lay-up, as well as from vapourization of dissolved moisture and cure reaction by products (if any) in the resin during heating. If voids are present in the final cured structure, they will have a deleterious effect on mechanical performance.

Microscopy techniques are often employed for observing the internal structure of materials. Although many branches of microscopy have now been developed (electron, infrared, ultraviolet, laser etc.), optical (light) microscopy is still one of the most popular techniques currently being used in material science. Advantages associated with optical microscopy include lower initial investment (equipment and training), lower maintenance costs (energy and consumables), and colour images (Kim, 2009). In the analysis of composite materials, micrographs can provide important information regarding void content, fibre morphology, and degree of resin impregnation. In their work on investigating resin flow in RFI manufactured parts, Thomas et al utilized both optical microscopy and ultrasound C-scan techniques to obtain “snapshots” of resin infiltration through woven preforms (Thomas et al., 2008; Thomas & Nutt, 2009). Infiltration was evaluated based on the location and amount of remaining voids. The micrographs revealed that at the start of infusion, voids existed primarily within the centre of the fibre tows. As the infusion progressed, resin flow encapsulated the tows and filled the void spaces simultaneously from all sides.

Although the void analysis was qualitative, Thomas et al's work provided useful insight into the pattern of resin flow in and around dry fibre bundles.

Grunenfelder et al and Hsiao et al utilized microscopy to assess the effects of dissolved moisture and vacuum quality on void content in MTM44-1/CF5804A twill and MTM45-1/CF2426A 5HS OOA prepregs, respectively (Grunenfelder & Nutt, 2010; Hsiao et al., 2011). Micrographs revealed that OOA specimens subjected to higher relative humidity conditioning resulted in increased porosity (from almost no porosity at 0 – 50 %RH conditioning, to up to three percent porosity at 90 %RH conditioning). However, autoclave prepreg specimens subjected to the same conditioning process consistently exhibited less than one percent porosity (Grunenfelder & Nutt, 2010). Similarly, decreasing vacuum quality resulted in increased levels of porosity (from 0.5% porosity at full vacuum to 3.5% porosity at 60% vacuum for 100 %RH conditioned OOA specimens) (Hsiao et al., 2011). Although three percent porosity seems small, it should be noted that the specimens used were laboratory sized panels (less than 30 cm x 30 cm; four to sixteen plies). Real production parts can be orders of magnitude larger, which would exacerbate any detrimental effects associated with dissolved moisture and low quality vacuum.

Recently, Farhang et al have performed void evolution studies on MTM45-1/CF2426A 5HS OOA prepregs using optical microscopy (Farhang & Fernlund, 2011a; Farhang & Fernlund, 2011b). For their experiments, multiple specimens

were prepared and partially cured to represent various points throughout its cure cycle. They categorized the observed voids into three groups as illustrated in Figure 2.6: “interlaminar voids” (voids located between lamina), “resin voids” (voids surrounded by resin), and “tow voids” (voids located inside fibre tows).

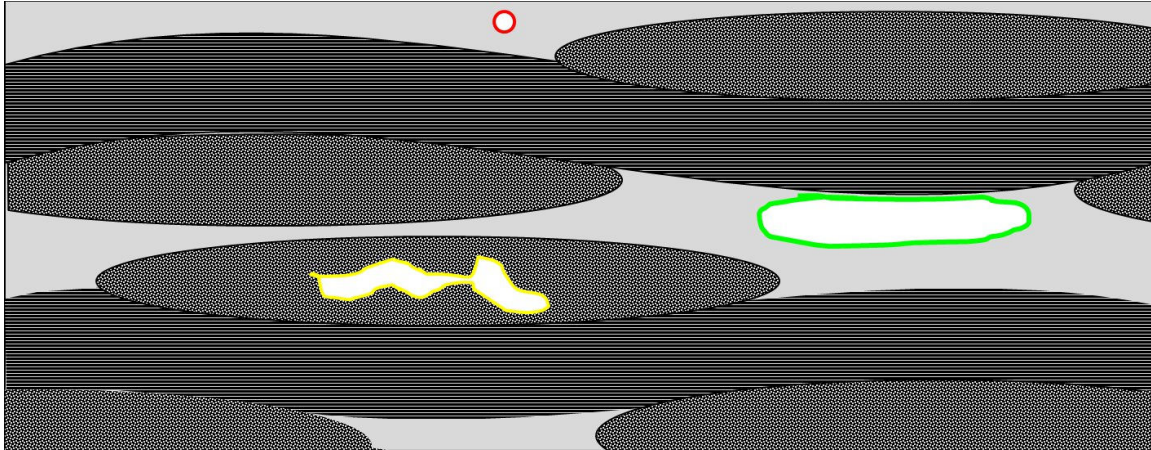


Figure 2.6. Void categorization during microscopy of OOA prepreg. Interlaminar voids are located between prepreg plies, and are represented by a green highlight. Fibre tow voids are located within individual fibre bundles, and are represented by a yellow highlight. Resin voids are isolated by the matrix, and are represented by a red highlight.

Interlaminar voids represented the greatest fraction of voids, followed by fibre tow voids and then resin voids. Farhang showed that both interlaminar and fibre tow voids fell sharply during the heating ramp, and eventually decreased to zero as they collapsed and became filled in. However, resin voids remained relatively constant throughout the entire cure cycle as they were trapped and could not be

removed. Additionally, a special method based on ASTM E2015-04 and Dillon's work was developed by Farhang to prepare uncured prepreg specimens for microscopy (ASTM International, 2009; Dillon, 2005). The method utilized a room-temperature cure low-viscosity mounting resin to fill the open pores in the uncured specimen. The mounting resin, once cured, provided support for the soft prepreg during grinding and polishing and reduced damage done to the viewing surface (i.e. resin smearing, fibre pull-out). Farhang specifically used the Epo-color (Buehler Co.) mounting resin, which had the added benefit of having a distinct colour so that it could be distinguished from the prepreg matrix. The uncured specimen preparation method developed by Farhang was used in the microscopy analysis performed in this thesis work.

2.4 WATER VAPOURIZATION

As discussed in Ch. 1, porosity can come from vapourization of absorbed moisture in the matrix phase during resin mixing or storage, as well as from volatiles generated by the cure reaction. Recent advancements in resin technology have led to the development of resin systems that are designed to generate lower (or zero) amounts of volatile by-products (Thomas, 2009; Thomas & Nutt, 2009). However, the presence of absorbed moisture remains an issue. Some studies have even suggested that vapourization of absorbed moisture is the primary cause of voids (Grunenfelder & Nutt, 2010; Kardos et al., 1980).

Numerous research groups have investigated the effects of moisture on the hygrothermal and mechanical properties of cured epoxy-based composite systems (Boll, Bascom, & Motiee, 1985; Lin & Chen, 2005; Loos & Springer, 1979; Shen & Springer, 1976; Vanlandingham et al., 1999). However, studies into the effects of moisture absorption during processing of uncured composites remains relatively limited. As mentioned previously, studies by Grunenfelder, Kay and Hsiao have individually investigated the effects of moisture on void formation in OOA prepregs and have demonstrated that an increase in porosity was observed with increasing levels of dissolved moisture (Grunenfelder & Nutt, 2010; Hsiao et al., 2011; Kay et al., 2011). According to a hypothesis presented by Kardos et al, absorbed moisture can lead to porosity if water molecules within the resin are able to diffuse together and form water voids (Kardos et al., 1980). During processing, the water voids can grow and expand if the vapour pressure inside the void surpasses the opposing resin pressure and surface tension forces. This can potentially become a significant problem during the cure cycle as temperatures reach the normal boiling point of water, causing voids to expand due to the volume change from water to steam. In autoclave processing, water void growth is more easily kept in check by high levels of applied pressure. However, for VBO processing, this is not an option. If the material system and cure cycle are not designed to allow evacuation of the vapourized water, extensive porosity will occur as a result.

As of the current literature review, very limited work has been done on determining the quantity of water vapour that is evolved from moisture absorption of OOA prepregs. Additionally, few have experimentally confirmed the conditions which cause vapourization of absorbed moisture to occur during vacuum bag processing. In this thesis work, studies were performed to quantify water vapourization in moisture conditioned CYCOM 5320/T650 PW and MTM45-1/CF2426A 5HS OOA prepreg laminates. Moisture absorption was predicted using a solubility model developed by Kardos (Kardos et al., 1980). Calculation of the pressures required for water vapourization at ambient temperatures was confirmed using the Clausius-Clapeyron relation, and the rate of water vapourization was compared to Langmuir's evaporation equation under room temperature vacuum conditions.

2.4.1 Application of Kardos' Solubility Model

Kardos developed an empirical parabolic solubility model based on prepreg moisture studies carried out collaboratively with Brand et al for the Air Force Wright Aeronautical Laboratories (AFWAL) (Brand, Brown, & McKague, 1984). In these experiments, Narmco 5208/T300 prepreg specimens were dried and then conditioned in 45, 62, and 71 %RH environments to measured weight gain from moisture absorption. Equation 4 was the parabolic model developed to fit the experimental data.

$$MC [wt. \%] = k(\%RH)^2 \quad \text{Equation 4}$$

In Equation 4, (MC) is the moisture content of the prepreg material, (k) is a unit-less proportionality constant, and ($\%RH$) is the relative humidity of the conditioning environment. For the Narmco 5208/T300 system, (k) was experimentally determined to be $5.58E-05$. For each prepreg system, (k) would have to be re-evaluated. By predicting the moisture content using Equation 4, the mass of absorbed moisture can be calculated using the definition of moisture content given in Equation 5 (Shen & Springer, 1976).

$$MC [wt. \%] = \frac{M_{H_2O}}{M_{Dry}} \times 100 \quad \text{Equation 5}$$

From Equation 5, (M_{H_2O}) is the mass of absorbed water and (M_{Dry}) is the mass of dry (0 %RH) prepreg. For the moisture vapourization studies presented in this thesis work, Kardos' parabolic solubility model was applied to moisture-conditioned CYCOM 5320/T650 PW and MTM45-1/CF2426A 5HS OOA prepreg laminates to predict moisture content. The mass of absorbed moisture was then compared against mass loss data obtained from the flow sensors during moisture vapourization testing.

2.4.2 Application of Clausius-Clapeyron Equation

The Clapeyron relation is a general equation which describes the co-existence curve between two phases of matter on a pressure-temperature (P-T) diagram.

For liquid-gas (i.e. water/water vapour) or solid-gas transitions at low temperatures and pressures (far below the critical point), the specialized Clausius-Clapeyron equation can be used instead (Fleagle & Businger, 1980). The Clausius-Clapeyron equation utilizes three assumptions (Fleagle & Businger, 1980; Salzman, 2005):

- Volume change of the phase transition is assumed to be equivalent to the volume of the gas only ($\Delta V = V_{gas} - V_{liquid} \approx V_{gas}$)
- Gas phase is assumed to be ideal
- Latent heat of vapourization is independent of temperature

The Clausius-Clapeyron equation can be used to relate the equilibrium vapor pressure of water at various temperatures to the latent heat of vapourization as given in Equation 6. If the vapourization pressure of water is known at one point (i.e. at the freezing or boiling temperature), the vapourization pressures at all other temperatures can be determined. The plot of vapourization pressure against temperature forms the co-existence curve of water and water vapour.

$$\ln \left(\frac{P_B}{P_A} \right) = \frac{L_{vap}}{R} \left(\frac{1}{T_A} - \frac{1}{T_B} \right) \quad \text{Equation 6}$$

In Equation 6, (P_A) and (P_B) are the water vapourization pressures at point A and B, (T_A) and (T_B) are the temperatures at point A and B, (R) is the gas constant, and (L_{vap}) is the latent heat of vapourization. In this thesis work, the Clausius-

Clapeyron equation was used to determine the vacuum pressure required to initiate water vapourization under ambient temperatures.

2.4.3 Application of Langmuir Evaporation Equation

In his work investigating the vapor pressure of metallic tungsten, Langmuir derived an equation which relates a substance's rate of evaporation to its vapour pressure (Langmuir, 1913). Langmuir envisioned a simple problem of a volume of gas with one side bounded by an interface with known surface area. Using the kinetic theory of gases and the ideal gas law, he described evaporation as the rate at which gas molecules will pass through the interface (Equation 7).

$$m_{flux} \left[\frac{kg}{m^2*s} \right] = P_V \sqrt{\frac{M}{2\pi RT}} \quad \text{Equation 7}$$

In Equation 7, (m_{flux}) is the mass flux, (P_V) is the substance's vapour pressure, (M) is the molecular weight, (R) is the gas constant, and (T) is the temperature. From Equation 7, increasing the vapour pressure increases the rate of mass loss. This equation can be used to describe the rates at which water evaporates and condenses within a closed container. At equilibrium, the rates of evaporation and condensation are equal. Equilibrium can also be defined as the condition when the partial pressure of water is equal to the vapour pressure of water at a fixed temperature, or in other words, at 100 %RH. The definition of relative humidity is given in Equation 8.

$$\%RH = \frac{\text{Partial Pressure of Water}}{\text{Vapour Pressure of Water}} \times 100 \quad \text{Equation 8}$$

Therefore, if Equation 7 describes the rate of water molecules evaporating (leaving through the interface), replacing the vapour pressure of water with its partial pressure will describe the rate of water molecules condensing (entering through the interface) (Powell, 2005). By subtracting the water partial pressure from its vapour pressure, the net evaporation rate can be obtained (Equation 9).

$$m_{flux} \left[\frac{kg}{m^2 \cdot s} \right] = (P_V - P_P) \sqrt{\frac{M}{2\pi RT}} \quad \text{Equation 9}$$

In the current thesis work, this variation of Langmuir's evaporation equation was applied to a numerical model developed by James Kay (University of British Columbia) to simulate water vapourization kinetics. The simulation was used to predict the time needed for complete moisture removal.

3 PERMEABILITY TESTING

3.1 METHODS

Permeability testing on 5320/T650 was carried out to characterize the gas transport behaviour of OOA prepregs. Steady-state gas flow tests were performed on laminate specimens and flow data was reduced using the 1D Darcy's Law gas transport model derived by Arafath et al (Arafath et al., 2009) to determine material permeability. Testing was done to quantify permeability for the in-plane and through-thickness directions under ambient and heated conditions. Ambient condition tests simulated gas transport during initial processing (i.e. debulking), whereas heated condition tests simulated gas transport during heat-up. A long debulk test was also performed to measure changes in in-plane permeability over long-term compaction. Microscopy was carried out to qualitatively observe specimen microstructures and void contents throughout cure. Both long debulk testing and microscopy was performed in the in-plane orientation because experimental evidence indicated that the majority of gas evacuation takes place along the fibre directions (Thorfinnson & Biermann, 1986; Thorfinnson & Biermann, 1987).

All permeability specimens were prepared by removing precut prepreg sheets from the freezer and thawing them in a Ziploc bag for approximately 20-30 minutes. This minimized moisture condensation on the prepreg as the material warmed up to room temperature. Once thawed, prepreg sheets were cut to over-

size dimensions (~1" greater than required) and then laid up together on a cutting mat to form laminate specimens. Rollers were used to increase ply compaction and ensure that each ply sat flush against one another. Laminates were cut to specimen dimensions using a sharp cutting knife. For the sake of consistency and to reduce the effects of material variability, all specimens were laid-up along their rolling direction. Additionally, all in-plane permeability tests were performed by setting the rolling direction to be the testing direction. Table 3.1 presents the testing matrix performed in this study along with details of the specimen dimensions from each test. The manufacturer's recommended cure cycle (MRCC) was used during heated permeability tests to replicate industry processing conditions as closely as possible.

Table 3.1. Permeability test matrix for 5320/T650.

	In-Plane	Through-Thickness
Long Debulk Test	3 repetitions 24 hour duration Specimen dimensions: 2-1/4" x 4" x 4 plies	N/A
Ambient Permeability Test	3 repetitions Specimen dimensions: 2-1/4" x 4" x 4 plies	3 repetitions Specimen dimensions: 3-1/4" x 3-1/4" x 8 plies
Heated Permeability Test	3 repetitions MRCC: (1-3 C/min ramp; 2 hour cure @ 120°C) Specimen dimensions: 2-1/4" x 4" x 4 plies	3 repetitions MRCC: (1-3 C/min ramp; 2 hour cure @ 120°C) Specimen dimensions: 3-1/4" x 3-1/4" x 8 plies
Microscopy Image Analysis	1 ply as laid up 4 ply as laid up 4 ply debulked 4 ply cured (vent side open) 4 ply cured (vent side closed) Specimen dimensions: 1/2" x 4" x varying thicknesses	N/A

3.1.1 In-Plane Setup

The experimental setup for in-plane permeability testing is illustrated in Figure 3.1A. Three isolated chambers containing vacuum ports (Torr Tech, 1/4" Vacuum Probe & QD11 1/4" NPT Plug) were created using sealant tape (Airtech, AT-200Y). One chamber was designated the "vent chamber" and was connected in series to a mass flow sensor and rotameter (OMEGA, FL-110 series) with access to atmospheric air. A second chamber was designated the "vacuum chamber"

and was connected in series to a second mass flow sensor and a vacuum pump (Leybold, TRIVAC D8A). Mass flow sensor equipment was on loan from Convergent Manufacturing Technologies Inc. A third and final chamber, designated the “leak test chamber”, was used to detect the presence of leaks. Inter-chamber and total-system leak tests were performed to determine if transverse gas flow and air-channel bridging existed in the setup. Illustrations of transverse gas flow and air-channel bridging are provided in Appendix C and Appendix D, along with the procedures for performing the inter-chamber and total-system leak tests. The permeability specimen was placed between the vent and vacuum chambers to serve as the sole pathway for inter-chamber gas flow. Sealant tape was applied to the specimen to isolate gas flow to the in-plane direction. Thermocouples (Omega, Type J) were attached to the specimen to measure temperature changes during heated tests. The mass flow sensors and thermocouples were hooked up to a computer equipped with a data acquisition (DAQ) device and LabView Signal Express software for logging flow data.

For ambient in-plane permeability testing, Figure 3.1B illustrates the tool and bagging materials used and their lay-up order. The specimen was laid up such that two breathing edges remain exposed in the in-plane testing direction. The exposed edges were covered by glass fibre bundles and placed in contact with layers of breather and vacuum ports to form complete pathways for gas removal. This bagging setup was designed to mimic Cytec’s recommended bagging scheme as closely as possible (CYTEC, 2009).

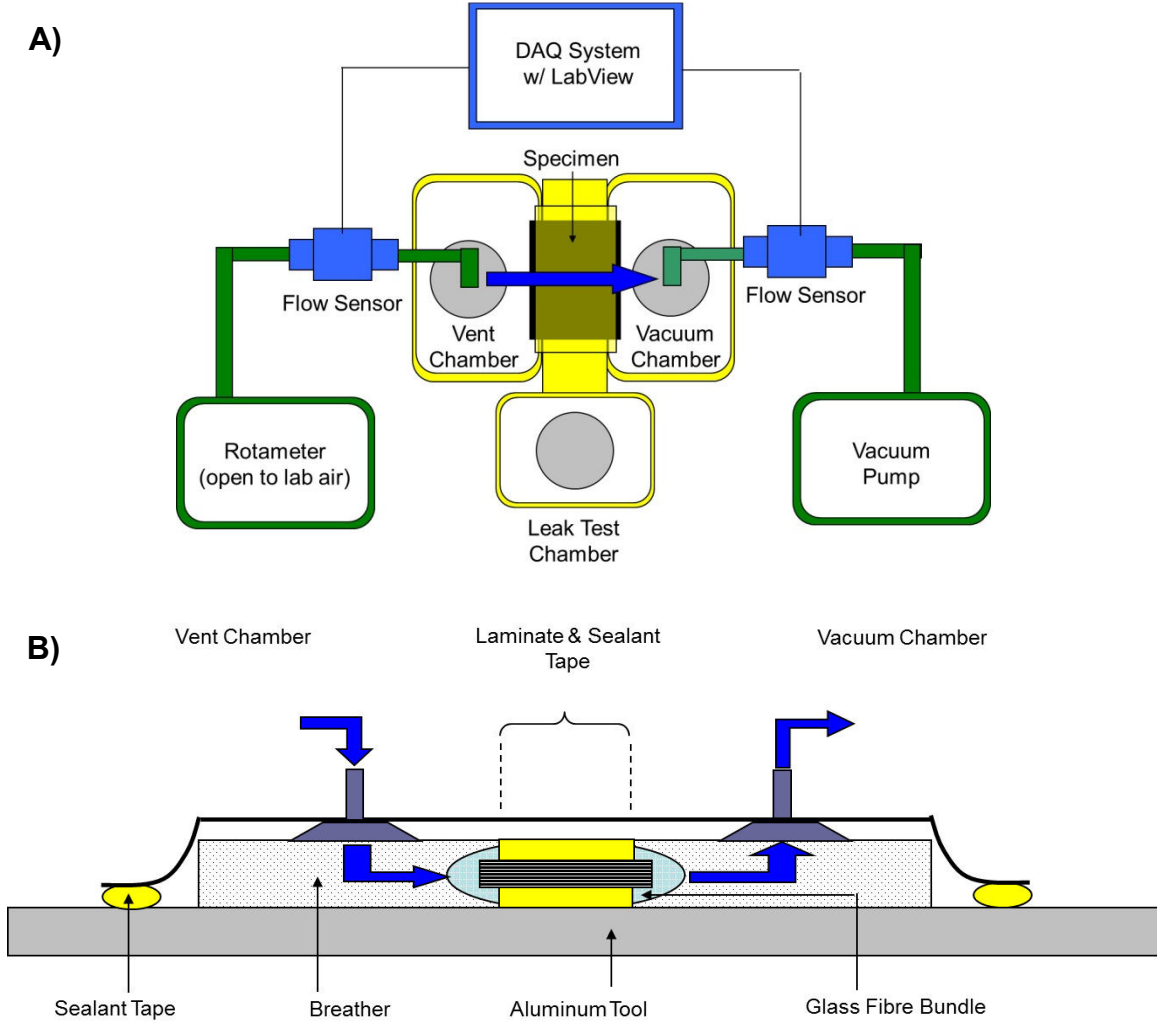


Figure 3.1. In-plane permeability test setup. A) Chamber configuration and test equipment layout; B) Lay-up order of consumables, and direction of in-plane gas flow.

In-plane permeability specimens were cut to 2- $\frac{1}{4}$ " long, but the actual length contained by sealant tape was 2" as shown in Figure 3.2. Since only 2" was truly subjected to 1D gas flow, the effective length (not the specimen length) was used for permeability calculation. Due to the difficulty of measuring the thickness of a

soft uncured prepreg, the nominal cured ply thickness was used to calculate the cross-sectional area of the specimen. 5320/T650 was found to have a nominal cured ply thickness of 0.20 mm, which translated to 0.80 mm for a four ply specimen.

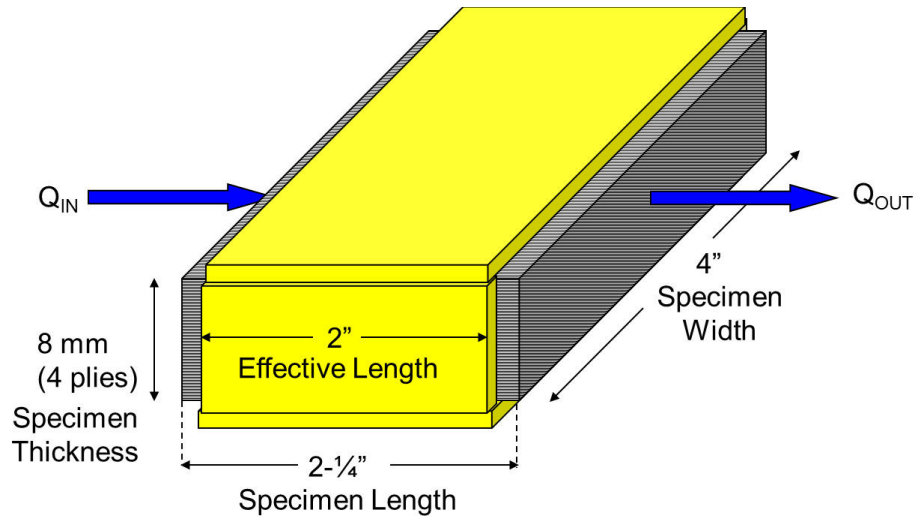


Figure 3.2. Isolated 1D gas flow in the in-plane direction. Effective length refers to the section of specimen truly subjected to 1-D in-plane gas flow (2") which is used in determining permeability.

During in-plane permeability testing, the vacuum pump was turned on to allow air to be continuously pulled through the specimen. Air flow rates were measured and reported by the mass flow sensors as standard volumetric flow (273.15 K; 1 atm). Once steady-state flow was achieved, flow rate data was logged for five to ten minutes and then saved and exported to Microsoft Excel for data reduction.

Heated in-plane permeability testing was identical to ambient testing except for the addition of an induction heating pad and several layers of aluminum tooling and ceramic tiles as illustrated in Figure 3.3A. Additionally, the setup was assembled within an enclosure lined with insulation as depicted in Figure 3.3B and Figure 3.3C. The induction heating pad was controlled via a temperature process controller (OMEGA®, Series CN7500) which enabled programming of accurate temperature ramp and soak cycles. The layers of aluminum tooling were included to even out thermal gradients generated from any uneven heating across the surface of the heating pad. The bottom layer of ceramic tiles served as insulation and protection for the table which the heating enclosure rested on.

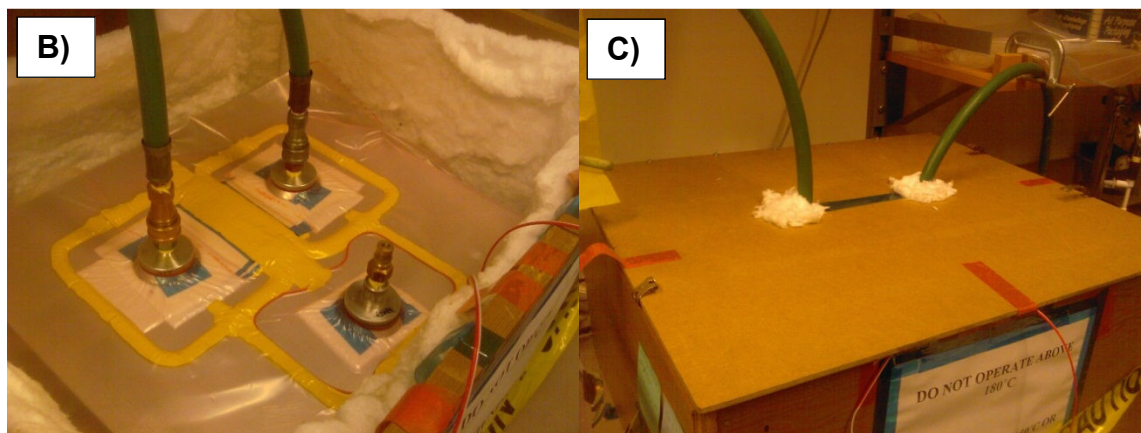
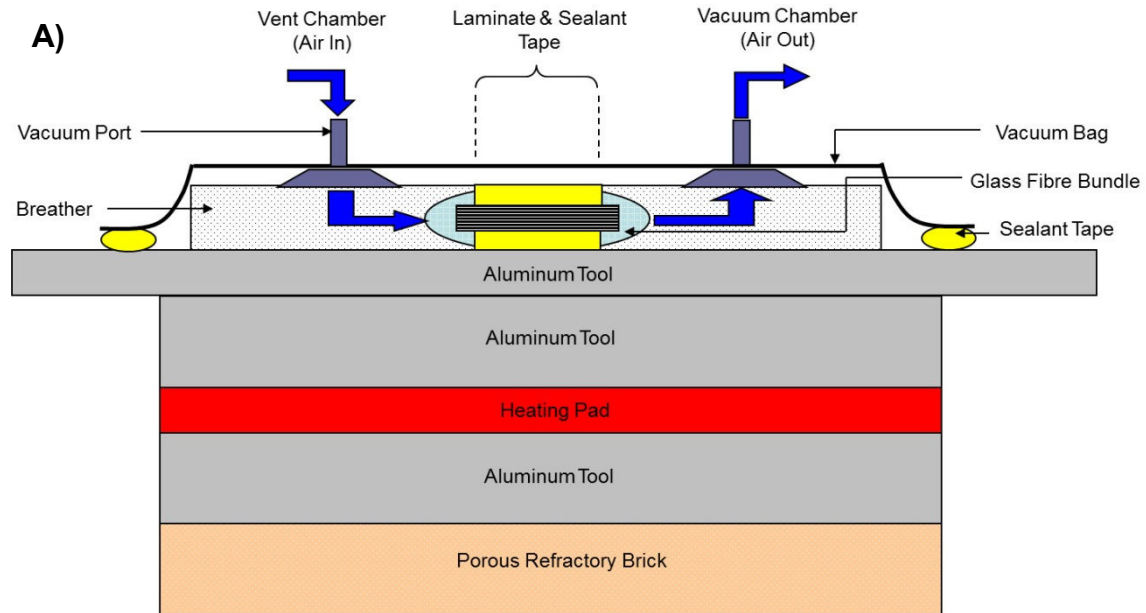


Figure 3.3. Heated in-plane permeability setup. A) Lay-up order of consumables, and direction of in-plane gas flow; B) Setup within heating enclosure; C) Setup during heated permeability testing.

Heated in-plane permeability tests were performed immediately after obtaining ambient flow data. The heating plate was turned on and the controller was pre-programmed to follow the MRCC for the duration of heating. Flow data was continuously logged for the entire duration of the cure cycle. Once testing was

completed, the heating plate was turned off and the enclosure opened to allow the setup to cool. Heated flow data was then exported for data reduction. A modified version of the heated in-plane permeability test was performed in addition to the standard setup. The modified setup involved placing the vent chamber under vacuum part way throughout the cure process (removing access to atmospheric air). This was carried out to observe differences in the resulting microstructure, and will be discussed in further detail in Ch. 3.2.4.

3.1.2 Long Debulk Setup

The setup for long debulk permeability testing was nearly identical to ambient in-plane testing (Figure 3.1). In ambient in-plane permeability experiments, the vent chamber was connected to a rotameter which had access to atmospheric air during the duration of testing (five to ten minutes). However, long debulk permeability experiments were twenty four hours in duration. Additionally, the vent chamber was disconnected from the rotameter and put under vacuum so that the permeability specimen could be compacted for extended periods. Flow measurements were taken at hourly intervals by re-connecting the vent chamber to the rotameter and allowing air flow (and the 1 atm pressure gradient) to return. The flow rates were allowed to reach steady-state before flow data was collected for five to ten minutes. After each measurement interval, the vent chamber was disconnected from the rotameter and vacuum was reapplied.

3.1.3 Through-Thickness

Experimental setups for through-thickness permeability testing followed the same principal described for in-plane permeability testing. Figure 3.4A illustrates the setup used in through-thickness permeability testing. Sealant tape was used to create two separate chambers, with the through-thickness permeability specimen serving as a gas pathway between the two isolated areas. The sealed area located below the specimen was designated the “vent chamber”, and was hooked up to a mass flow sensor and a rotameter. The sealed area located above the specimen was designated the “vacuum chamber” and was connected to a second mass flow sensor and a vacuum pump. A leak test chamber was not created for through-thickness permeability testing due to size limitations imposed by the tool. Thermocouples were attached to the specimen to measure temperature changes during heated tests.

Figure 3.4B illustrates the tool and bagging materials used their lay-up order. Sealant tape was used to seal the edges of the permeability specimen and facilitate 1D gas transport in the through-thickness direction. The specimen was placed on a porous ceramic tile that was pre-cut to the same dimensions as the laminate. Once again, fibre glass and breather layers were placed over the exposed specimen surface to form pathways for gas removal.

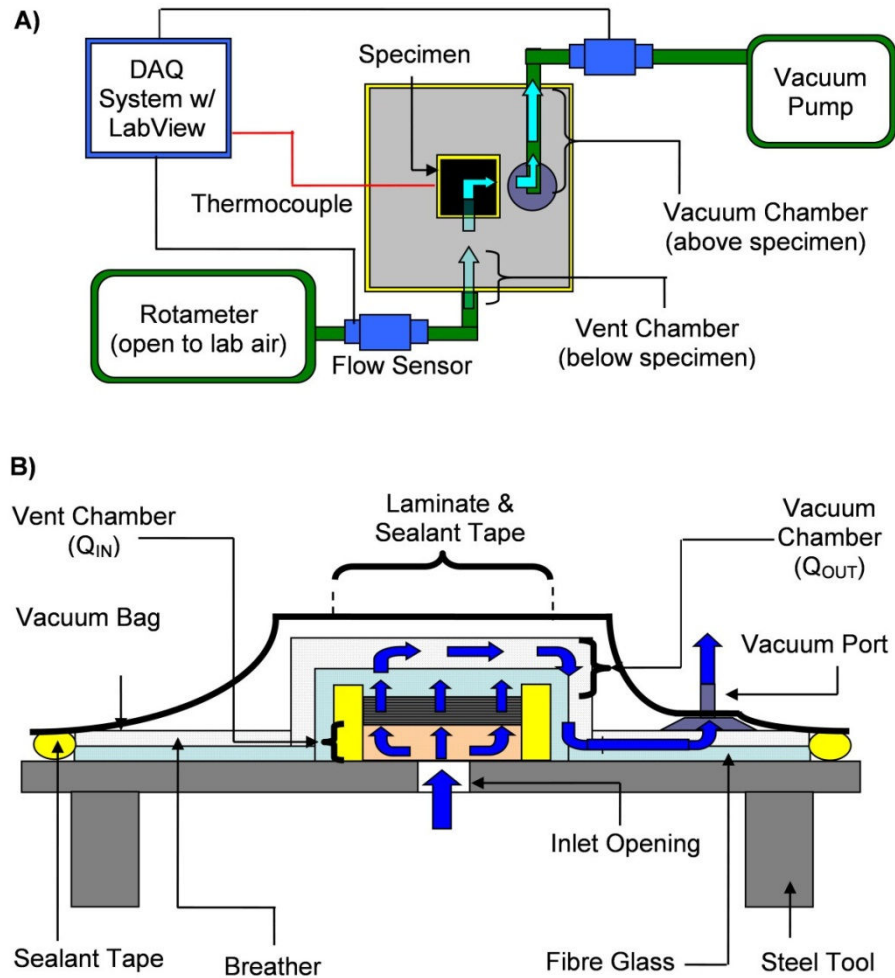


Figure 3.4. Through-thickness permeability test setup. A) Chamber configuration and test equipment layout; B) Lay-up order of consumables, and direction of through-thickness gas flow.

In through-thickness permeability testing, the effective length in the direction of 1D gas flow was equivalent to the cured ply thickness of the permeability specimen (8 plies, or 1.60mm) as shown in Figure 3.5. Figure 3.5 also illustrates the purpose of the ceramic tile. Since the inlet opening machined into the bottom of the tool had a much smaller cross-section than the exposed surface of the

During ambient through-thickness permeability testing, the vacuum pump was turned on to allow air to be continuously pulled through the specimen. Once steady-state flow had been reached, flow rate data was logged for five to ten minutes and then saved and exported for further analysis.

Heated through-thickness permeability testing was identical to the ambient through-thickness test except the entire setup was placed inside an oven. The oven was controlled by an OMEGA® Series CN9000 TPC which enabled temperature ramp and soak cycles. Heated through-thickness permeability tests were performed immediately after obtaining ambient flow data. The oven was turned on and the controller was pre-programmed to follow the MRCC for the duration of heating. Flow data was continuously logged for the entire duration of the heated permeability test. When testing had completed the oven was turned off and the oven door opened to allow for the setup to cool. The heated flow data was then exported for analysis.

3.1.4 Microscopy

Microscopy specimens were prepared according to guidelines found in ASTM E2015-04 “Standard guide for preparation of plastic and polymeric specimens for micro-structural examinations” (ASTM International, 2009) and sample preparation procedures developed by Farhang (Farhang & Fernlund, 2011a) for uncured prepreg specimens. The goal of performing microscopy was to observe the evolution of voids throughout processing, from an as-laid up single sheet of

prepreg to a cured laminate stack. This was achieved by mounting microscopy specimens in a special coloured, low-viscosity mounting resin (Buehler Co., Epo-color). The coloured mounting resin served two purposes: a) it provided a qualitative indication of void content by filling void spaces and causing them to appear as a separate colour from the fibre and matrix phases under the microscope, and b) it helped “lock” specimen microstructures in place once it was cured and minimized damage to the viewing surface during grinding and polishing.

A total of five specimens were prepared for image analysis on their in-plane cross-sections: 1 Ply Uncured (As Laid-Up), 4 Ply Uncured (As Laid-Up), 4 ply Uncured (Debulk), 4 Ply Cured (Vent Open), and 4 Ply Cured (Vent Closed). The first three (uncured) specimens were freshly prepared whereas the final two (cured) specimens were sectioned from previous permeability specimens. The 4 Ply Cured (Vent Open) specimen was obtained from a regular heated in-plane permeability test where the vent chamber had access to atmospheric air. The 4 Ply Cured (Vent Closed) specimen was obtained from the modified heated in-plane permeability test where the vent chamber was put under vacuum (as described at the end of Ch. 3.1.2). The 4 Ply Cured (Vent Closed) specimen was prepared because it represented typical industry processing conditions. All microscopy specimens were sectioned to identical dimensions of 4” long by ½” wide. Uncured specimens were sectioned using a fresh, clean cutting knife. Sectioning of uncured specimens was especially difficult due the softness of the

material and the potential of causing deformation and fibre pull-out to the specimen microstructure and viewing surface. Therefore, care was taken to maintain a consistent cutting action in order to minimize damage and smearing. Cured specimens were easier to process due to the rigid (cured) matrix phase, and were sectioned using a slow speed diamond-saw (Buehler Co., Isomet). Specimen thicknesses varied depending on the number of plies (1 or 4 plies), degree of cure (uncured or fully cured), and processing method (As-Laid Up, Debulked, Vent Open, or Vent Closed). Figure 3.6 illustrates the five different specimens prepared for image analysis.

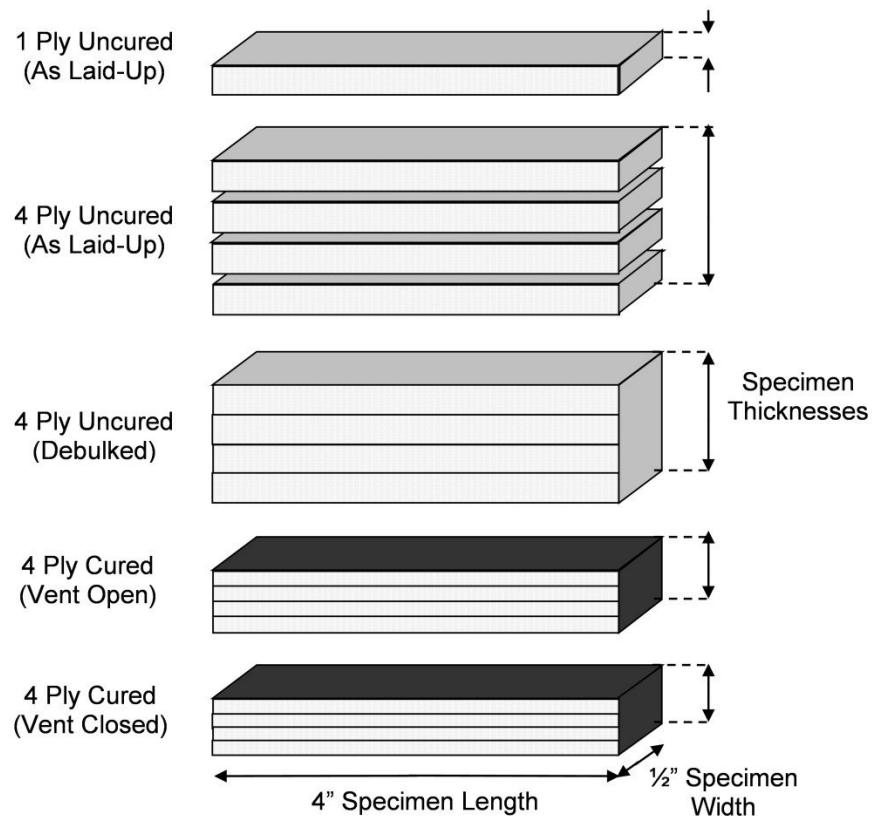


Figure 3.6. 5320/T650 microscopy specimens.

The microscopy specimens were placed within the centre of a mould for mounting as illustrated in Figure 3.7A. The inner dimensions of the mould were 6-½” long, by 1-½” wide, by $\frac{15}{16}$ ” deep. The microscopy specimens were stacked adjacent to one another, with a layer of FEP film separating each specimen. Blocks of filler material (in this case silicone rubber) material were used to fill the empty volume around the specimens. The rubber blocks provided support to keep the specimens standing upright, and also reduced the total quantity of mount resin needed to fill the mould. The specimens were slightly elevated on the bottom by several small blocks of rubber wrapped in double-sided tape as depicted in Figure 3.7B. The double-sided tape fixed the specimens in place and prevented them from floating when the mount resin was poured. The specimens were elevated to allow the mounting resin to infiltrate them from both top and bottom surfaces.

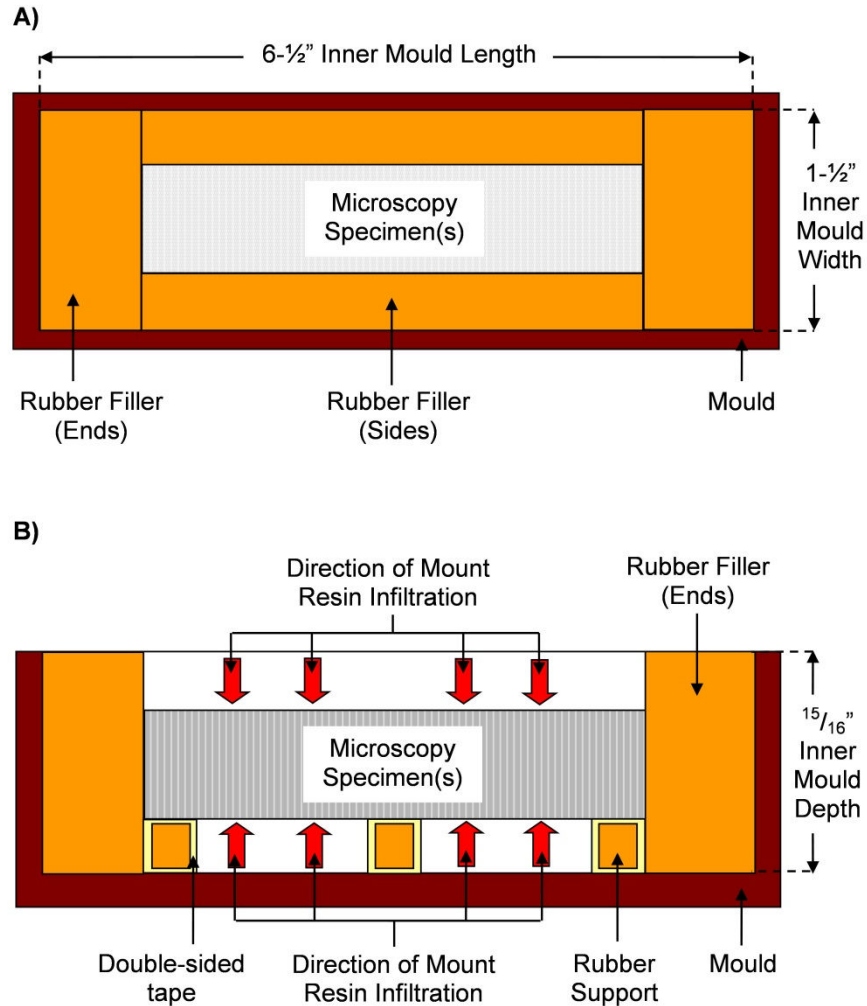


Figure 3.7. Microscopy mount preparation. A) Top view; B) Side view.

Microscopy specimens were elevated to allow mount resin infiltration from both top and bottom directions

The mounting resin was first mixed and degassed, and then slowly poured into the mould from one fixed end to allow the resin to infiltrate and fill up void spaces while minimizing air entrapment. The resin was then left to cure at room temperature for at least 24 hours. The cured mount was removed from the mould and subjected to polishing and grinding. The grades of grinding paper

used included: 120 grit, 320 grit, 600 grit, and 1200 grit (LECO Corp.). Specimen surfaces were checked to ensure that all scratch marks were removed from the previous grade of grinding paper before moving onto the finer grade. Polishing was performed using a 6-micron and a 1-micron polishing cloth with the associated diamond polishing suspension (LECO Corp.). Specimen surfaces were observed under a microscope to determine whether all the scratches had been removed prior to moving onto the finer polishing cloth.

Image analysis was carried out using an optical microscope equipped (Nikon, Eclipse LV 100) with bright field and dark field imaging lenses. A mosaic image of all five specimen surfaces was generated using a separate optical microscope (Nikon, Epiphot 300) equipped with a motorized stage and the Clemex software (version PE 6.0). The images were then qualitatively analyzed to observe changes in fibre architecture and void evolution between uncured and cured specimens. Voids were characterized as interlaminar voids (between plies) or fibre tow voids (within the fibre bundles).

3.2 RESULTS

3.2.1 In-Plane Results

The results for ambient in-plane permeability are shown in Figure 3.8. Calculated in-plane permeabilities under ambient temperature conditions were on the order of $1\text{E-}14\text{ m}^2$. This is similar to ambient in-plane permeability values reported for other prepreg systems (both autoclave and OOA) (Arafath et al., 2009; Louis et al., 2010).

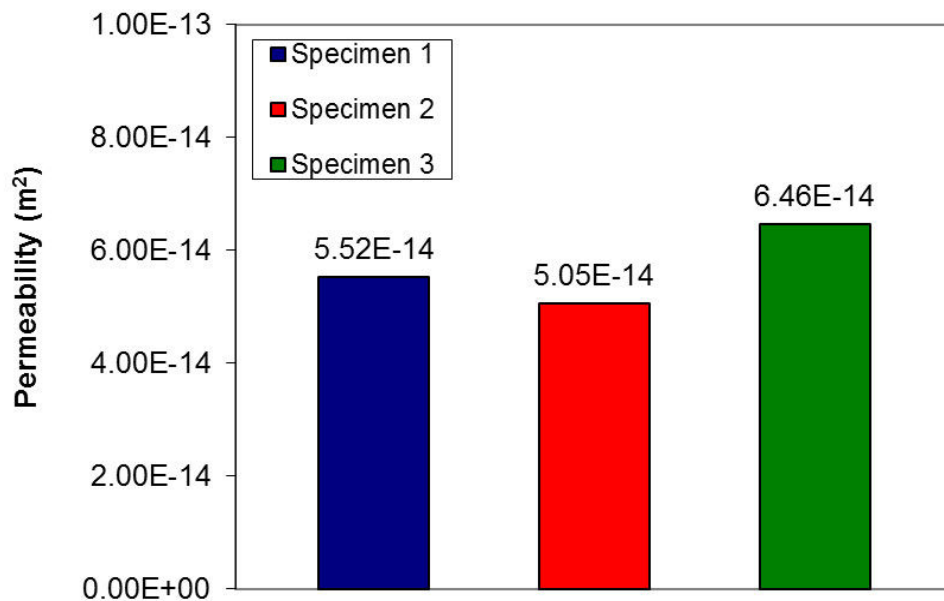


Figure 3.8. Ambient in-plane gas permeability. 5320/T650 four ply specimens with three repeats.

Heated in-plane permeability results are shown in Figure 3.9 and Figure 3.10. Permeability was initially constant, but began to noticeably decrease when the

specimen was heated to 50°C. Permeability then continued to steadily decrease with increasing temperature until approximately 80-90°C, where measured readings suddenly “opened-up”. As the 120°C hold temperature was reached, permeability values increased dramatically to the order of 1E-13 m² (ten times the starting ambient value). One of the specimens did not exhibit the “opening-up” effect, and it was theorized that this may have been due to defects in the material (excess resin etc.) or errors in the handling and lay-up process (sealant tape or vacuum bag “pinching”) which inhibited the material from breathing even as resin viscosity fell.

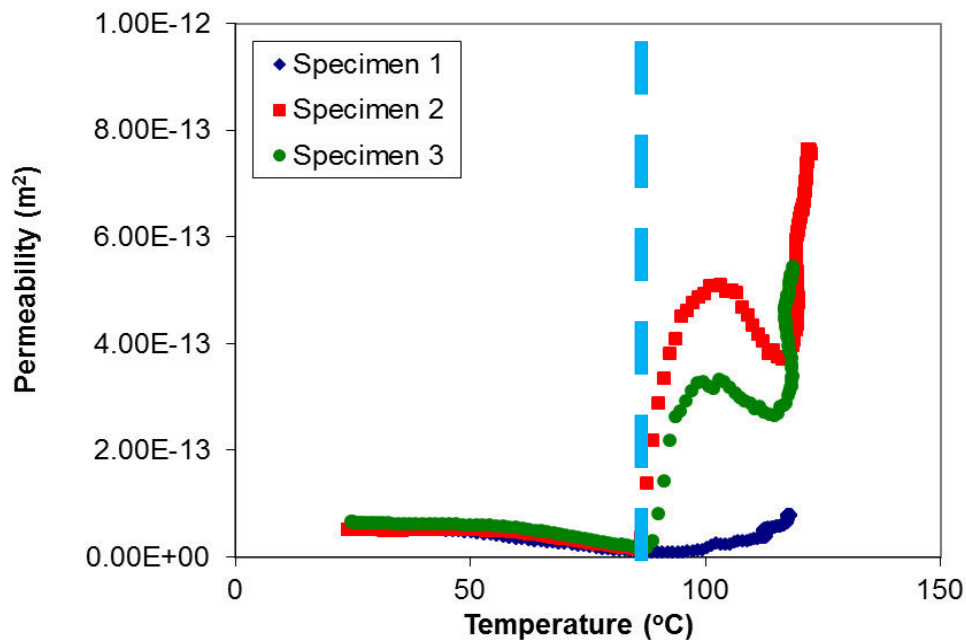


Figure 3.9. Heated in-plane gas permeability. 5320/T650 four ply specimens with three repeats. Critical “opening-up” temperature occurred at approximately 90°C.

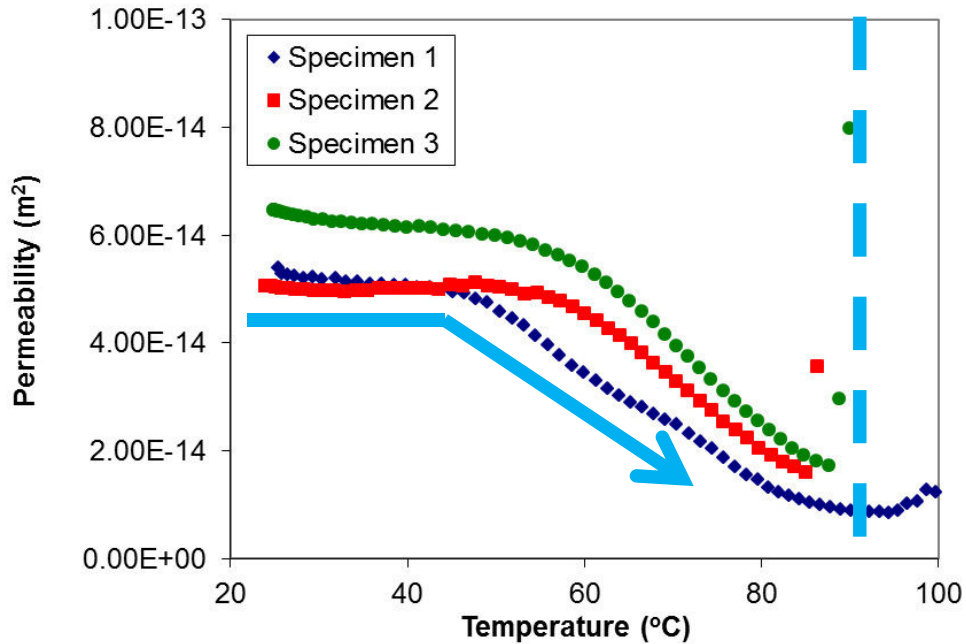


Figure 3.10. Close-up of heated in-plane gas permeability. 5320/T650 four ply specimens with three repeats. Critical “opening-up” temperature occurred at approximately 90°C.

3.2.2 Long Debulk Results

Results from the long debulk permeability experiments are presented in Figure 3.11 and Figure 3.12. It was observed that permeability was initially around 1E-13 m², but dropped sharply within the first half hour of debulking. After the first half hour, permeability decreased steadily but at a slower rate until the end of the test. Final permeability values were approximately 6E-14 m², which was half of the starting permeability. It was hypothesized that the initial rapid drop in permeability was due to the loss of large interconnected voids that existed between the plies. During debulking, these interconnected void pathways

collapse and become disconnected, leaving the dry fibre tows as the remaining means of gas extraction. Additionally, the viscoelastic nature of the semi-solid resin under long term compaction may have resulted in resin cold-flow into the dry fiber tows, leading to the slow but continual drop in permeability. However, this drop appears to have plateaued out towards the end of testing, indicating that significant levels of permeability were retained and that gas evacuation was still possible.

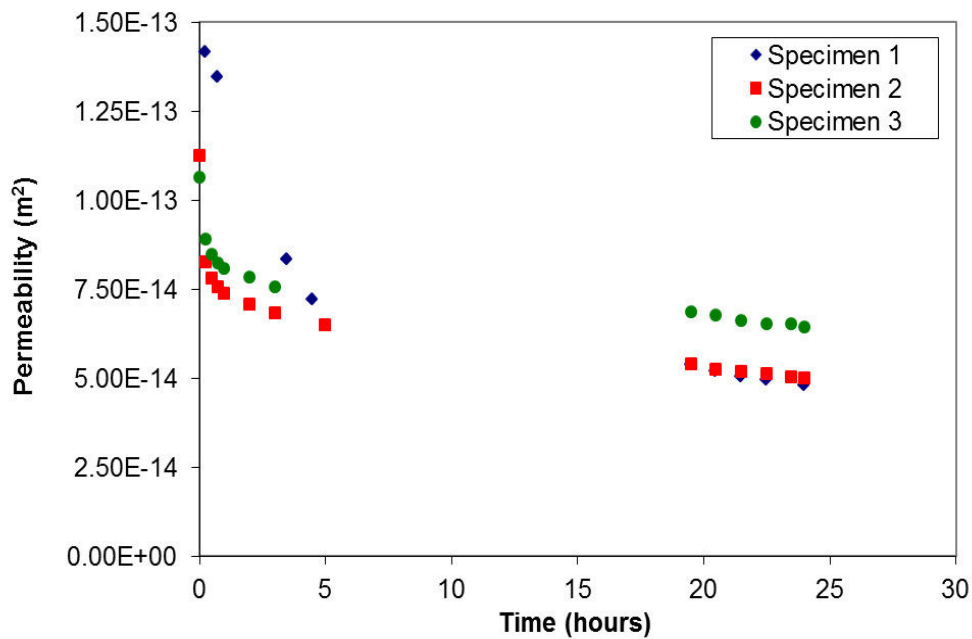


Figure 3.11. Long debulk permeability. 5320/T650 four ply specimens with three repeats. Half of total permeability loss occurred within the first half hour of testing.

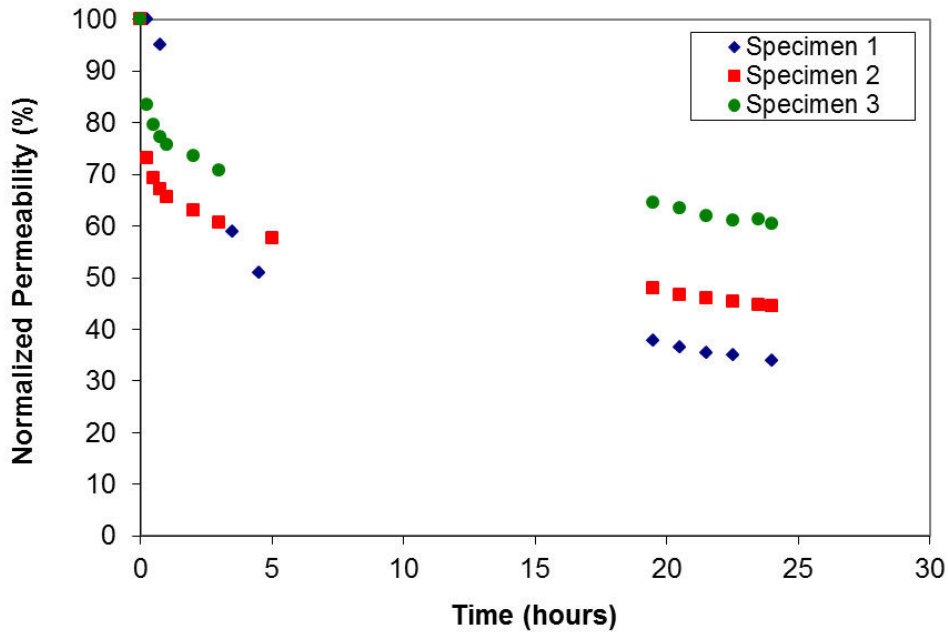


Figure 3.12. Normalized long debulk permeability. 5320/T650 four ply specimens with three repeats. Half of total permeability loss occurred within the first half hour of testing.

3.2.3 Through-Thickness Results

Results for ambient through-thickness testing are presented in Figure 3.13. Through-thickness permeabilities were found to be on the order of $1\text{E-}17\text{ m}^2$, approximately three orders of magnitude (1000x) lower than in-plane permeabilities. Measured through-thickness permeabilities for 5320/T650 were greater than the values reported for other prepreg systems (both autoclave and OOA) (Arafath et al., 2009; Louis et al., 2010). Heated through-thickness permeability results showed a three order magnitude difference compared to heated in-plane results. From Figure 3.14 and Figure 3.15, it was observed that

through-thickness permeability also decreased with rising temperature. When the specimens were heated past 40°C, the rate of permeability loss increased. Similar to what was observed for in-plane heated specimens, heated through-thickness specimen permeabilities “opened” up upon reaching a critical temperature range (approximately 75-80°C). For these tests, the measured flow rates actually grew beyond the limits of the flow sensors. Therefore, specimen through-thickness permeabilities after “opening-up” were undetermined.

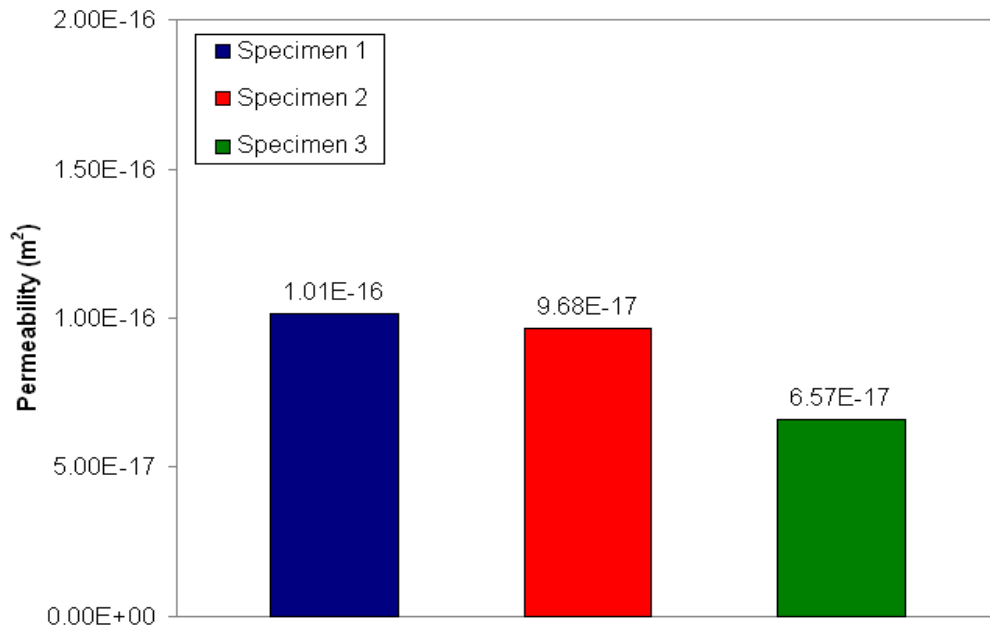


Figure 3.13. Ambient through-thickness gas permeability. 5320/T650 eight ply specimens with three repeats.

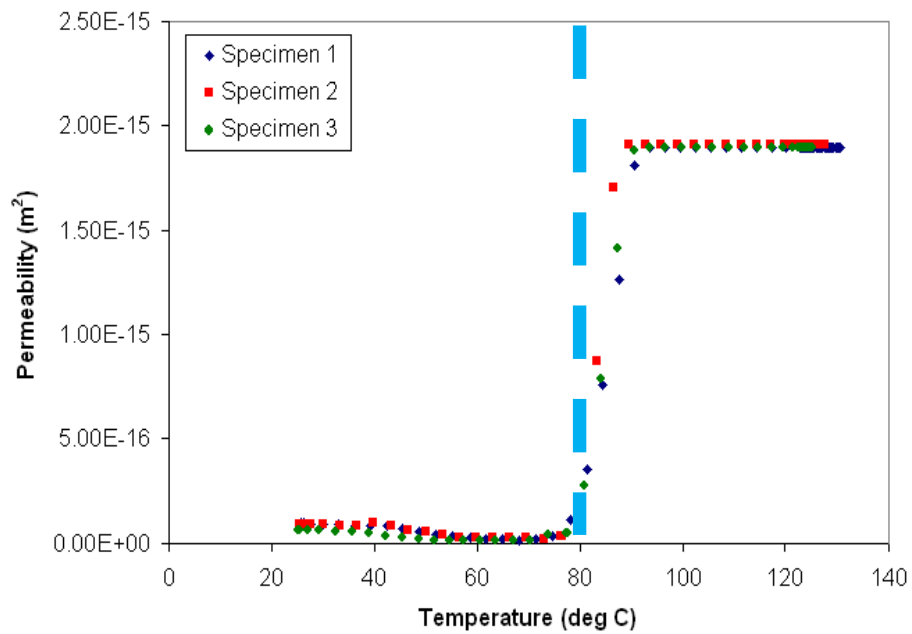


Figure 3.14. Heated through-thickness gas permeability. 5320/T650 eight ply specimens with three repeats. Critical “opening-up” temperature occurred at approximately 80°C.

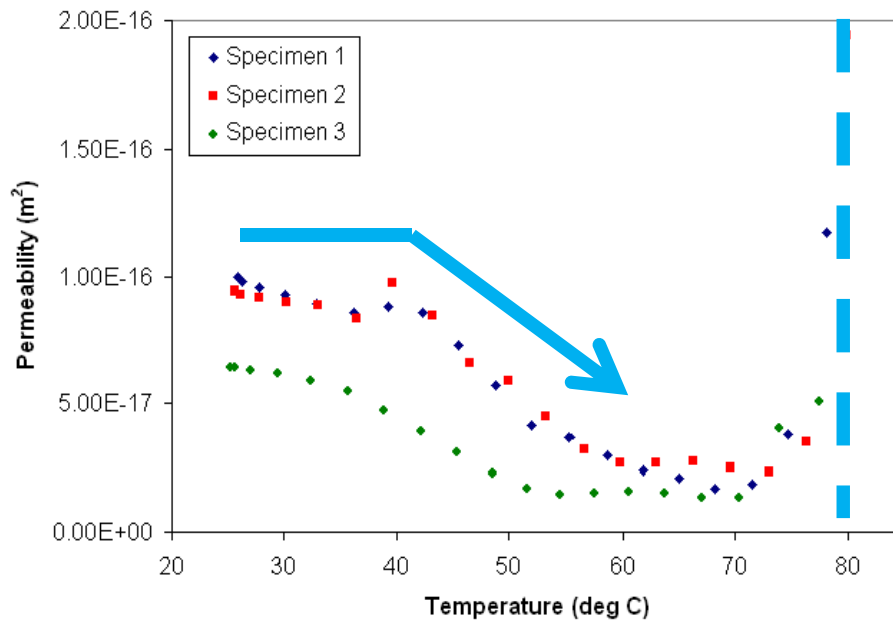


Figure 3.15. Close-up of heated through-thickness gas permeability. 5320/T650 eight ply specimens with three repeats. Critical “opening-up” temperature occurred at approximately 80°C.

3.2.4 Microscopy Results

Microscopy results illustrated the changes in prepreg microstructure and void evolution with respect to the processing history. Figure 3.16 is a micrograph showing the cross-section of the 1 Ply Uncured (As Laid-Up) specimen viewed under dark field imaging. The micrograph depicts the cross-ply (one-over, one-under) pattern of 5320/T650 fibre tows. Fibre tows in the rolling direction are perpendicular to the cut surface and appear as long black elliptical cross-sections. Fibre tows in the transverse direction appear as long fibre bundles that follow a sinusoidal curve across the cut surface.

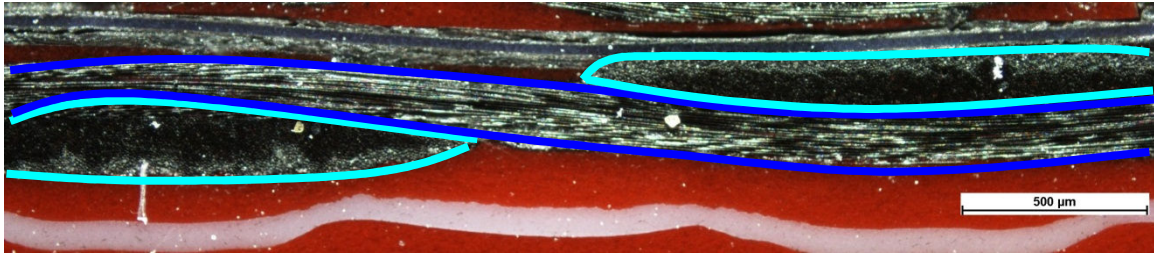


Figure 3.16. Micrograph of 1 Ply Uncured (As Laid-Up) 5320/T650 laminate specimen. Fibre tows in the in-plane rolling direction are indicated by a light blue highlight. Fibre tows in the transverse in-plane direction are indicated by a dark blue highlight.

Figure 3.17A, also taken under dark field imaging, provides a cross-sectional image of the 4 Ply Uncured (As Laid-Up) specimen. The large inter-ply areas filled with red mounting resin indicate the presence of numerous interlaminar voids within the laminate. The shapes of the interlaminar voids appear long and elliptical, and are consistent with the interlaminar voids found in uncured and undebulked laminates of other similar OOA prepreg systems (Farhang & Fernlund, 2011b). The presence of red mounting resin was also found within the rolling direction fibre tows as shown in Figure 3.17B. This observation confirms the presence of fibre tow voids. As this specimen was not subjected to heating or vacuum compaction, the high volume of interlaminar and fibre tow voids observed was expected. The white and shiny areas that appear around the fibre tows in Figure 3.17 consist of uncured prepreg resin and diamond polishing media. The uncured prepreg resin takes on the colour of surroundings materials,

and its soft and adhesive nature allows loose particles to become trapped on its surface (i.e. the reflective diamond polishing media) (Farhang & Fernlund, 2011b). This was consistently observed on all of the uncured prepreg microscopy specimens.

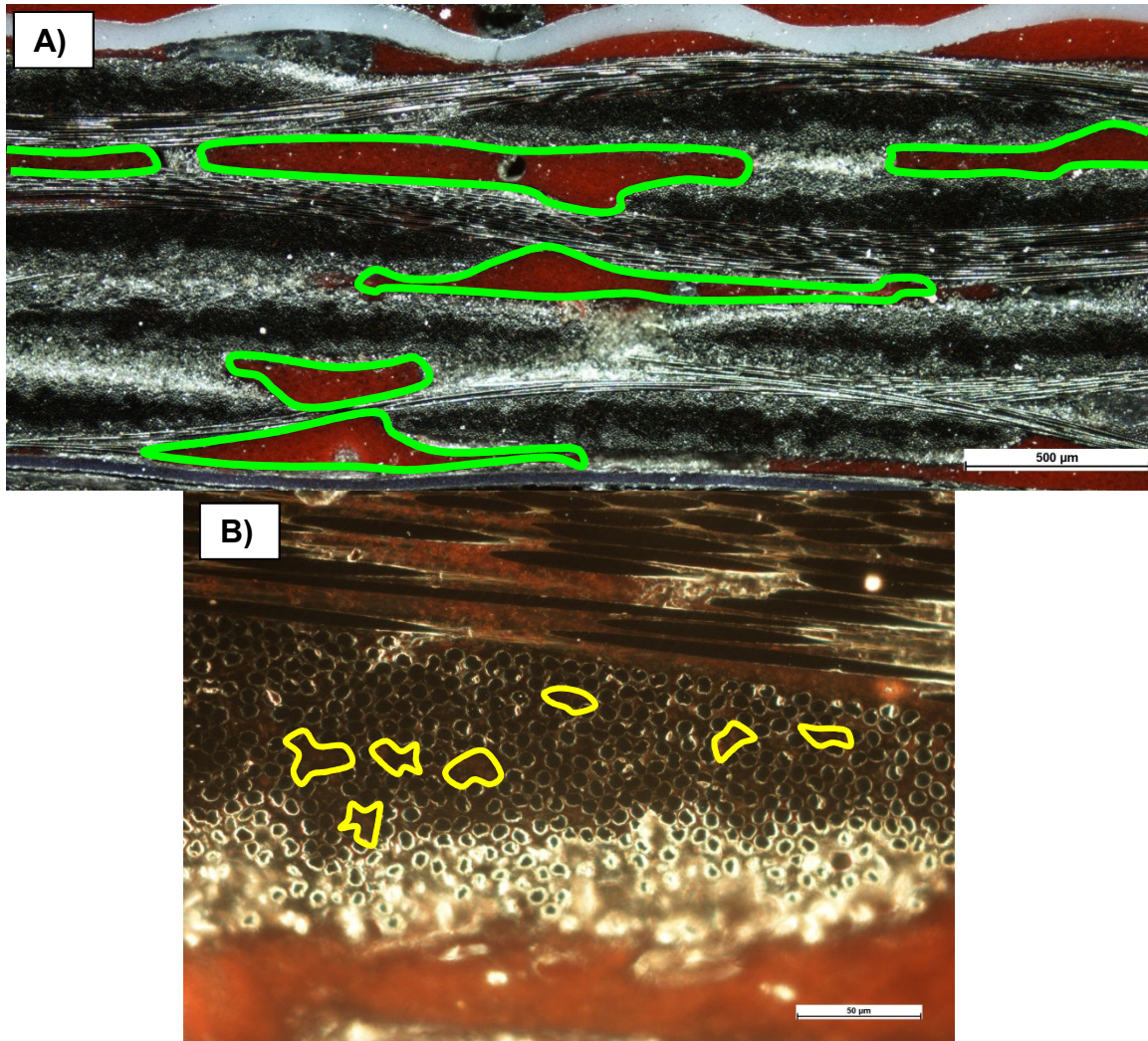


Figure 3.17. Micrograph of 4 Ply Uncured (As Laid-Up) 5320/T650 laminate specimen. A) Laminate cross-section. Interlaminar voids are indicated by a green highlight; B) Close-up image of fibre tow cross-section. Fibre tow voids are indicated by a yellow highlight

When subjected to a debulking step, the laminate became consolidated as vacuum was applied and internal air was removed. For the 4 Ply Uncured (Debulked) specimen, Figure 3.18A shows that the inter-ply regions filled with red mounting resin have disappeared due to the collapse of the interlaminar voids. The overall thickness of the laminate has also been reduced compared to the as-laid up state. However, red mounting resin is still present within the fibre tow bundles in Figure 3.18B.

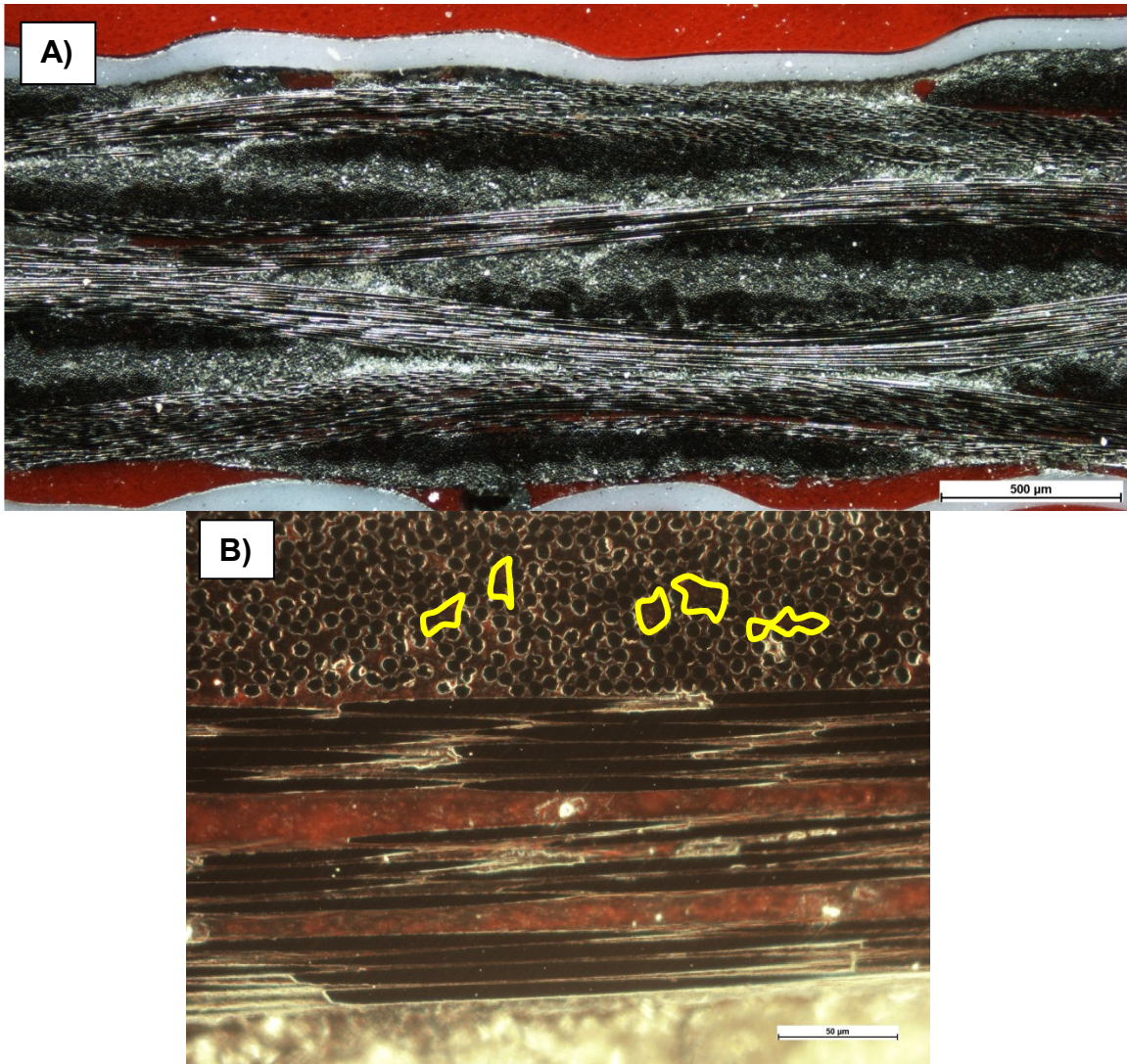


Figure 3.18. Micrograph of 4 Ply Uncured (Debulked) 5320/T650 laminate specimen. A) Laminate cross-section with no observable interlaminar voids; B) Close-up image of fibre tow cross-section. Fibre tow voids are indicated by a yellow highlight.

Once the laminate has been subjected to debulking, vacuum bagging, and curing, additional changes occur to its microstructure and void content. During heating, the resin begins to soften and flow into the open spaces within the fibre

tow bundles. This results in further consolidation, which is locked in place as the resin cures. For the 4 Ply Cured (Vent Closed) specimen, Figure 3.19A and Figure 3.19B show that the laminate thickness has decreased further and that no red mounting resin is visible in the regions between individual plies and within fibre tows. This indicates that the majority of voids within the laminate have been filled by the matrix resin. The highlighted area in Figure 3.19A shows a region that has been covered with debris. The unclear topography of the area suggests that the region's topography is not at the same height as the rest of the viewing surface. By adjusting the height of the stage and determining when the region came into focus, it was revealed that the region was actually deeper than the viewing surface. This indicates that the region was originally a void space that had become filled with debris during the grinding and polishing process.

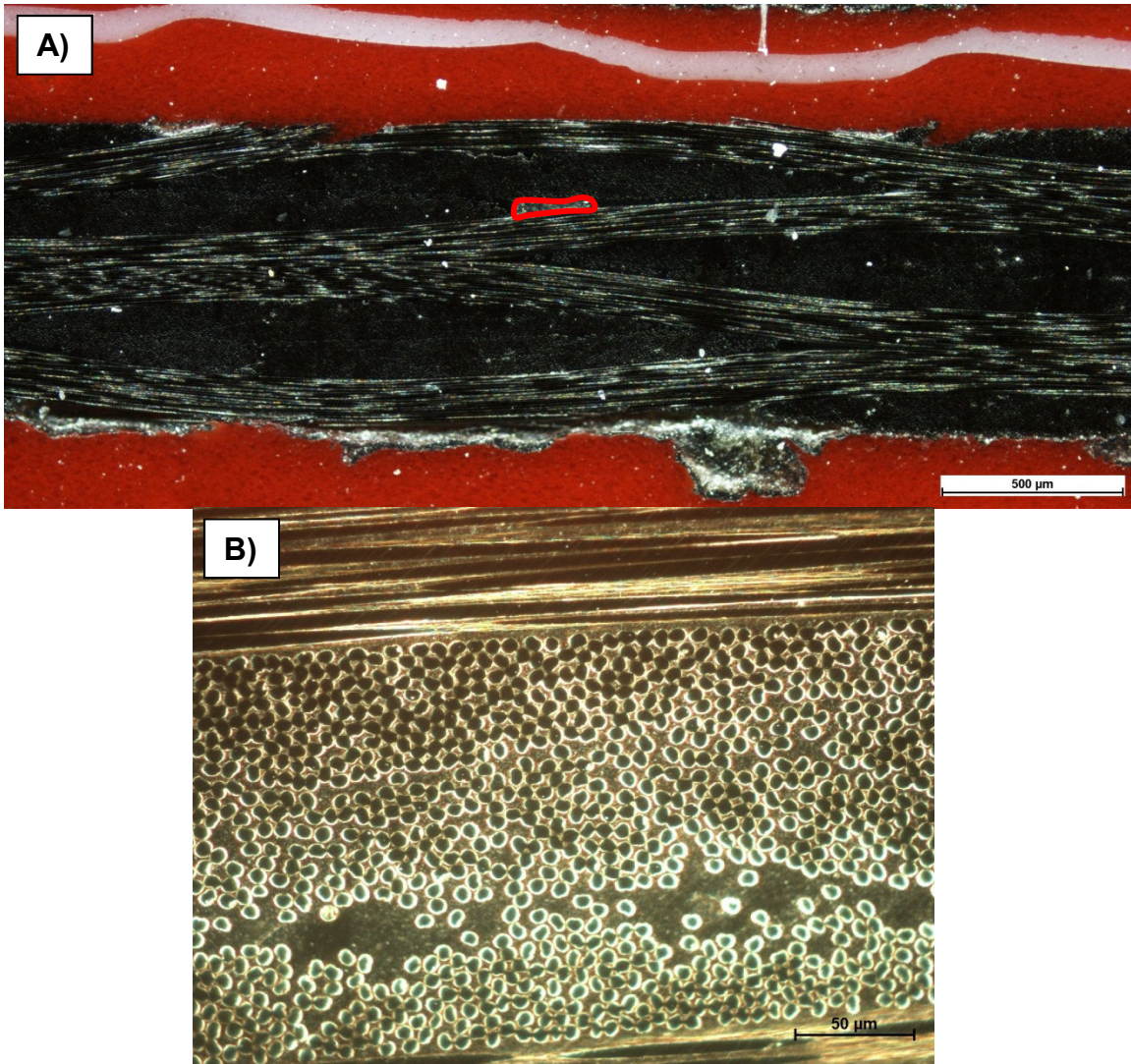


Figure 3.19. Micrograph of 4 Ply Cured (Vent Closed) 5320/T650 laminate specimen. A) Laminate cross-section with no observable interlaminar voids except for a void filled with polishing media (highlighted in red); B) Close-up image of fibre tow cross-section with no observable fibre tow voids.

Where the 4 Ply Cured (Vent Closed) specimen represented actual vacuum-bag processing conditions, the 4 Ply Cured (Vent Open) specimen obtained from the regular permeability test represented a worst-case scenario of a vacuum-bag

setup with a severe bag leak (a continuous supply of air being pulled through the laminate). Figure 3.20A shows a cross-section of the 4 Ply Cured (Vent Open) specimen. Although the specimen had undergone significant compaction, the micrograph shows that the interlaminar regions filled with red mounting resin have returned, along with the void areas filled with debris. The increase in void volume is not surprising considering that air was constantly being supplied to the specimen during the heated permeability test. Any gas pathways forced open by air channels would become locked into the microstructure during resin gelation and cure. Red mounting resin was not observed within the fibre tows as illustrated in Figure 3.20B. The results of microscopy suggest that during heated permeability testing, air pressure may have forced aside low-viscosity resin regions between plies and re-opened pathways. Once the specimen has been cured, these pathways become filled with either the red mounting resin or debris from grinding and polishing.

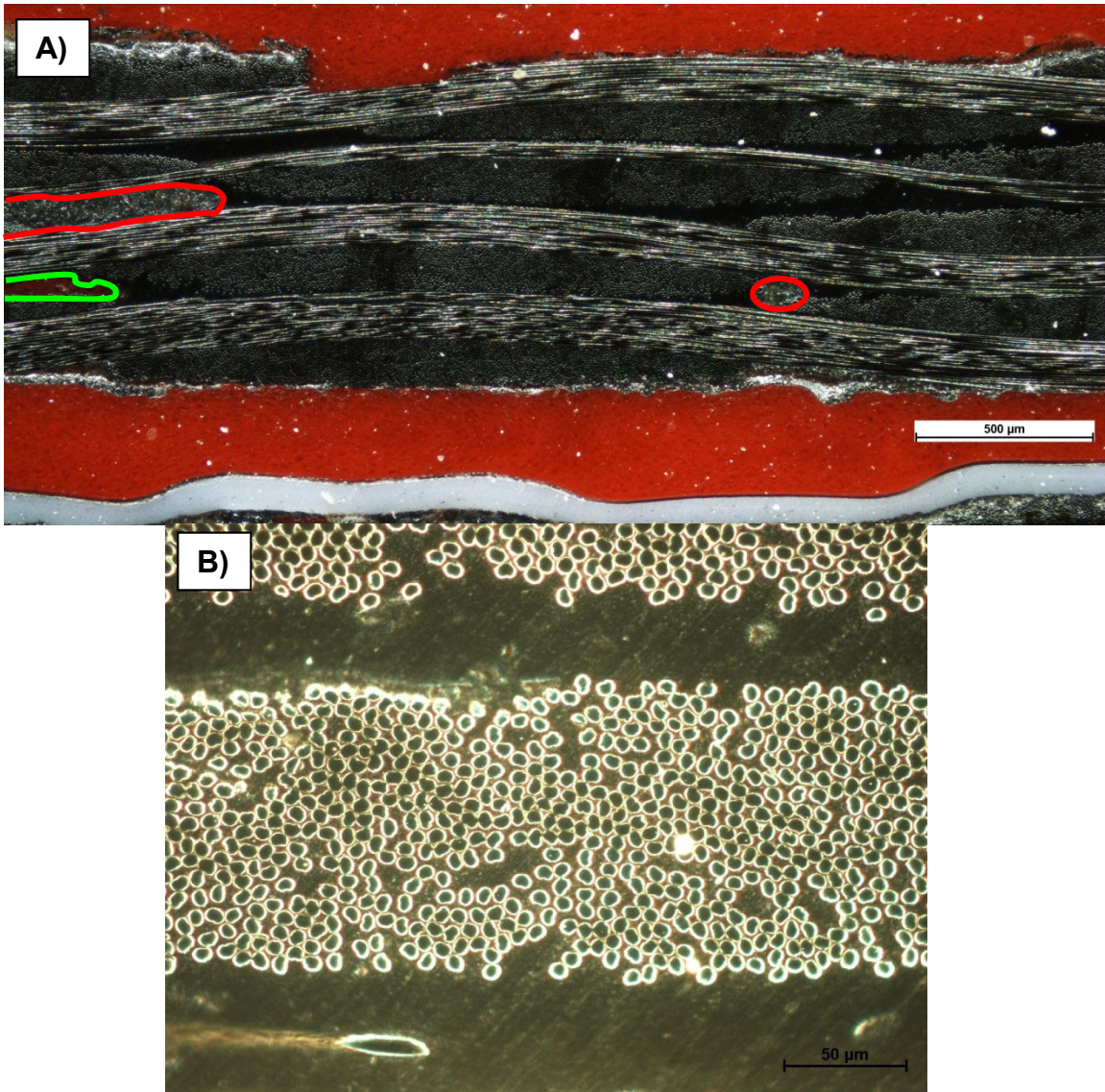


Figure 3.20. Micrograph of 4 Ply Cured (Vent Open) 5320/T650 laminate specimen. A) Laminate cross-section. Interlaminar voids filled with polishing media are indicated by a red highlight. Interlaminar voids filled with mounting resin are indicated by a green highlight; B) Close-up image of fibre tow cross-section with no observable fibre tow voids.

4 WATER VAPOURIZATION TESTING

4.1 METHODS

Water vapourization testing on 5320/T650 was conducted to quantify water vapour generation from OOA prepregs during processing. Comparative testing was also done on MTM45-1/CF2426A, a similar OOA prepreg system. The effect of process humidity on moisture content was determined. Pressure levels required for rapid vapourization of water under ambient temperature conditions were verified against Clasius-Clapeyron predictions, and vapourization rates were modeled using a numerical approach with Langmuir's evaporation equation. Additionally, the time scales involved for vapourization of water from an open surface versus within a porous medium were compared. The kinetics of water vapourization was also compared against Langmuir model predictions. Heated vacuum bagged tests were conducted to quantify water vapour and to observe the temperature ranges which it occurs. The contributions of moisture vapourization from test laminates and bagging consumables were also identified.

All water vapourization specimens were laid-up along their rolling direction for consistency and to minimize the effects of material variability. Specimens prepared for vacuum-bag processing were cured according to the MRCC. The test matrix used for water vapourization experiments on laminate specimens is presented below in Table 4.1. A similar test matrix is provided in Table 4.2 for experiments performed on the bagging consumables. The bagging consumable materials selected for testing were ones commonly found in vacuum bag

processing of aerospace parts. Details of the specimen dimensions are also provided.

Table 4.1. Moisture vapourization test matrix for 5320/T650 and MTM45-1/CF2426A

	5320/T650	MTM45-1/CF2426A	Open Beaker
Humidity Conditioning	<p>1 repetition at each condition</p> <p>Conditioning levels: 0 %RH, ambient, 75 %RH, 100 %RH</p> <p>Specimen dimensions: 2-1/2" x 2-1/2" x 4 plies</p>	<p>1 repetition at each condition</p> <p>Conditioning levels: 0 %RH, ambient, 75 %RH, 100 %RH</p> <p>Specimen dimensions: 2-1/2" x 2-1/2" x 4 plies</p>	N/A
Water Vapourization	N/A	<p>Porous medium (dry & moist composite tests):</p> <p>1 repetition at each condition</p> <p>Conditioning levels: 0%RH, 100%RH</p> <p>Specimen dimensions: 4" x 4" x 16 plies</p>	<p>Open surface (water beaker tests):</p> <p>1 repetition at each setup</p> <p>Water beaker setups: Baseline (empty) Limited (1 g water) Infinite (>100 g water)</p>
Vacuum Bagged Vapourization	<p>1 repetition at each condition</p> <p>Conditioning levels: 0%RH, ambient, 100%RH</p> <p>MRCC (1-3 C/min ramp; 2 hour cure @ 120 C)</p> <p>Specimen dimensions: 12" x 2-1/2" x 4 plies</p>	<p>1 repetition at each condition</p> <p>Conditioning levels: 0%RH, ambient, 100%RH</p> <p>MRCC (1-3 C/min ramp; 4 hour cure @ 120 C)</p> <p>Specimen dimensions: 12" x 2-1/2" x 4 plies</p>	N/A

Table 4.2. Water vapourization test matrix for bagging consumables

	Bagging Consumables
Humidity Conditioning	<p>Consumables: vacuum bag, breather, FEP release film, peel ply, sealant tape</p> <p>1 – repetition at each condition for each type of consumable</p> <p>Conditioning Levels: 0%RH, ambient, 75%RH</p> <p>Specimen dimensions: 2-½" x 2-½" x 1 ply – vacuum bag, breather, FEP release film 2-½" x ½" x 1 ply – peel ply, sealant tape</p>
Vacuum Bagged Vapourization	<p>2 – repetitions</p> <p>Conditioning Levels: ambient</p> <p>Specimen dimensions: *not measured, although all tests used roughly the same amount of each type of consumable</p>

4.1.1 Humidity Conditioning Test

In order to observe the effects of process humidity on water vapour generation in laminate and bagging consumable specimens, a conditioning procedure developed by James Kay of the UBC Composites Group for achieving controlled humidity environments was used (Hsiao et al., 2011). An initial trial was performed to determine the length of time needed for the moisture content of the specimens (laminates and consumables) to equilibrate with their surroundings. The trial also provided for a way to calculate the diffusion coefficient of 5320/T650 and MTM45-1/CF2426A at ambient conditions. Details of the procedures for the initial trial are provided in the Appendix E. The results of the trial indicated that five days was sufficient conditioning time for the laminate and

bagging consumable specimens to reach equilibrium in a humid environment (75 %RH for laminates, 100 %RH for bagging consumables) from an initially dry state (0 %RH). Therefore, all subsequent conditioning followed a five day regime.

For humidity conditioning experiments, a total of four polypropylene containers were used to create four environments with different relative humidity levels. As shown in Figure 4.1, each container contained a different medium to achieve distinct humidity levels of ~0 %RH, ~75 %RH, and ~100 %RH. The fourth container was left open to atmosphere to obtain the relative humidity of the lab air. Lab air relative humidity varied day-to-day, although it was observed to be typically around 15-25 %RH during winter and 40-50 %RH during summer.

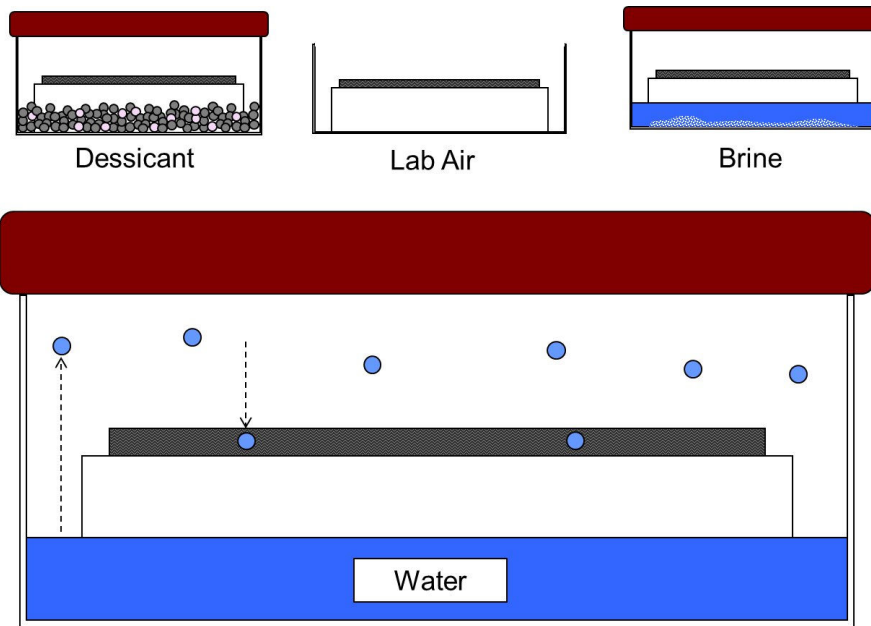


Figure 4.1. Humidity conditioning test setup. Four different mediums are used to achieve four separate relative humidity levels. Lab air humidity varies from 20 %RH in the winter to 50 %RH in the summer. Brine consists of a saturated solution of salt water in equilibrium with solid salt.

4.1.2 Water Vapourization Test

Previous studies have suggested that moisture absorption in the resin phase can adversely affect void content and final part quality of cured composite structures (Grunenfelder & Nutt, 2010; Hsiao et al., 2011; Kardos et al., 1980; Kay et al., 2011; Olivier, Cottu, & Ferret, 1995). Moisture is of particular concern in OOA processing, where atmospheric compaction pressure may be inadequate at keeping water bubbles in solution (Grunenfelder & Nutt, 2010). This can lead to severe porosity and delamination problems as large quantities of water vapour are generated during the cure cycle. However, limited work has been done in

quantifying laminate vapourization of absorbed moisture and identifying when it occurs during the cure cycle. Furthermore, there currently exists no standard approach for conducting water vapourization measurements during processing. In this study, a new approach for measuring water vapourization from laminate specimens during processing was proposed using mass flow sensor equipment. Data measured by the mass flow sensors were reported as standard volumetric flow (273.15 K; 1 atm). Although the sensors were designed and calibrated for measuring air, it was not known how well they would handle water vapour. A simple vapourization test was therefore devised to verify the accuracy of the flow sensors. Additionally, a quick calibration was made to the measured flow data to account for the differences in density and heat capacity between air and water vapour (OMEGA, 2000). The flow calibration calculation is provided in Appendix F. Setup for the vapourization test is illustrated in Figure 4.2.

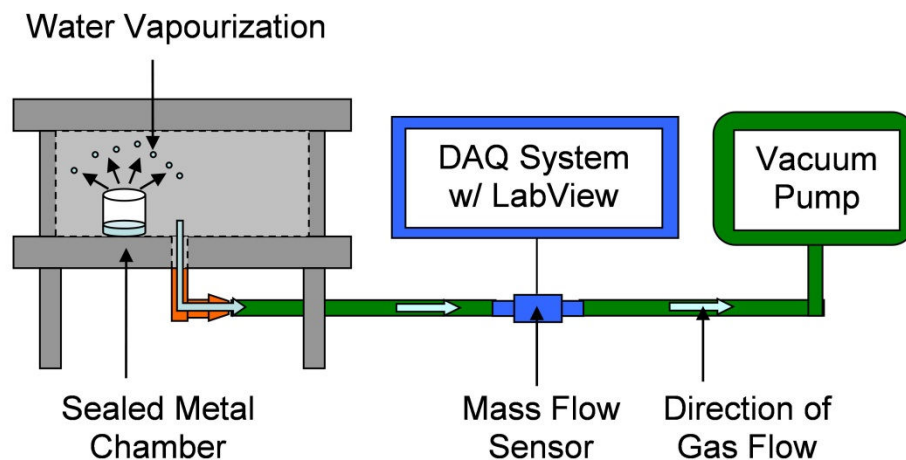


Figure 4.2. Water vapourization test setup and equipment layout.

The setup involved an air-tight metal chamber, a computer with data acquisition capabilities, and a vacuum pump all connected in series. A source of water (i.e. beaker containing water, moist laminate) was placed within the sealed metal chamber, and vacuum was pulled on the chamber. As gas was removed, the flow sensors continuously measured the flow rates. When pressures within the chamber fell low enough to allow boiling at room temperature, the rapid vapourization of water was detected by the flow sensors as an increase in the measured flow rate. This provided a convenient approximation of when boiling occurred. Flow rate data from these tests were integrated over time to calculate total mass of water vapour generated, and the results were verified against measured weight losses in the beaker or moist laminate specimens. The calculated pressure at the onset of vapourization was compared against vapour pressure predictions for water based on the Clausius-Clapeyron relation. Additionally, the Langmuir evaporation equation was applied to a numerical model to predict the time needed for complete water vapourization from the beaker.

Water vapourization tests were performed using two different arrangements: one where applied vacuum had direct access to the water source (open beaker tests), and the other where applied vacuum must penetrate a porous medium to reach the water source (moist laminate tests). A total of three tests using the beakers were carried out. These tests consisted of an empty 250 mL beaker (“baseline”), a 50 mL beaker containing one gram of water (“limited”), and a 250

mL beaker containing over 100 g of water (“infinite”). The 50 mL beaker had a circular cross-section of 11.4 cm², whereas the 250 mL beaker had a circular cross-section of 31.7 cm². A 0 %RH (“dry”) and 100 %RH (“moist”) conditioned specimen was also prepared for water vapourization testing. The time scales involved in vapourizing water from an open beaker, versus a dry or moist laminate, provided insight into how quickly and effectively absorbed moisture could be removed during processing.

4.1.3 Vacuum Bagged Water Vapourization Test

Water Vapourization experiments involving vacuum bagged laminates were carried out to measure vapourization of absorbed moisture under industry processing conditions. Laminate specimens were prepared using the conditioning regime described in Ch. 4.1.2, and then vacuum bagged and cured according to the MRCC. Figure 4.3A illustrates the lay-up of the bagged laminate experiments. Specimens were laid up on an aluminum tool, with a layer of FEP release film placed between the test laminate and the tool surface. Strips of peel ply, prepared so that they extend beyond the edges of the release film, were distributed across the specimen surface to act as pathways (incompressible channels) facilitating gas extraction. A type J thermocouple was placed next to the laminate to measure the specimen temperature during testing. A second sheet of FEP release film was placed on top of the specimen to control resin bleed. Several layers of breather were used to cover the setup and form a path to the vacuum port. The entire lay-up was finally vacuum-bagged using nylon

bag material and sealant tape as shown in Figure 4.3B, leak-tested, and then placed into a wooden heating enclosure to be cured. Details of the leak test process can be found in Appendix G.

In addition to water vapourization testing on vacuum bagged laminates, tests were also performed on ambient conditioned bagging consumables by following the setup shown in Figure 4.3A, but without the inclusion of a laminate specimen. Figure 4.3C depicts the experimental setup used in conducting the vacuum bagged water vapourization tests. The setups were connected in-line to mass flow sensors and a vacuum pump. Flow sensors were hooked up to a computer to measure and log gas flow rates and specimen temperatures during testing.

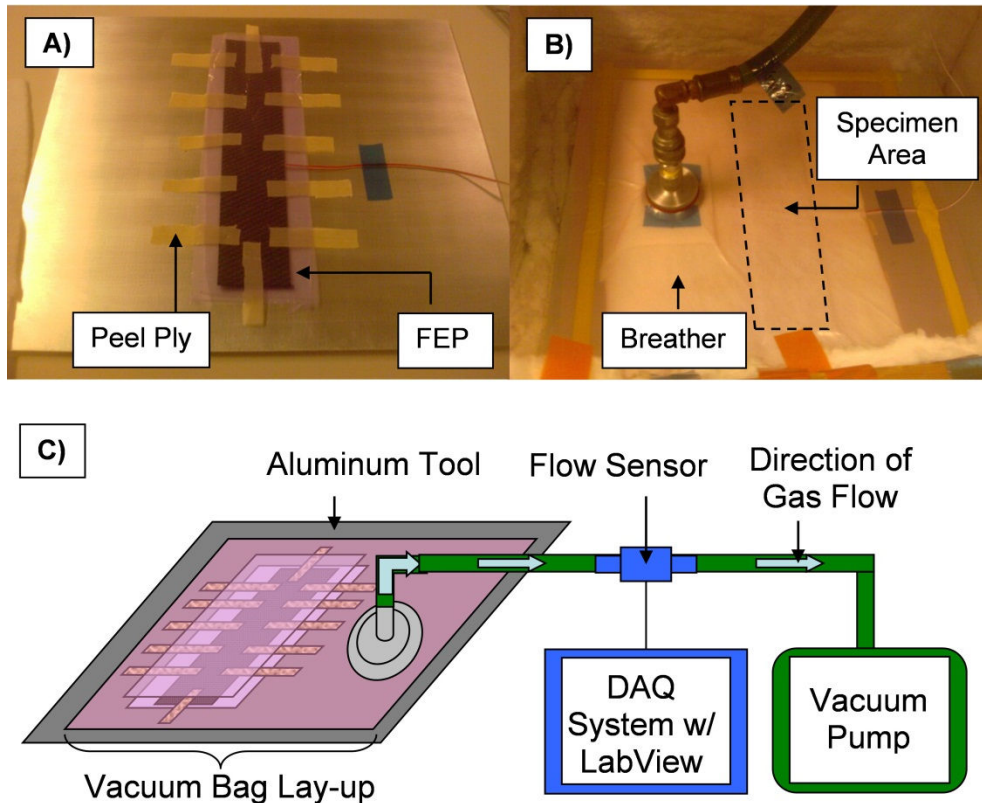


Figure 4.3. Vacuum bag water vapourization test setup. A) Specimen Lay-up; B) Vacuum bagged setup in heating enclosure; C) Vacuum bagged setup and equipment layout.

At the start of the test, vacuum was applied to remove air contained under the vacuum bag. Flow rate data from the initial air evacuation step contained significant amounts of noise and were not included in the analyses. Test flow rates were allowed to stabilize before heating and logging of flow and temperature data were initiated. Using the same principle from the water vapourization test, measured increases in the gas flow rate after initial air evacuation were taken to be indications of water vapourization. From this

experiment, the volume of water vapour generated from the test laminate and bagging consumables were quantified. Additionally, the temperatures where moisture vapourization initiates, reaches a maximum, and then subsides were identified.

4.2 RESULTS

4.2.1 Humidity Conditioning Results

The relationship between relative humidity and equilibrium moisture content for 5320/T650 and MTM45-1/CF2426A laminate specimens are illustrated in Figure 4.4 and Figure 4.5, respectively. The blue data points represent experimental moisture contents measured at nominal relative humidities, whereas the dotted curve represents predicted equilibrium moisture contents as a function of relative humidity. Predicted moisture contents were obtained using the parabolic solubility model developed by Kardos et al (Kardos et al., 1980).

Although Kardos' solubility model was developed for a different prepreg system (Narmco 5208/T300), it was found that the model worked well for approximating the equilibrium moisture contents of 5320/T650 and MTM45-1/CF2426A (Hsiao et al., 2011). Empirical values of the proportionality constant for 5320/T650 and MTM45-1/CF2426A were determined to be $7.0E-05$ and $5.6E-05$, respectively. Figure 4.4 and Figure 4.5 shows that the equilibrium moisture contents of both OOA prepreg systems follow the Kardos model closely until 100 %RH. Upon

reaching 100 %RH, large scatter in the moisture content results are observed. The scatter is suspected to originate from moisture condensation, which forms a water film on the surface of the laminate specimens and increases measured weight. Average equilibrium moisture contents for both material systems are approximately 0.6 wt.% at 100 %RH. The diffusion coefficients of uncured 5320/T650 and MTM45-1/CF2426A laminates are determined to be approximately $2.45\text{E-}08$ to $3.63\text{E-}08$ cm^2/s and $1.06\text{E-}06$ to $1.28\text{E-}06$ cm^2/s , respectively. These results are greater than typical diffusion coefficients found in cured prepregs. A hypothesis for this is that uncured resin has a greater open structure which increases available free volume (molecular-sized holes) for water molecule transport (Diamant, Marom, & Broutman, 1981; Vanlandingham et al., 1999). Diffusion coefficients for cured autoclave prepreg resins have been reported to range from $1\text{E-}10$ to $1\text{E-}08$ cm^2/s (Kaelble & Dynes, 1977; Maggana & Pissis, 1999; Vanlandingham et al., 1999).

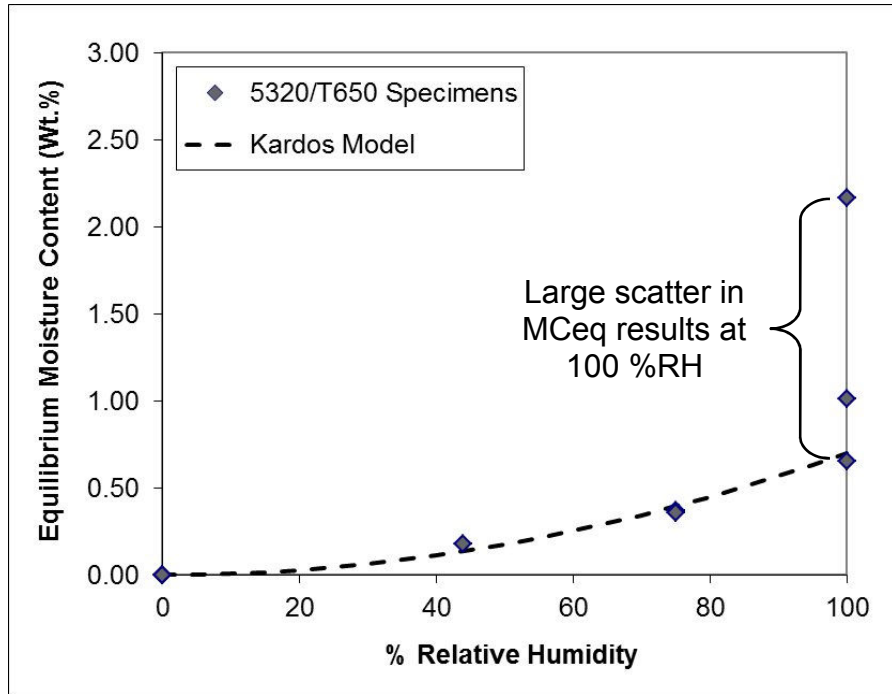


Figure 4.4. Humidity conditioning results for 5320/T650. Experimental results follow Kardos' solubility model (Kardos et al., 1980) up until 100 %RH, where large scatter in the results are observed.

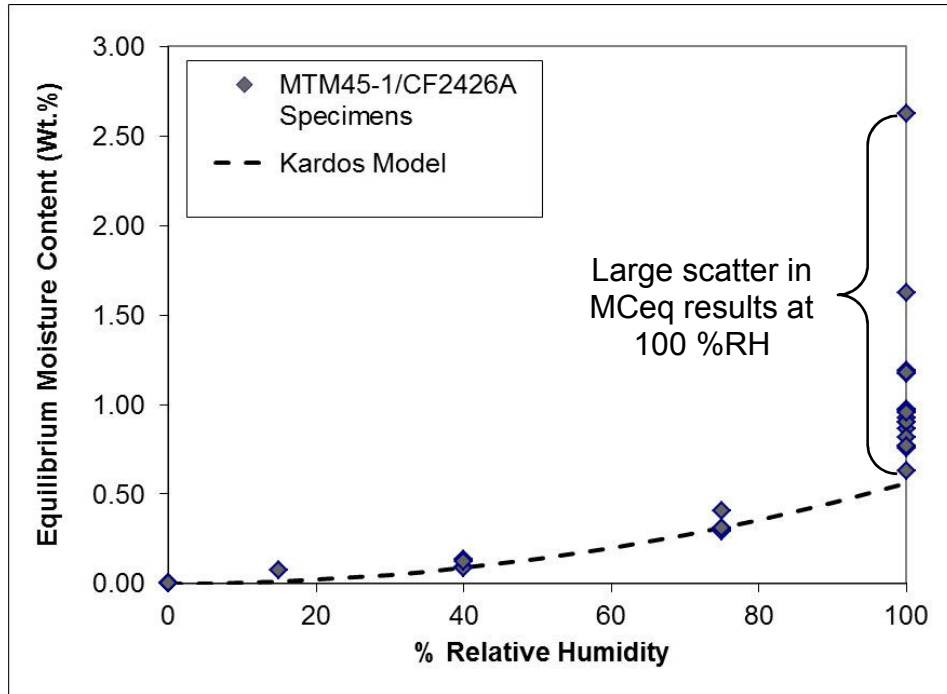


Figure 4.5. Humidity conditioning results for MTM45-1/CF2426A. Experimental results follow Kardos' solubility model (Kardos et al., 1980) up until 100 %RH, where large scatter in the results are observed.

Testing was also performed on the five types of bagging consumables. Figure 4.6 shows that the nylon vacuum bag has the highest moisture content for a given relative humidity level. Compared to laminate specimens, equilibrium moisture contents of the nylon vacuum bag is ten times greater. This indicates that significant volumes of water vapour can potentially be generated from the bagging consumables and their contribution must be accounted for when analyzing the vapourization results of the vacuum-bagged experiments. By using Kardos' model to approximate a curve for the vacuum bag data points, the value of the proportionality constant was empirically determined to be $8.0E-04$.

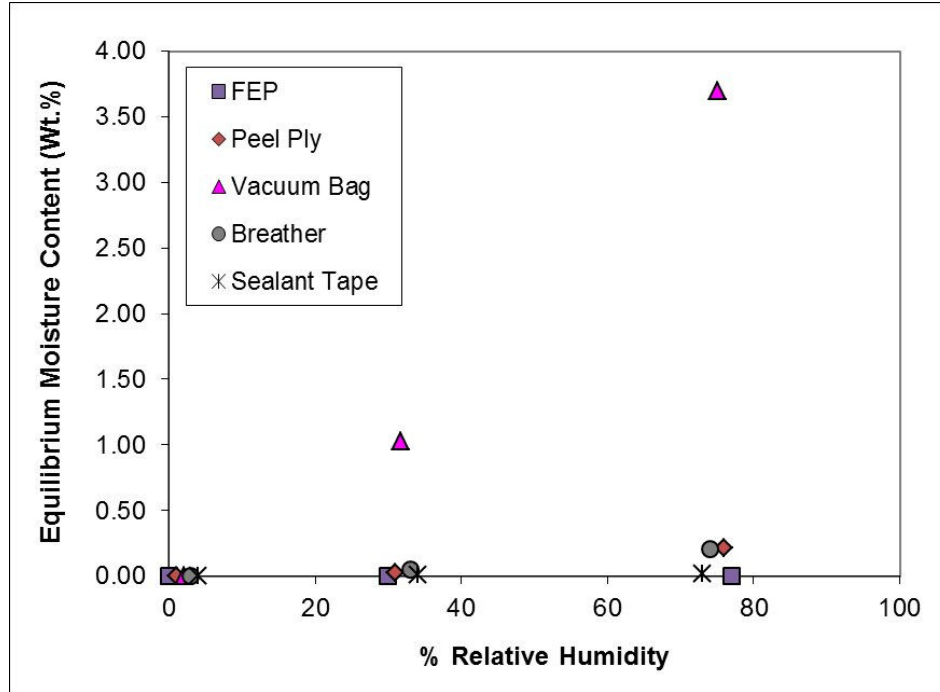


Figure 4.6. Humidity conditioning results for bagging consumables. The nylon vacuum bag consumable shows the greatest level of moisture content at a given relative humidity.

4.2.2 Water Vapourization Results

Results from the water vapourization tests are presented as plots of standard flow rate versus time. Data from the tests using open beakers are provided in Figure 4.7. The three plots represent the baseline, limited water, and infinite water tests. A plot of internal chamber pressure versus time is also included. Internal chamber pressures were calculated from total remaining air volumes in the baseline test using the Ideal Gas Law. From Figure 4.7, as internal pressure falls, the measured flow rates drop rapidly until reaching a critical pressure level

(~0.06 atm or 28 in.Hg vacuum) where they begin to diverge. This critical pressure level is taken as the vapour pressure of water. At room temperature (20°C), the Clausius-Clapeyron relation predicts that pure water will have a vapour pressure of ~0.03 atm (in other words, ~29 in.Hg vacuum is required to cause boiling), which is close to the measured/calculated vapour pressure. As testing proceeds, the baseline flow rate falls to zero whereas the limited water and infinite water flow rates begin leveling out. Flow rates from the limited water test are lower than the infinite water test. The difference in flow rate is likely affected by the available water surface area exposed to vacuum (11.4 cm² in a 50 mL beaker from the limited water test; 31.7 cm² in a 250 mL beaker from the infinite water test). In the limited water test, once the single gram of water contained in the beaker is completely vapourized and removed, the flow rate joins the baseline test curve at zero. For the infinite water test, a sufficient amount of water (>100g) is present to keep the vapourization process going throughout the duration of the experiment. Figure 4.7 also illustrates that the mass flow sensors are able to detect when flow rates increase from the onset of vapourization, as well as when they diminish due to the water source being exhausted. Measured flow rate data was used to calculate the total volume of gas extracted from each test. The total calculated volume from the baseline test is within ten percent of the actual drum volume, which verifies the accuracy of the sensors for measuring air flow. For the limited water and infinite water tests, total calculated volumes were first subtracted by flow results from the baseline test to obtain the volumes of water vapourized. Volumes of water vapourized were

converted into mass quantities and compared against weight changes in the beakers before and after testing. Calculated mass of water vapourized from the limited and infinite water tests are within ten percent of the measured beaker weight change results. Figure 4.8 provides the calculated and measured values for the volume of the drum (baseline test) and the mass of water vapourized (limited water and infinite water tests). The results from Figure 4.8 helps to verify the accuracy of the flow sensors for measuring water vapour flow.

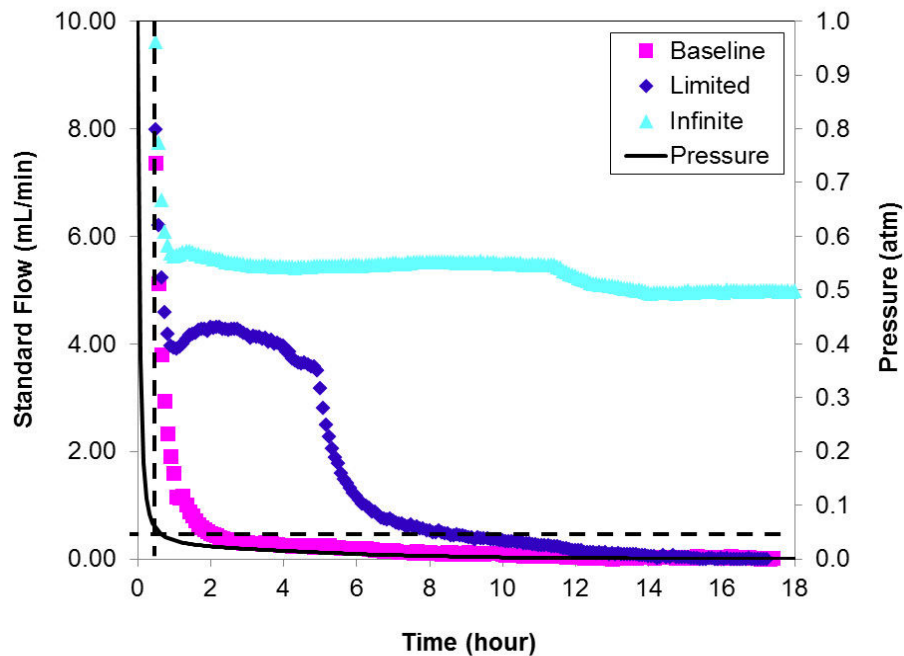


Figure 4.7. Water vapourization results from beaker tests. The baseline curve represents an empty beaker. The limited water curve represents a beaker containing a single gram of water. The infinite water curve represents a beaker containing over a hundred grams of water. The pressure curve represents falling pressure inside the metal chamber during testing.

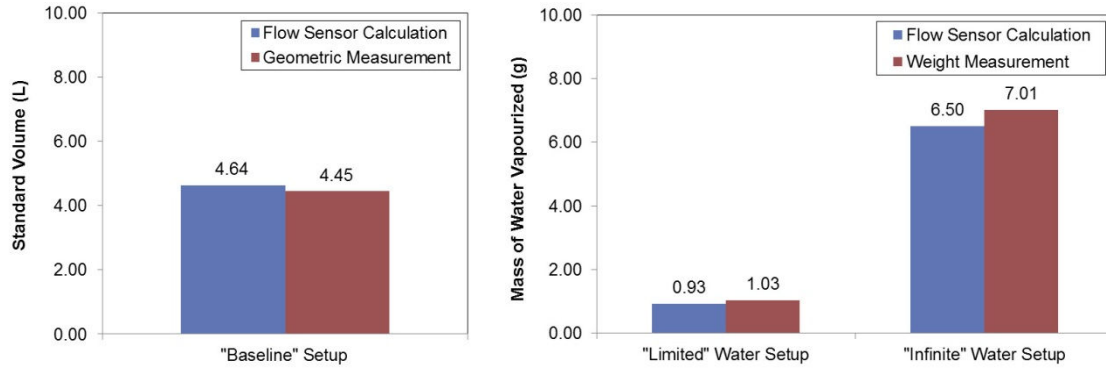


Figure 4.8. Water vapourization results from the beaker tests. The baseline (empty beaker) setup is compared against the known volume of the metal chamber to verify the accuracy of air flow measurements. The limited water (1 g) and infinite water (> 100 g) setups are compared against measured mass changes in the beakers to verify the accuracy of water vapour flow measurements.

An attempt was made to model the rates of water vapourization from the beaker. Modeling of the water vapourization flow rates was performed by incorporating Langmuir’s evaporation equation into a finite difference model. The simulation and experimental flow results for the limited water test are compared in Figure 4.9. Figure 4.9 shows that the simulation closely approximates the falling flow rates and captures the “elbow” of the experimental curve indicating that water is completely removed from the beaker.

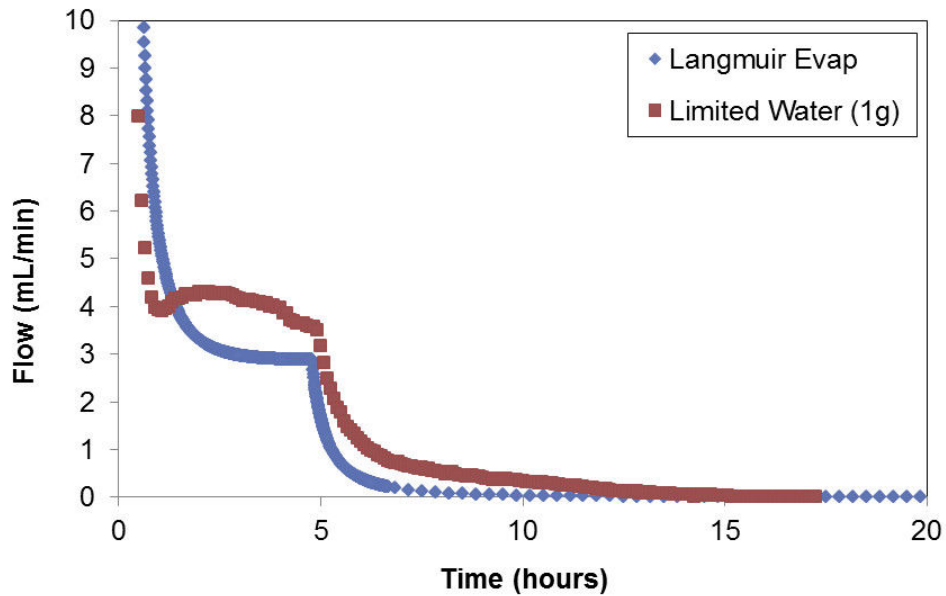


Figure 4.9. Modeling of water vapourization flow rate from the limited water test.

Modeling was conducted using a finite difference model using Langmuir's evaporation equation.

In addition to the open beaker tests, testing was performed on 0 %RH (“dry”) and 100 %RH (“moist”) conditioned MTM45-1/CF2426A laminate specimens. Water vapourization results from dry and moist composite testing are plotted in Figure 4.10. The baseline and limited water curves are included for comparison. The dry composite test curve approximately follows the baseline curve since both tests contained negligible sources of water. Calculated water vapour volume for the dry composite specimen is within ten percent of the actual drum volume. This demonstrates that asides from absorbed moisture, there are no other significant sources of gas generation in the prepreg laminates. The moist

composite specimen absorbed less water (0.52 g) compared to the limited water setup (1.11 g), resulting in a lower calculated volume. The calculated mass of water vapourized is less than the measured mass change in the moist composite, falling outside a ten percent difference. Although the mass change results did not show complete agreement, interesting information was still derived from the flow curves. From Figure 4.10, it is observed that flow rates from the moist composite test (1 to 2 mL/min) are lower than the limited water test (up to 5 mL/min), but vapourization lasts seven hours longer. It is hypothesized that vapourization from the moist composite is restricted by the timescales required for vacuum to penetrate the laminate specimen, resulting in lower flow rates and longer periods for complete vapourization. Comparisons between limited versus infinite water (open beaker tests) and limited water versus moist composite results support this hypothesis, suggesting that accessibility of the water source plays a key role in not only the rate of vapourization, but also in the duration required for complete moisture removal. Figure 4.11 provides the calculated and measured values for the volume of the drum (dry Composite) and the mass of water vapourized (moist Composite).

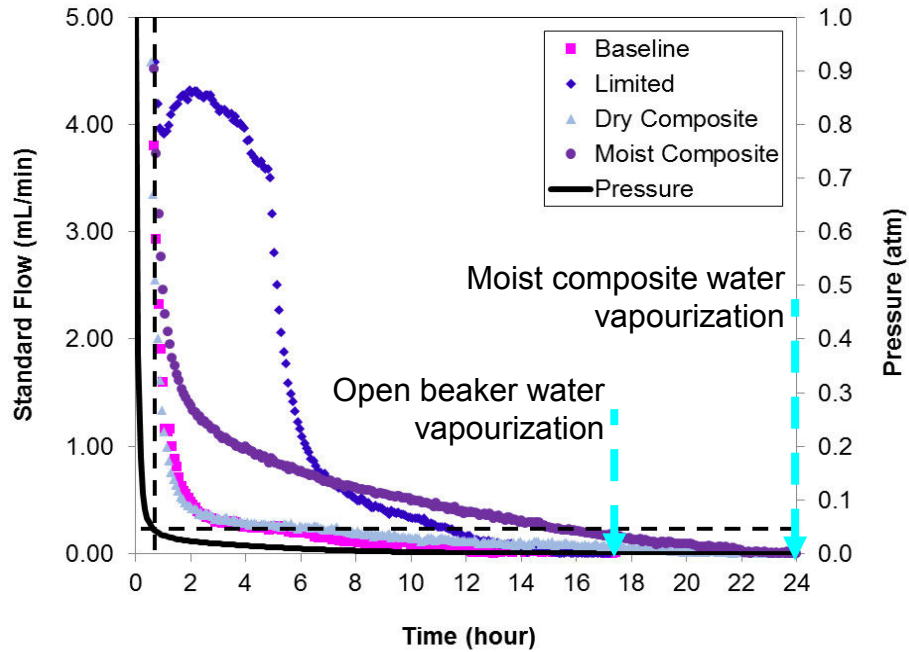


Figure 4.10. Water vapourization results from composite tests. The dry composite curve represents a 0 %RH conditioned specimen. The wet composite curve represents a 100 %RH conditioned specimen. The limited water setup is included for comparison.

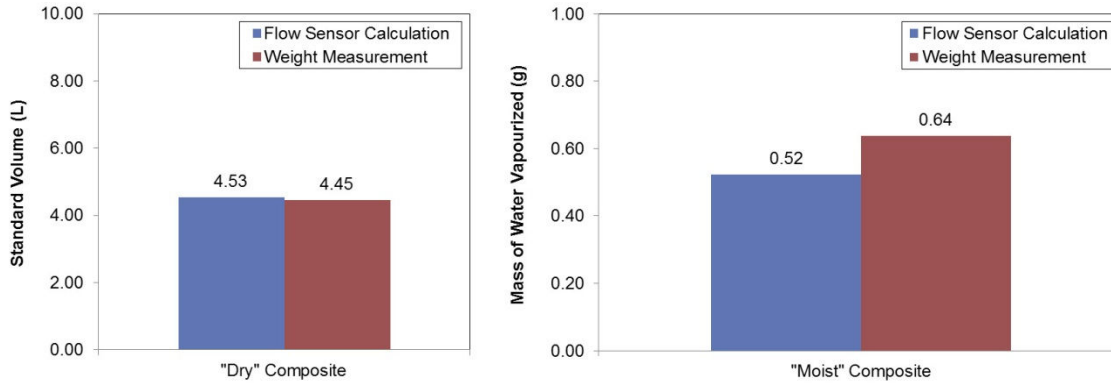


Figure 4.11. Water vapourization results from the composite tests. The dry composite (0 %RH) setup is compared against the known volume of the metal chamber. The moist composite (100 %RH) setup is compared against measured mass changes in the composite.

4.2.3 Vacuum Bagged Water Vapourization Results

Results for the vacuum bagged water vapourization tests on laminate specimens and bagging consumables are presented as plots of standard volume flow rate versus temperature. The results for 5320/T650 and MTM45-1/CF2426A are shown in Figure 4.12 and Figure 4.13, respectively. From the combined plot in Figure 4.12, it is observed that water vapourization begins as soon as heating is initiated, reaching a maximum around 40-70°C before receding as heating continued past 100°C. Figure 4.13 also shows a similar trend, but several of the tests did not exhibit significant moisture vapourization until reaching 50°C. This is likely an experimental artifact which occurred due to an inconsistency in the testing procedure. Under normal procedures, vacuum would be vented from the bagged setup after leak checking. But in several earlier experiments, this step

was neglected and the setup was kept under vacuum prior to starting the test. It is hypothesized that keeping the lay-up stack under vacuum may have caused pre-emptive vapourization of absorbed moisture from the specimen and bagging consumable surfaces prior to the start of the test. Therefore, subsequent vapourization from the specimen would require more time for absorbed moisture to diffuse out before it can be removed. Additionally, the extended compaction period may have affected gas pathways, impairing gas evacuation and vacuum penetration into the specimen.

Both Figure 4.12 and Figure 4.13 show that 100 %RH conditioned laminates produce the greatest amount of water vapour. This is expected since data from the humidity conditioning experiments presented in Ch. 4.2.1 demonstrates that specimens prepared under elevated relative humidity conditions show greater equilibrium moisture levels. Water vapour amounts generated from 0 %RH and ambient conditioned laminates are comparable. Figure 4.14 compares water vapour mass calculated from flow sensor data against Kardos' solubility model predictions for humidity conditioned 5320/T650 and MTM45-1/CF2426A laminates, and ambient condition bagging consumables. Although not all calculated and predicted water vapour results were within 10% of each other, the two results clearly follow the same trend. Figure 4.14 also illustrates that, under ambient condition testing, the majority of vapourization actually comes from absorbed moisture in the bagging consumables as opposed to the laminates.

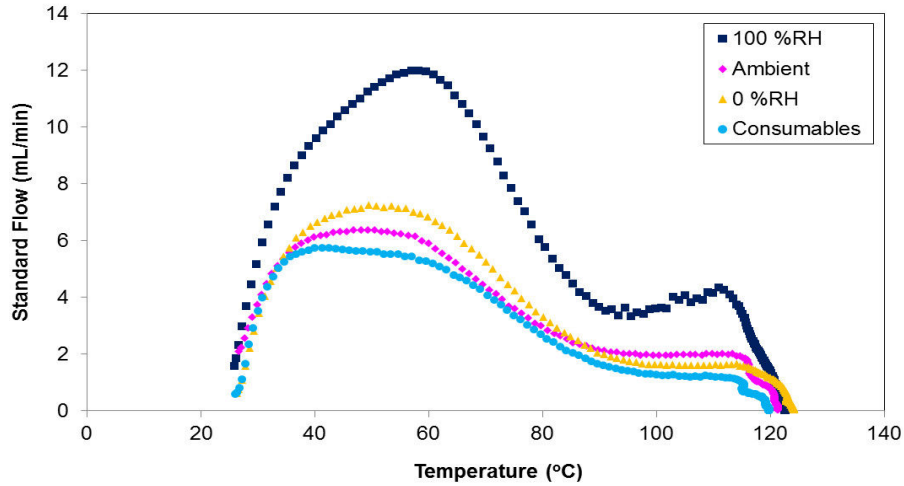


Figure 4.12. Water vapourization results of vacuum bagged 5320/T650 4 ply specimens conditioned at 100 %RH, ambient, and 0 %RH. Results of the consumables conditioned at ambient humidity are also included.

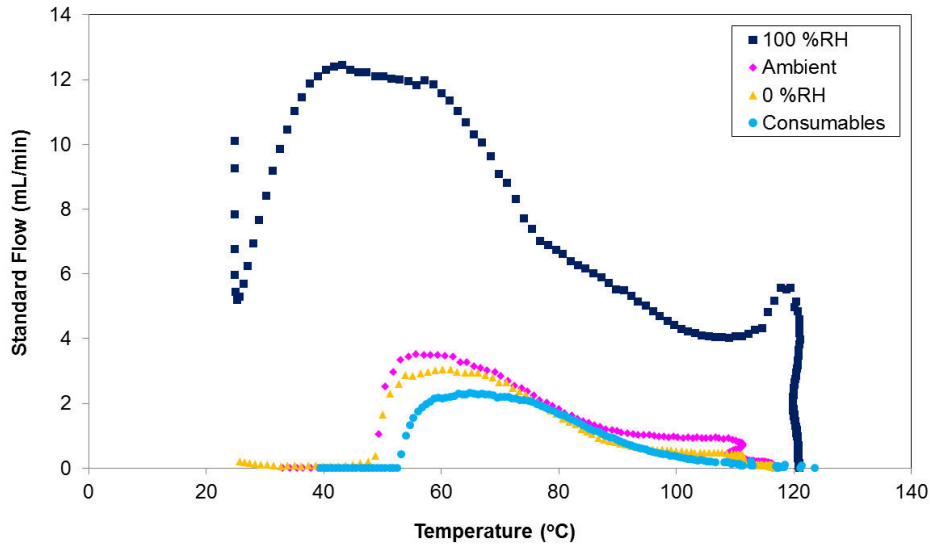


Figure 4.13. Water vapourization results of vacuum bagged MTM45-1/CF2426A 4 ply specimens conditioned at 100 %RH, ambient, and 0 %RH. Results of the consumables conditioned at ambient humidity are also included.

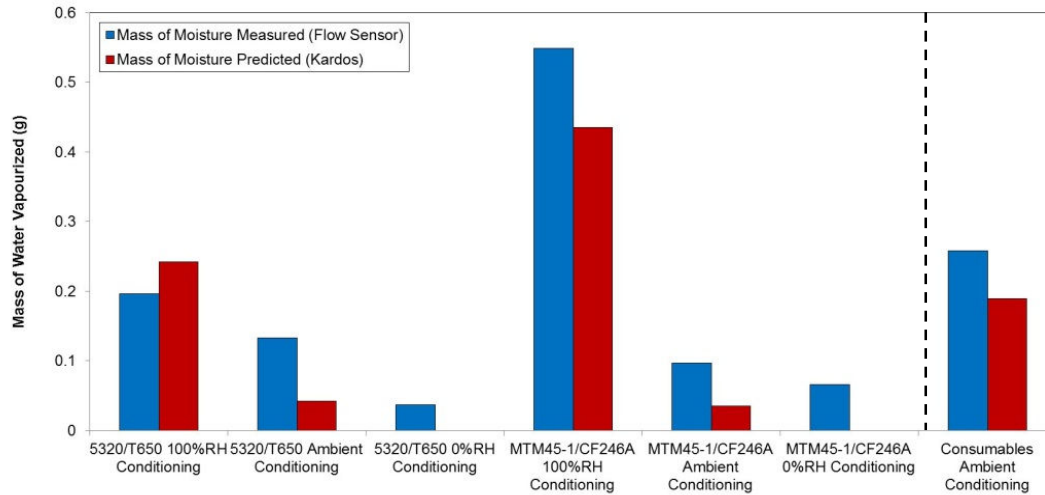


Figure 4.14. Water vapourization results of vacuum bagged 5320/T650 and MTM45-1/CF2426A 4 ply specimens conditioned at 100 %RH, ambient, and 0 %RH. Results of the consumables conditioned at ambient humidity are also included.

5 DISCUSSION

5.1 Anisotropy of Gas Transport

Gas transport was shown to be highly anisotropic in 5320/T650 prepregs, with in-plane gas transport being 1000 times more effective than through-thickness gas transport under both ambient and heated conditions. To put things in perspective, the time it takes for entrapped gas to travel one millimetre in the through-thickness direction is equivalent to it having travelled one metre in the in-plane direction. Gas transport work performed by Kratz, Louis, and Farhang et al on MTM45-1/CF2426A prepregs revealed similar trends of anisotropy (Farhang & Fernlund, 2011a; Kratz, 2009; Louis et al., 2010; Louis, 2010). The hypothesis for this anisotropy is that gas transport effectiveness depends on the nature of existing void spaces within the fibre bundles and resin film. For in-plane gas transport, it is theorized that gas is primarily extracted through intralaminar void spaces residing within the fibre tows. In continuous reinforcement prepregs, these void spaces can run the entire span of the structure to form a “vascular” network (Louis, 2010). However, for through-thickness gas transport, it is theorized that available void spaces exist as pockets in the resin film and cavities between nested fibre bundles. These are often generated randomly during resin impregnation and lay-up and therefore have limited interconnectivity. Furthermore, because these void spaces rarely align perfectly, the resulting pathways are highly tortuous (see Ch. 2, Figure 2.2) (Kardos et al., 1980; Louis, 2010).

Gas transport anisotropy is likely created as a result of the impregnation process. In prepreg manufacturing, the two most common impregnation techniques are hot-melt impregnation and resin-filming (F. C. Campbell, 2004). In both of these techniques, resin is applied to the surfaces of the fibre layers while the intralaminar regions are kept dry (thereby forming the EVaCs) (Figure 5.1). Using this surface-wetting approach, it seems intuitive that through-thickness gas transport would be inhibited by the resin layers while in-plane gas transport would remain relatively intact. Additionally, the application of resin on the surfaces mean that void spaces between the layers will be reduced and isolated, thereby limiting gas transport between plies. This likely explains why various prepreg manufacturers describe EVaCs as being primarily within the fibre tow regions (ACG, 2007; Boyd, 2003; CYTEC, 2009; Nutt & Boyd; Ridgard, 2009).

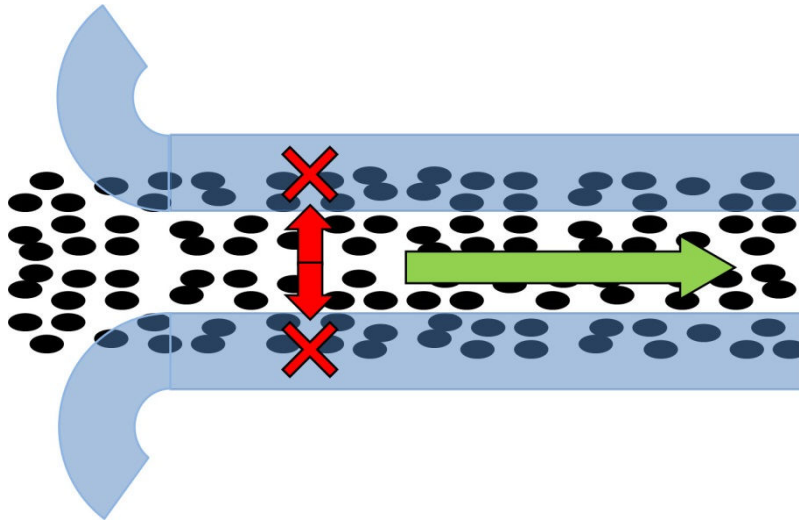


Figure 5.1. Illustration of partial impregnation and gas transport anisotropy.

The magnitude of in-plane 5320/T650 gas permeabilities measured in this thesis work was found to be on the same order as results reported by Kratz, Louis, and Farhang et al for MTM45-1/CF2426A (Farhang & Fernlund, 2011a; Farhang & Fernlund, 2011b; Kratz, 2009; Louis, 2010). This seems to suggest that both OOA prepreg systems are produced using similar resin impregnation techniques. However, the through-thickness permeabilities measured for 5320/T650 was two to three orders of magnitude greater than that reported for MTM45-1/CF2426A. It is theorized that this may be because of different fibre weave patterns employed in each prepreg system. The 5320/T650 prepreg consists of a plain weave pattern (Figure 5.2A), whereas the MTM45-1/CF2426A prepreg has a five-harness-satin weave pattern (Figure 5.2B). From the two photos of the prepreps, one can observe that the plain weave found in 5320/T650 contains more “openings” than MTM45-1/CF2426A’s five-harness-satin weave. Another factor that may affect through-thickness permeability is the thickness of the resin

layers applied to the prepreg surfaces. During handling of both prepregs, it was observed that MTM45-1/CF2426A had a much glossier and tackier surface compared to 5320/T650, suggesting that thicker resin layers were applied onto MTM45-1/CF2426A during impregnation. A thicker resin layer on the surface will likely hinder through-thickness gas transport and reduce permeability.

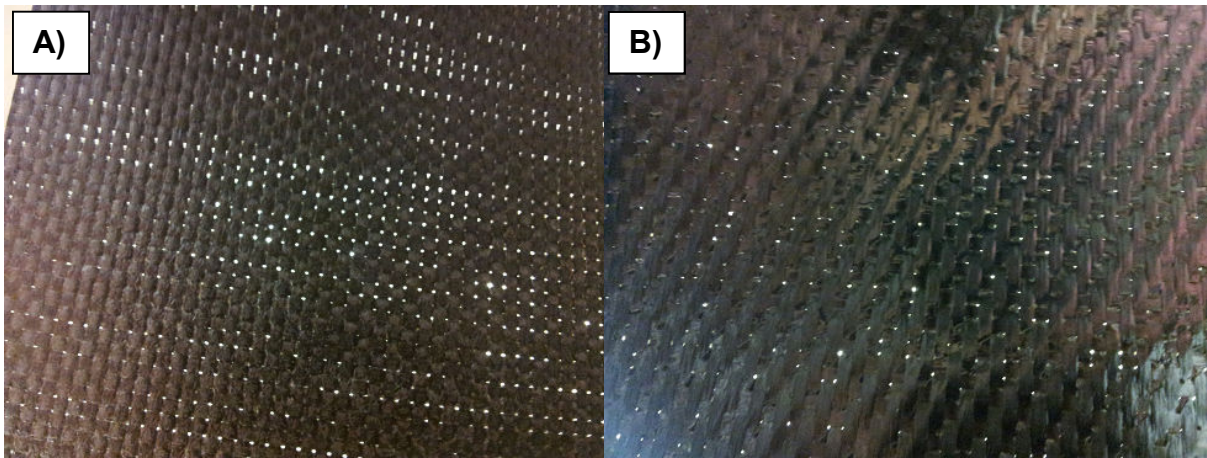


Figure 5.2. Photos of prepreg weave pattern (single ply). A) 5320/T650; B) MTM45-1/CF2426A

5.2 Evolution of Gas Transport with Process History

It was demonstrated that in-plane gas permeability in 5320/T650 decreased during the debulking process. This can potentially create problems during the manufacture of large or complex geometry structures, where prolonged debulking procedures (upwards of 16 hours or more) may be required to sufficiently remove porosity before heating (CYTEC, 2009). In-plane permeability decreased by approximately 50 % over the duration of the long debulk test.

Permeability reduction was observed to undergo two phases: a rapid reduction that occurs during the first two hours of debulking, followed by a gradual reduction that approaches steady state through the remainder of the test. It is hypothesized that the initial rapid reduction was a result of the loss of interlaminar voids. These interlaminar voids are initially present and interconnected during lay-up, but eventually collapse and become isolated as air is removed by vacuum. This is clearly evident from the microscopy results presented in Ch. 3.2.4, where Figure 3.17 and Figure 3.18 illustrate the loss of interlaminar voids when going from lay-up to debulking. The gradual permeability reduction during the second phase is hypothesized to take place because of resin cold-flow (Louis, 2010). Since the resin exists as a viscoelastic semi-solid at room temperature, it has the ability to “flow” overtime and slowly penetrate the dry fibre tows during vacuum compaction. However, for 5320/T650, the resin viscosity at room temperature was not low enough to allow complete infiltration of the fibre tows. Therefore, a sufficient portion of the EVaCs remained open to continue gas extraction. This is critical as it demonstrates that large or complex structures made from 5320/T650 can be subjected to prolonged debulking procedures without fear of impairing the EVaCs.

During heating, both in-plane and through-thickness permeabilities were found to initially decrease with temperature. This is due to the resin viscosity falling, allowing the resin to better infiltrate and wet-out the EVaCs. Figure 5.3 shows the change in resin viscosity with respect to temperature for 5320/T650.

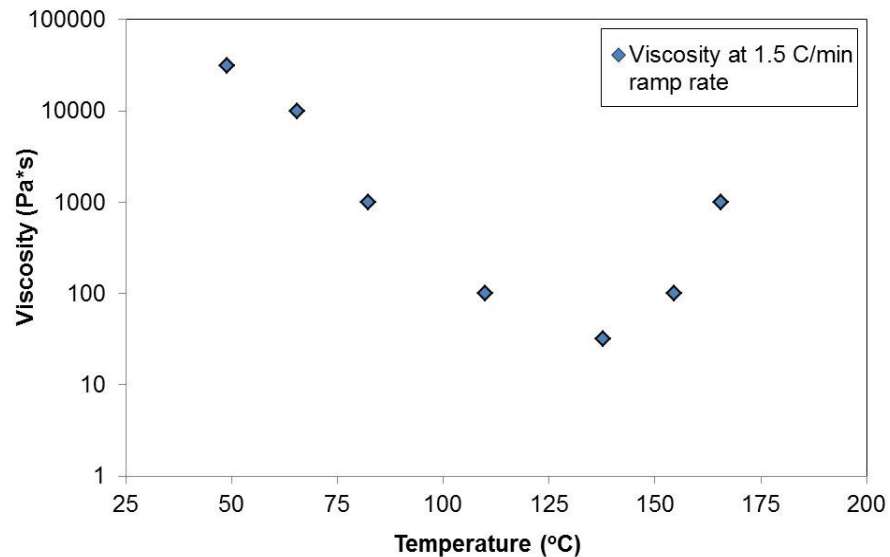


Figure 5.3. 5320/T650 matrix viscosity evolution with temperature. Plot is reproduced from Cyttec datasheet (CYTEC, 2009)

As testing progressed, observed in-plane and through-thickness permeabilities “open-up” when the laminates reached 80 to 90°C. These observations are consistent with observations from studies performed by Louis on MTM45-1/CF2426A (Louis et al., 2010; Louis, 2010). This is thought to be an artifact of the permeability test due to the necessity of maintaining steady state air flow. As the resin viscosity drops with temperature, resin pressures may fall below atmospheric pressure and enable air flow to force open previously filled pathways. During permeability testing, these pathways stayed open past gelation and cure and resulted in high porosity (Ch. 3.2.4, Figure 3.20). Under actual process conditions, it is unlikely that pathways would be forced open

unless significant vacuum bag leaks, moisture vapourization, or off-gassing occurs. However, if the resin pressure and viscosity falls low enough, entrapped gases can potentially “bubble” out of the laminate in a fashion similar to that found in bleed resin cure systems (Boyd, 2003; Louis, 2010). This means that even after resin has filled in the vacuum channels, gas removal can still continue to occur until resin gelation sets in. Because the test laminates had their pathways altered by steady-state air flow, the in-plane and through-thickness permeabilities measured beyond the “opening-up” temperature were not considered representative of actual process conditions. Therefore, true in-plane and through-thickness permeabilities were only measured up to the “opening-up” temperature.

5.3 Effect of Humidity on Moisture Content

Humidity was shown to effect the moisture content of 5320/T650 and MTM45-1/CF2426A prepregs. With increasing relative humidity, the moisture content of the prepregs also increased. The experimental values of moisture content with increasing relative humidity were found to closely follow Kardos’ solubility model (Kardos et al., 1980). Going from 0 to 100 %RH resulted in both prepregs having a moisture content of about 0.6 wt%. Although that may seem like a small amount of moisture, the transformation from liquid water to water vapour under partial vacuum conditions at room temperature results in a volume expansion of approximately 1300 times. For the 2.5” x 2.5” x 0.8 mm specimens used in the this study, the 0.6 wt% moisture content would generate around thirteen times

the volume of the laminate in water vapour. If not evacuated, high porosity levels and even delamination can occur as the laminate may literally “blow up” due to the volume change.

In Ch. 4.2.1, it was mentioned that a large scatter in the moisture content data was observed at 100 %RH. It is thought that temperature fluctuations in the lab and humidity conditioning chambers may be responsible for this phenomenon. Relative humidity, as defined in Equation 8, is the ratio of water partial pressure to water vapour pressure. When temperatures inside the conditioning chambers rise or fall, the water vapour pressure adjusts accordingly based on the Clausius-Clapeyron relation. This alters the pressure ratio so that an increase in the temperature results in a lower relative humidity and vice versa. If the system within the 100 %RH conditioning chamber was initially at equilibrium (equal rates of evaporation and condensation), increasing the temperature leads to an increased net evaporation until 100 %RH is re-established. However, decreasing the temperature will result in a net condensation of liquid water out of the gas phase since it is impossible to have relative humidity levels above 100%. It is hypothesized that some of this water may have condensed on the surfaces of the test laminates and increased their measured weights, therefore changing their moisture contents during 100 %RH conditioning.

5.4 Water Vapour Flow Measurements with Mass Flow Sensors

It was demonstrated that the mass flow sensors were capable of measuring water vapour flow during vapourization testing. Total mass of water vapourized as calculated from flow sensor data were within ten percent of the measured weight changes from the beakers (Figure 4.8), and the calculated pressure level in the metal chamber when the baseline, limited water, and infinite water vapourization plots diverged was close to the Clausius-Clapeyron prediction for water vapour pressure (Figure 4.7). Errors between calculated and measured mass change results may have stemmed from the fact that the flow sensors were calibrated for air whereas actual testing involved water vapour or air-water vapour mixtures. This was partially accounted for by multiplying the measured flow rate results with a correlation factor which takes into account the differences in density and heat capacity between air and water vapour (OMEGA, 2000). However, the actual mole ratios of air to water vapour during testing remained unknown. Therefore, it was assumed that gas flow initially only consisted of air, until pressure within the metal chamber reached the calculated water vapour pressure. After this point, the gas flow was assumed to be purely water vapour.

Water vapourization flow rates from the limited water test were simulated using a finite difference model incorporating Langmuir's evaporation equation. The model closely approximated experimental water vapour flow rates and captured the "elbow" of the plot as water was depleted from the beaker (Figure 4.9). However, the numerical model slightly under predicts the experimental flow rate

by about 1 mL/min when vapourization occurred. It was thought that this may again be due to temperature fluctuations during testing (which ran for 24 hours). As discussed in Ch. 5.3, water vapour pressure varies across temperature based on the Clausius-Clapeyron relation. If the temperature gets warmer inside the metal chamber, water vapour pressure rises and leads to increased rates of evaporation and vapour flow. This may have occurred during the experiments as ambient lab temperatures reach a high in the afternoon, and then fall in the evening and morning hours. However, the temperature parameter was constant for the model. Therefore, the simulation would not have captured changes in the rate of water vapourization due to temperature variations.

5.5 Timescales for Moisture Removal

Water vapourization testing demonstrated that moisture removal from prepreg laminates involves significant timescales. The test results illustrated that vapourizing a gram of water absorbed within a laminate took ten hours longer than vapourizing a gram of water sitting in an open beaker (Figure 4.10). The timescales associated with moisture removal from a laminate are linked to two main phenomena: moisture diffusion in the resin, and vapour advection through the void channels (Hsiao et al., 2011). To escape, absorbed moisture must first diffuse through the resin to the nearest available pathway. This rate of diffusion is limited by the diffusivity of water in resin. Previous studies have shown that water diffusion in resin is dependent on resin molecular structure and water-resin affinity (Adamson, 1980; Wong & Broutman, 1985). Therefore, changes in cross-

link density and the availability of hydrogen bonding sites can significantly alter the diffusion kinetics (Vanlandingham et al., 1999). As mentioned in Ch. 4.2.1, the diffusivity of water in uncured prepregs was found to be higher than in cured prepregs, suggesting that polymerization reduces the available number of molecular vacancies and hydrogen bonding sites. This could result in the moisture removal process becoming more difficult as the prepreg structure progresses along its cure cycle.

Moisture that diffuses to the resin-void channel interface will vapourize if the pressure conditions are satisfied (based on the Clausius-Clapeyron relation). The vapourized water can then be removed by advection through the EVaCs. The rate at which water vapour is removed via advection depends on the volume and tortuosity of available pathways (i.e. the prepreg permeability), the geometry of the laminate structure, and the pressure gradient driving advection. Processing factors such as debulk times and temperature ramps can significantly reduce the volume of open pathways, whereas material factors like fibre architecture and degree of resin impregnation can influence pathway tortuosity and anisotropy. For larger and more complex geometry parts, gas removal becomes increasingly difficult as entrapped gases must travel further before reaching and escaping through laminate edges and surfaces. Last, but not least, the magnitude of the pressure gradient driving advection depends on the quality of vacuum as well as the ease with which vacuum can penetrate the porous prepreg (related to permeability). Therefore, enough time must be set aside for

the removal of absorbed moisture as it is a complex process involving both diffusion transport through the resin and advection transport through the EVaCs. Cyttec recommends vacuum dwell times between four to sixteen hours (depending on the complexity of the part) in order to adequately remove moisture and entrapped gas (CYTEC, 2009).

5.6 Water Vapourization During VBO Processing

Testing performed on vacuum-bagged moisture conditioned 5320/T650 and MTM45-1/CF2426A laminates showed that vapourization of absorbed moisture occurred immediately as heating began. The test results revealed that vapourization was most prominent when laminate temperatures reached 40 to 60°C. Therefore, it is critical that prepreg manufacturers design their prepreg systems so that existing EVaCs can stay open as long as possible (especially around this temperature range) in order to maximize water vapour and air removal. The observations from this study seem to be in agreement with early empirical trials performed by ACG, who found that vacuum dwells around 70 – 80°C appeared to be most effective for reducing laminate void content (Ridgard, 2009). For 5320/T650, heated in-plane and through-thickness gas permeabilities were shown to decrease with temperature. However, some permeability was still retained all the way up to the critical “opening-up” temperature. This suggests that evacuation of vapourized moisture from 5320/T650 laminates can take place if the EVaCs remain open or if internal gas pressure can force open new pathways.

The results presented in Ch. 4.2.3 illustrated that moisture vapourization from the 0 %RH and ambient conditioned test laminates were quite similar. From Figure 4.4 and Figure 4.5, it appeared that moisture contents did not increase significantly until reaching roughly 30 %RH. Moisture experiments performed by Hsiao et al seem to show agreement with this observation (Hsiao et al., 2011). This suggests that at low to ambient relative humidities, vapourization of absorbed moisture from the laminates is small, and the majority of vapourization actually occurs from the vacuum bag consumables (most notably, the nylon vacuum bag). As seen in Figure 4.12 and Figure 4.13, the plots of the 0% RH conditioned specimen, ambient conditioned specimen, and consumables only tests followed one another closely throughout the cure cycle. However, even under ambient relative humidity conditions, the 0.1 – 0.2 wt% moisture content can still pose serious porosity issues by generating up to three or four times the volume of the laminate (12" x 2.5" x 0.8 mm) in water vapour.

From Figure 4.14, it can be seen that there were some errors associated with the water vapourization measurements and calculations in the laminate. One source, as mentioned previously, was that the mass flow sensors were calibrated for air flow instead of water vapour flow. Another source of error originated from the way water vapourization testing and quantification was performed. During testing of vacuum bagged laminates, both the laminates and consumables contributed to the total measured water vapour volume. It was assumed that

100% of the moisture contents in both the laminates and consumables were converted to water vapour. In order to isolate water vapourization from the laminate, additional testing was performed purely on the consumables so that vapourization from the consumables could be subtracted from the total measured vapourization in the vacuum-bagged laminates (Figure 5.4A). However, day-to-day fluctuations in the lab's relative humidity resulted in different moisture content of consumables between the vacuum-bagged tests and the consumables only test (Figure 5.4B). This meant that subtraction of the consumables portion from total measured water vapourization would not equal vapourization in the laminate.

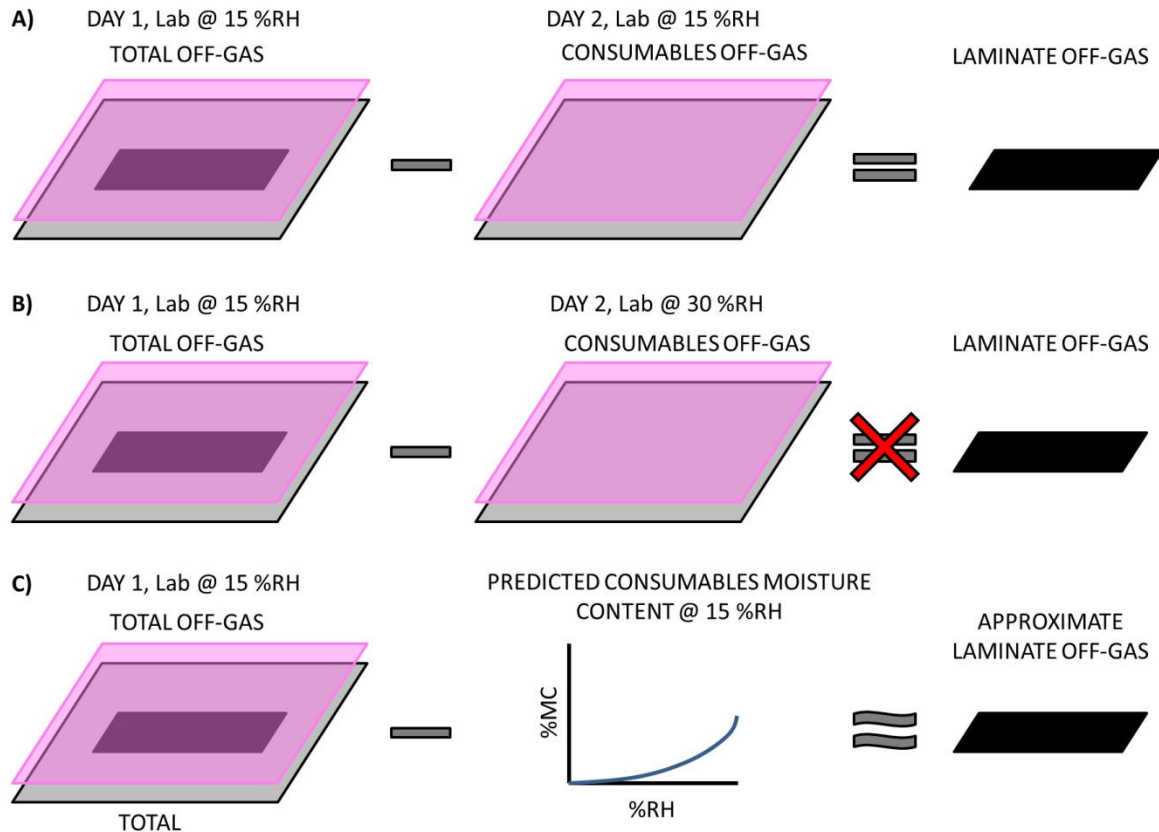


Figure 5.4. Determination of water vapourization in the laminate. A) Ideal scenario with unchanging lab relative humidity; B) Actual scenario with fluctuating lab relative humidity; C) Using Kardos' model to approximate actual consumable moisture contents

In this study, there was insufficient time for performing a consumables-only moisture vapourization test for each corresponding vacuum-bagged laminate test. Therefore, the Kardos' model was used to predict the nominal moisture contents of the consumables at any lab relative humidity (Figure 5.4C). Using this approach allowed for the determination of moisture vapourization from the

lamine, but also introduced error into the results as true moisture vapourization from the consumables was not obtained.

6 CONCLUSION

The objective of this study was to characterize gas transport and water vapourization characteristics of out-of-autoclave (OOA) prepregs during processing. The primary prepreg material used in this study was Cytec's CYCOM 5320/T650 PW. A second prepreg material, Advanced Composite Group's (ACG) MTM45-1/CF2426A 5HS, was used to provide comparisons to 5320/T650. Gas transport characterization was performed through permeability testing and microscopy analysis. Characterization of water vapourization was performed through relative humidity conditioning and vapourization testing. The following conclusions are reached from this study:

1) Gas transport is highly anisotropic

In-plane gas permeability of 5320/T650 was found to be much greater than through-thickness gas permeability under both ambient and heated conditions. This anisotropy is due to the nature of available interconnected void spaces (degree of interconnectivity, tortuosity of pathways etc.). Anisotropy is mainly a result of the impregnation process, where resin is often only applied to the fibre surfaces. Other factors such as weave "tightness" and resin film thickness can also significantly affect permeability.

2) Gas transport characteristics evolve with processing history

Debulking altered the gas permeability of 5320/T650. Permeability loss was observed to undergo two phases: a rapid reduction that occurs during initial vacuum application followed by a gradual reduction that led to steady state permeability. Based on microscopy analysis, the rapid reduction is associated with the collapse of interlaminar voids, whereas the gradual reduction is hypothesized to be a result of viscoelastic resin cold-flow into dry fibre bundles. Since the EVaCs remained upon after prolonged debulking, gas extraction was still possible.

Temperature was also found to have an effect on permeability. Increasing the temperature caused both in-plane and through-thickness permeabilities to decrease. This was due to a falling resin viscosity, which enabled the resin to flow and fill in void spaces. However, there existed a critical resin viscosity level where air pressure overcame resin pressure and re-opened closed pathways. During permeability testing, the imposed steady-state air flow caused the pathways to “open-up”. In actual processing, it is unlikely that this phenomenon would occur unless vacuum bag leaks or significant levels of internal gas generation (moisture vapourization or off-gassing) were present.

3) Moisture from the environment can lead to high porosity due to vapourization

Moisture content of 5320/T650 was found to increase with relative

humidity. This increase in moisture content with relative humidity was well approximated by Kardos' solubility model (Kardos et al., 1980) up to around 95 %RH. The transformation from liquid water to water vapour results in a volume change of 1300 times at room temperature, which if not removed, will cause severe porosity and delamination in the final structure. Moisture conditioning performed on several common types of vacuum bagging consumables revealed that the nylon vacuum bag absorbed more moisture than any other type of consumable.

Removal of absorbed moisture is a slow and complex process that involves both water diffusion through the resin and water vapour advection through interconnected voids (Hsiao et al., 2011). Vapourization testing illustrated that moisture removal from a moist laminate took roughly ten hours longer than from an open beaker for a single gram of water. The timescales associated with moisture removal depend on factors such as the availability of open molecular sites in the resin structure, the resin-water affinity, the permeability of the prepreg, the geometry of the structure, and the quality of the vacuum.

During testing, moisture vapourization from 5320/T650 occurred immediately with heating and peaked between 40 to 60°C. Evacuation of vapourized moisture from the laminate can be facilitated as long as gas permeability is retained during heating. For low relative humidity

conditioned laminates (0 %RH to ambient condition), the plots of water vapourization versus time were quite similar, suggesting that laminate moisture contents did not change significantly until the laminates were exposed to higher levels (> 30 %RH) of relative humidity conditioning (Hsiao et al., 2011). However, even ambient level moisture contents in the laminate can translate to serious porosity problems if not adequately removed. Therefore, it is advisable that storage and processing of both prepreg and consumable materials be performed in controlled humidity environments to minimize their moisture contents.

4) Water vapourization measurements can be performed using mass flow sensors

It was demonstrated that mass flow sensors can be used to measure moisture vapourization from laminates during vacuum bag processing. The sensors were able to detect when rapid vapourization began (as predicted based on pressure calculations and the Clausius Clapeyron relation), as well as when it concluded (as simulated by numerical modeling using Langmuir's evaporation equation). Errors associated with mass flow sensor measurements were attributed to the fact that the sensors were calibrated for air as opposed to water vapour.

To achieve effective void removal, OOA prepregs should be designed so that EVaCs remain open for as long as possible (especially through peak

vapourization temperatures). Resins should also be tailored so that viscosities are high during ambient temperature debulking and initial heating in order to reduce cold flow infiltration and maximize gas evacuation time. However, once all of the gas has been removed, resin viscosities must become low enough to completely wet-out the dry fibres. Last, but not least, incorporating vacuum dwells during peak vapourization temperatures may help facilitate the moisture removal process (Ridgard, 2009).

6.1 Future Work

Based on the conclusions from this study, several recommendations can be made for future work:

1) Linking resin rheology and microscopy studies to permeability

In the current study, gas permeability was shown to decrease with increasing temperature until reaching the “opening-up” temperature. Beyond this point, true gas permeability of prepregs was not determined. To obtain a better understanding of what happens past the “opening-up” temperature, resin viscosity data should be linked with permeability results to predict how long EVaCs will stay open during processing. Additionally, more detailed microscopy studies should be performed at various points throughout the cure cycle to correlate void evolution with permeability. Other analysis methods such as CT scan or ultrasonic testing may also be

useful in revealing the interconnectivity of in-plane and through-thickness void spaces throughout the cure cycle.

2) Moisture conditioning and flow sensors

During moisture conditioning, large scatters in moisture content data were observed at 100 %RH. Subsequent conditioning of “moist” specimens should be performed at slightly lower relative humidity levels (i.e. 75 %RH) to avoid condensation due to temperature variations. This will allow for more consistent moisture content results.

Water vapourization testing was performed using mass flow sensors. Although it was shown that the flow sensors can accurately detect water vapourization and quantify water vapour flow to within ten percent error, the sensors used were calibrated for air and not water vapour. Future vapourization testing should be performed with mass flow sensors specifically calibrated for water vapour in order to improve the accuracy of measurements.

3) Vapourization of absorbed moisture with respect to heating rate, hold temperature, and degree of cure

The effects of heating rates and hold temperature on laminate moisture vapourization during processing should be studied. Since OOA prepregs are required to be curable over a range of temperatures, knowing what the

peak vapourization temperatures are and how long moisture vapourization will last will aid in the design of more effective cure cycles. This could be especially important when large temperature gradients are anticipated (i.e. in thick laminate parts). Additionally, moisture conditioning and moisture vapourization testing should be performed on specimens at various degrees of cure to observe how polymerization affects the moisture absorption and removal process.

4) Modeling of the moisture removal process

Water vapourization from an open beaker was simulated using numerical modeling and Langmuir's evaporation equation. Although the simulation and experimental vapourization curves followed each other closely, the model was not able to capture the effects of temperature on water vapourization. Future attempts at modeling water vapourization should include temperature as a parameter. The next logical step in the modeling process is to simulate water vapourization from a moist laminate. Since the moisture removal process involves both diffusion and advection, future models will need to incorporate both of these phenomena to accurately simulate moisture removal.

REFERENCES

- ACG. (2007). *MTM45-1 matrix resin product data sheet* (PDS1205/11.07/3 ed.)
Advanced Composites Group.
- Adamson, M. J. (1980). Thermal expansion and swelling of cured epoxy resin used in graphite-epoxy composite materials. *Journal of Materials Science*, *15*, 1736-1745.
- Ahn, K. J., Seferis, J. C., Price, J. O., & Berg, A. J. (1991). Permeation measurements through prepreg laminates. *SAMPE Journal*, *27*, 19-26.
- Ahn, K. J., Seferis, J. C., & Berg, J. C. (1991). Simultaneous measurements of permeability and capillary pressure of thermosetting matrices in woven fabric reinforcements. *Polymer Composite*, *12*(3), 146-152.
- Arafath, A. R. A., Fernlund, G., & Poursartip, A. (2009). Gas transport in preregs: Model and permeability experiments. Paper presented at the *Gas Transport in Preregs: Model and Permeability Experiments*, Edinburgh, Scotland.
- ASTM International. (2009). *ASTM E2015-04 (reapproved 2009) "standard guide for preparation of plastics and polymeric specimens for microstructural examination"*
- Boeing. (2012). *787 dreamliner program fact sheet*. Retrieved March, 18, 2012, from <http://www.boeing.com/commercial/787family/programfacts.html>

- Boey, F. Y. C., & Lye, S. W. (1992). Void reduction in autoclave processing of thermoset composites - part 1: High pressure effects on void reduction. *Composites*, 23(4), 261-265.
- Boll, D. J., Bascom, W. D., & Motiee, B. (1985). Moisture absorption by structural epoxy-matrix carbon-fiber composites. *Composites Science and Technology*, 24, 253-273.
- Bombardier. (2012). *A new meaning to traveling light*. Retrieved March 18, 2012, from <http://cseries.com/en/?docID=0901260d800091f9#/cseries/technology/advancedmaterial/>
- Bond, G. G., Griffith, J. M., Han, G. L., Bongiovanni, C., & Boyd, J. (2008). Non-autoclave prepreg manufacturing technology. Paper presented at the Long Beach, California.
- Boyd, J. (2003). Vacuum bag only composite part manufacturing. Paper presented at the Dayton, Ohio.
- Brand, R. A., Brown, G. G., & McKague, E. L. (1984). *Processing science of epoxy resin composites* (Final No. AFWAL- TR-83-4 124). OH: Air Force Materials Laboratory Wright Patterson AFB,. Retrieved from <http://oai.dtic.mil/oai/oai?verb=getRecord&metadataPrefix=html&identifier=ADB083264>

Campbell, F. C. (2004). *Manufacturing process for advanced composites*. The Boulevard, Langford Lane, Kidlington, Oxford OX5: Elsevier Advanced Technology.

Campbell, K. (2009). *Airbus to start manufacturing parts for new A350 XWB in late '09*. Retrieved March 18, 2012, from <http://www.engineeringnews.co.za/article/airbus-to-start-manufacturing-parts-for-new-a350-xwb-in-late-09-2009-05-11>

Chen, X., & Penumadu, D. (2008). Permeability measurement and numerical modelig for refractory porous materials. Paper presented at the *Permeability Measurement and Numerical Modelig for Refractory Porous Materials*, AFS (American Foundry Society) 2008 Atlanta, Georgia. , 116. pp. 1-15.

Costa, M. L., Almeida, S. F. M., & Rezende, M. C. (2001). The influence of porosity on the interlaminar shear strength of carbon/epoxy and carbon/bismaleimide fabric laminates. *Composites Science and Technology*, 61, 2101-2102-2108.

CYTEC. (2009). *CYCOM 5320 datasheet* (Revision 1.3 - 03.18.09 ed.) CYTEC.

Diamant, Y., Marom, G., & Broutman, L. J. J. (1981). The effect of network structure on moisture absorptions of epoxy resins. *Journal of Applied Polymer Science*, 26, 3015.

- Dillon, G. P. (2005). *Influence of prepreg microstructures on structural performance of polymer matrix composites* (Final No. ADA437260) Air Force Office of Scientific Research (AFOSR).
- Farhang, L., & Fernlund, G. (2011a). Void evolution and gas transport during cure in out-of-autoclave prepreg laminates. Paper presented at the Long Beach, California.
- Farhang, L., & Fernlund, G. (2011b). Void morphology, void evolution and gas transport in out-of-autoclave prepregs. Paper presented at the Montreal, Quebec.
- Fleagle, R. G., & Businger, J. A. (1980). *An introduction to atmospheric physics, volume 25* (2nd ed.) Academic Press.
- Gebart, B. R., & Lidstrom, P. (1996). Measurement of in-plane permeability anisotropic fiber reinforcements. *Polymer Composite*, 17(1), 43-51.
- Gode, P., Lindbergh, G., & Sundholm, G. (2002). In-situ measurements of gas permeability in fuel cell membranes using a cylindrical microelectrode. *Journal of Electroanalytical Chemistry*, 518(2), 115-122.
- Grunenfelder, L. K., & Nutt, S. R. (2010). Void formation in composite prepregs - effect of dissolved moisture. *Composites Science and Technology*, 70, 2304-2309. Retrieved from Elsevier database.

- Gutowski, T. G., Cai, Z., Bauer, S., Boucher, D., Kingery, J., & Wineman, S. (1987). Consolidation experiments for laminate composites. *Journal of Composite Materials*, 21, 650-669.
- Ho, C. K., & Webb, S. W. (Eds.). (2006). *Gas transport in porous media (theory and applications of transport in porous media)* (1st ed.). Dordrecht, Netherlands: Springer.
- Hsiao, K., Kay, J., & Fernlund, G. (2011). Gas transport and water evaporation in out-of-autoclave prepregs. Paper presented at the Montreal, Quebec.
- Kaelble, D. H., & Dynes, P. J. (1977). Methods for detecting moisture degradation in graphite-epoxy composites. *Materials Evaluation*, , 103.
- Kang, M. K., Jung, J. J., & Lee, W. I. (2000). Analysis of resin transfer moulding process with controlled multiple gates resin injection. *Composites Part A*, 31, 407-422.
- Kardos, J. L., Dudukovic, M. P., & Dave, R. (1980). Void growth and resin transport during processing of thermosetting - matrix composites. *Advances in Polymer Science*, 80, 101-123.
- Kay, J., Farhang, L., Hsiao, K., & Fernlund, G. (2011). Effect of process conditions on porosity in out-of-autoclave prepreg laminates. Paper presented at the *Effect of Process Conditions on Porosity in Out-of-Autoclave Prepreg Laminates*, Jeju Island, Korea.

- Kim, O. (2009). *Electron microscopes vs optical (light) microscopes*. Retrieved March, 30, 2012, from <http://www.microbehunter.com/2009/01/22/electron-microscopes-vs-optical-light-microscopes/>
- Kratz, J. (2009). Processing composite sandwich structures using out-of-autoclave technology. (Master's of Engineering, McGill University).
- Lam, R. C., & Kardos, J. L. (1989). The permeability and compressibility of aligned and cross-ply fiber beds during processing of composites. Paper presented at the pp. 1408-1412.
- Langmuir, I. (1913). The vapor pressure of metallic tungsten. *Physical Review Second Series*, 2(5), 329-342.
- Lin, Y. C., & Chen, X. (2005). Moisture sorption-desorption-resorption characteristics and its effect on the mechanical behavior of the epoxy system. *Polymer*, 46, 11994-12003.
- Liu, L., Zhang, B. M., Wang, D. F., & Wu, Z. J. (2006). Effects of cure cycles on void content and mechanical properties of composite laminates. *Composite Structures*, 73, 303-309.
- Loos, A. C., & Springer, G. S. (1979). Effects of thermal spiking on graphite-epoxy composites. *Journal of Composite Materials*, 13, 17-34.
- Loos, A. C., & Springer, G. S. (1983). Curing of epoxy matrix composites. *Journal of Composite Materials*, 17, 135-169.

- Louis, B. (2010). Gas transport in out-of-autoclave prepreg laminates. (Master of Applied Science, University of British Columbia).
- Louis, B., Hsiao, K., & Fernlund, G. (2010). Gas permeability measurement of out of autoclave prepreg MTM45-1/CF2426A. Paper presented at the Seattle, Washington.
- Maggana, C., & Pissis, P. (1999). Water sorption and diffusion studies in an epoxy resin system. *Journal of Polymer Science: Part B*, 37, 1165-1182.
- Marks, P. (2005). *Aviation - the shape of wings to come*. Retrieved March, 18, 2012, from <http://www.newscientist.com/article/dn7552-aviation--the-shape-of-wings-to-come.html?full=true>
- Michaud, V., & Mortensen, A. (2007). On measuring wettability in infiltration processing. *Scripta Materialia*, 56(10), 859-862.
- Naceri, A. (2009). Modeling of the mechanical behavior of composite at different relative humidities. *Strength of Materials*, 41(4), 444-448.
- Nam, J. D., Seferis, J. C., Kim, S. W., & Lee, K. J. (1995). Gas permeation and viscoelastic deformation of prepreps in composite manufacturing process. - *Polymer Composites*, 16(5), 370-377. doi:- 10.1002/pc.750160505
- Nield, D. A., & Bejan, A. (Eds.). (2006). *Convection in porous media* (3rd ed.) Springer.

Noman, R., & Zubair Kalam, M. (1990). Transition from laminar to non-darcy flow in porous media. Paper presented at the *Transition from Laminar to Non-Darcy Flow in Porous Media*, SCA (Society of Core Analysts) London, UK. pp. 447-462.

Nutt, S. R., & Boyd, J. *Advanced composites for aerospace - new materials development: Out-of-autoclave processing with vacuum-bag-only (VBO) prepregs* USC Viterbi School of Engineering Gill Foundation Composites Center.

Olivier, P., Cottu, J. P., & Ferret, B. (1995). Effects of cure cycle pressure and voids on some mechanical properties of carbon/epoxy laminates. *Composites*, 26(7), 509-515.

OMEGA. (2000). *Electronic mass flowmeters - flow reference section*. Retrieved April, 26, 2012, from http://www.omega.com/Green/pdf/MASS_FLOW_REF.pdf

Powell, A. (2005). *Multicomponent evaporation kinetics*. Retrieved April 05, 2012, from <http://teaching.matdl.org/teachingarchives/wiki/ReSources>

Price, T. L., Dalley, G., McCullough, P. C., & Choquette, L. (1997). *Manufacturing advanced composite components for airframes* (Handbook No. DOT/FAA/AR-96/75) FEDERAL AVIATION ADMINISTRATION WASHINGTON DC OFFICE OF AVIATION RESEARCH.

- Putnam, J. W., & Seferis, J. C. (1995). Prepreg gas permeation as a function of fibre orientation and aging time. *Journal of Advanced Materials*, 26(3), 35-41.
- Repecka, L., & Boyd, J. (2002). Vacuum-bag-only-curable-prepregs that produce void-free parts. Paper presented at the Long Beach, California.
- Ridgard, C. (2009). Out of autoclave composite technology for aerospace, defense, and space structures. Paper presented at the *Out of Autoclave Composite Technology for Aerospace, Defense, and Space Structures*, Baltimore, Maryland.
- Ridgard, C. (2010). Next generation out of autoclave. Paper presented at the *Next Generation Out of Autoclave*, Seattle, Washington.
- Sakhaee-Pour, A., & Bryant, S. L. (2011). Gas permeability of shale. Paper presented at the *Gas Permeability of Shale*, Denver, Colorado. pp. 1-14.
- Salzman, W. R. (2005). *Clapeyron and clausius-clapeyron equations.*, April, 1, 2012, from <http://web.archive.org/web/20070607143600/http://www.chem.arizona.edu/~salzmanr/480a/480ants/clapeyro/clapeyro.html>
- Scheidegger, A. E. (1974). *The physics of flow through porous media* (3rd ed.). Toronto, Ontario: University of Toronto Press.
- Shen, C. H., & Springer, G. S. (1976). Moisture absorption and desorption of composite materials. *Journal of Composite Materials*, 10(2), 2-20.

Shim, S. B., Ahn, K. J., Seferis, J. C., Berg, A. J., & Hudson, W. (1994). Flow and void characterization of stitched structural composites using resin film infusion process (RFIP). *Polymer Composites*, 15(6), 453-463.

Shim, S. B., & Seferis, J. C. (1997). Thermal and air permeation properties of a carbon fiber/toughened epoxy based prepreg system. *Journal of Applied Polymer Science*, 65(1), 5-16.

Sobera, M. P., & Klejin, C. R. (2006). Hydraulic permeability of ordered and disordered single-layer arrays of cylinders. *Physical Review E*, 74(3), 036301-1-036301-2 to 036301-10.

Tavares, S. S., Michaud, V., & Manson, J. -. E. (2009). Through thickness air permeability of prepregs during cure. *Composites Part A: Applied Science and Manufacturing*, 40(10), 1587-1596.

The Engineering ToolBox. (2009). *STP - standard temperature and pressure & NTP - normal temperature and pressure*. Retrieved September, 2011, 2011, from http://www.engineeringtoolbox.com/stp-standard-ntp-normal-air-d_772.html

The Engineering ToolBox. (2011). *Air - absolute and kinetic viscosity*. Retrieved October, 2011, 2011, from http://www.engineeringtoolbox.com/air-absolute-kinematic-viscosity-d_601.html

- Thomas, S. (2009). Vacuum bag only processing of composites. (Doctor of Philosophy (Materials Science), University of Southern California).
- Thomas, S., Bongiovanni, C., & Nutt, S. R. (2008). In situ estimation of through-thickness resin flow using ultrasound. *Composites Science and Technology*, *68*, 3093-3098.
- Thomas, S., & Nutt, S. R. (2009). Temperature dependence of resin flow in a resin film infusion (RFI) process by ultrasound imaging. *Applied Composite Materials*, *16*(3), 183-196.
- Thorfinnson, B., & Biermann, T. F. (1986). Production of void free composite parts without debulking. Paper presented at the *Production of Void Free Composite Parts without Debulking*, Las Vegas, Nevada. pp. 480-490.
- Thorfinnson, B., & Biermann, T. F. (1987). Degree of impregnation of prepregs - effects on porosity. Paper presented at the *Degree of Impregnation of Prepregs - Effects on Porosity*, Anaheim, California. pp. 1500-1509.
- Vanlandingham, M. R., Eduljee, R. F., & Gillespie, J. W. (1999). Moisture diffusion in epoxy systems. *Journal of Applied Polymer Science*, *71*, 787-798.
- Wong, T. C., & Broutman, L. J. (1985). Water in epoxy resins part ii. diffusion mechanism. *Polymer Engineering and Science*, *25*(9), 529-534.

Wood, J. R., & Bader, M. G. (1995). Modelling the behaviour of gas bubbles in an epoxy resin: Evaluating the input parameters for a diffusion model using a free-volume approach. *Journal of Materials Science*, 30, 916-922.

Wood, K. (2010). *Learjet 85 composite pressurized cabin a cost cutter* Retrieved March 18, 2012, from <http://www.compositesworld.com/articles/learjet-85-composite-pressurized-cabin-a-cost-cutter>

Zhu, C., Jiang, L., Teng-Man, C., & Kin-Kai, H. (2002). A comparative study of artificial membrane permeability assay for high throughput profiling of drug absorption potential. *European Journal of Medicinal Chemistry*, 37(5), 399-407.

APPENDICES

A) Derivation of Modified Darcy's Law

Arafath's derivation for 1-D fluid flow through a porous medium is based on Darcy's Law and the Ideal Gas Law as shown below (Arafath et al., 2009; Louis, 2010):

$$Q = -\frac{AK}{\mu} \frac{dP}{dx} \quad (\text{Equation A1})$$

$$PV = nRT = C(\text{constant}) \quad (\text{Equation A2})$$

The Ideal Gas Law can also be presented as a flow rate by using (\dot{V}) as volumetric flow rate (m^3/s) and (\dot{n}) as molar flow rate ($moles/s$):

$$P\dot{V} = \dot{n}RT = C(\text{constant}) \quad (\text{Equation A3})$$

$$(\dot{V}) = (Q)$$

Since the right hand side is constant, Equation A3 reduces to:

$$PQ = C(\text{constant}) \quad (\text{Equation A4})$$

Equation A4 can be rearranged to isolate for (Q) and then substituted back into Darcy's Law:

$$\frac{C}{P} = -\frac{AK}{\mu} \frac{dP}{dx} \quad (\text{Equation A5})$$

Equation A5 can be rearranged and integrated on both sides to obtain Equation A6. The limits of integration are from 0 to L and vacuum (v) to atmosphere (a) for distance (left hand side) and pressure (right hand side), respectively:

$$C \int_0^L dx = -\frac{AK}{\mu} \int_a^v P dP$$

$$CL = -\frac{AK}{\mu} \frac{P_v^2 - P_a^2}{2} \quad (\text{Equation A6})$$

The constant (C) can be replaced by (pQ) from Equation A4. At atmospheric conditions, this becomes:

$$P_a Q_a L = -\frac{AK}{\mu} \frac{P_v^2 - P_a^2}{2}$$

$$Q_a = -\frac{AK}{2\mu} \frac{P_v^2 - P_a^2}{P_a}$$

$$Q_a = \frac{AK}{2\mu} \frac{P_a^2 - P_v^2}{P_a} \quad (\text{Equation A7})$$

B) Verification of Laminar Flow

Reynolds number is determined for gas flow in the in-plane and through-thickness directions to confirm that flow was indeed in the laminar region.

The generic form of Darcy's law is given as:

$$v = -\frac{K}{\mu} \left(\frac{\Delta P}{L} \right) \text{ (Equation A8)}$$

In Equation A8, v (m/s) is Darcy velocity of the gas, K (m²) is gas permeability, μ (Pa · s) is dynamic viscosity of air, and $\frac{\Delta P}{L}$ (Pa/m) is the pressure gradient. For in-plane gas permeability specimens, K was 5.67E-14 m², and $\frac{\Delta P}{L}$ was 1.99E6 Pa/m. For through-thickness gas permeability specimens, K was 8.79E-17 m², and $\frac{\Delta P}{L}$ was 6.33E7 Pa/m. Using Equation A8, Darcy velocity for in-plane and through-thickness gas flow was determined to be 5.71E-3 m/s and 2.78E-4 m/s, respectively.

The Reynolds number for in-plane and through-thickness gas flow can be determined using Equation A9:

$$Re_K = \frac{\rho v K^{1/2}}{\mu} \text{ (Equation A9)}$$

Equation A9 is a permeability-based Reynolds number, where ρ (kg/m³) is density. Substituting in air density, air dynamic viscosity, Darcy velocity, and gas

permeability, the Reynolds number for in-plane and through-thickness gas flow can be determined. For in-plane gas flow, Reynolds number was determined to be $8.26E-5$. For through-thickness gas flow, Reynolds number was determined to be $1.59E-7$. In both cases, the Reynolds number for gas flow was much less than one, indicating that in-plane and through-thickness gas flow were indeed in the laminar regime (Nield & Bejan, 2006).

C) Total System Leak Test

The total system leak test is to detect the presence of vacuum bag leaks. The testing procedure is performed as described below:

1. Apply vacuum to the vent, vacuum, and leak test chambers.
2. Once full vacuum has been achieved in all three chambers, disconnect the line from the vacuum pump and observe if vacuum drops in any of the chambers (Figure C.1). If no leaks are present, full vacuum will be maintained in all three chambers.

According to the CYCOM 5320 datasheet, full vacuum should be within 2 in. Hg of absolute vacuum (30 in. Hg) for a given altitude. Additionally, vacuum bagged setups should not show more than 5 in. Hg loss within five minutes (CYTEC, 2009).

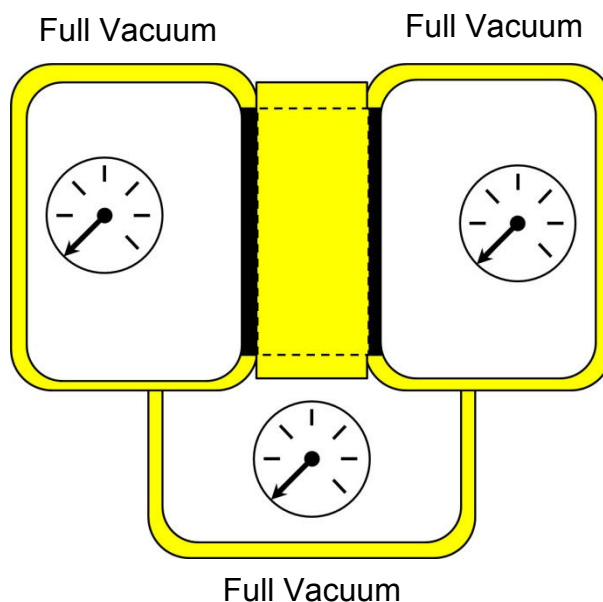


Figure C.1. Total system leak test setup.

D) Inter-Chamber Leak Test, Transverse Gas Flow, and Air-Channel Bridging

The inter-chamber leak test is broken down into two segments as described below. It is used to confirm that gas transport is isolated to the 1-D direction (no transverse gas flow), and that gas transport occurs through the laminate (and not through laminate-sealant tape interface).

The method for testing transverse gas flow is as follows:

1. Apply vacuum to the vent, vacuum, and leak test chambers.
2. Once full vacuum has been achieved in all three chambers, disconnect the line from the vacuum pump and release vacuum in the leak test chamber. Observe if vacuum drops in either the vent or vacuum chambers (Figure D.). If no transverse gas flow is present, full vacuum will be maintained in the two remaining chambers

The method for testing air-channel bridging is as follows:

1. Apply vacuum to the vent, vacuum, and leak test chambers.
2. Once full vacuum has been achieved in all three chambers, disconnect the line from the vacuum pump and release vacuum in the vacuum chambers. Observe how quickly vacuum drops in the vent chamber (Figure D.). If no air-channel bridging is present, the vacuum level in the vent chamber will decrease slowly over time as air permeates to equalize pressure in the vacuum chamber. If air-channel bridging is present, the rate of vacuum

loss will be much more rapid (zero transverse gas flow must be confirmed beforehand).

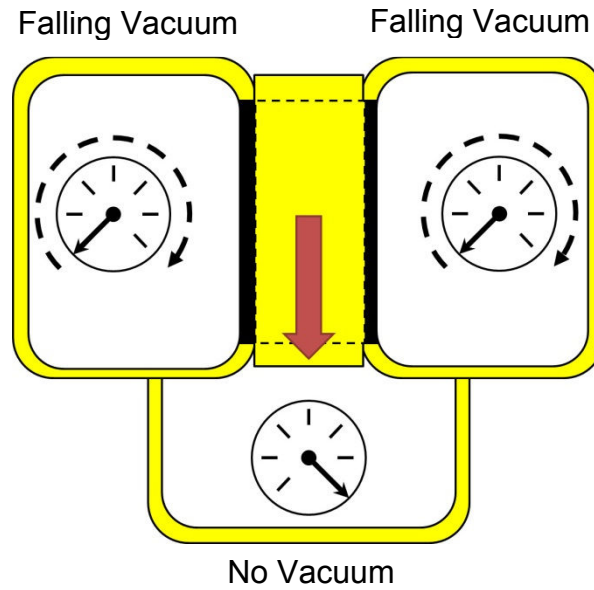


Figure D.1. Inter-chamber leak test setup for transverse gas flow.

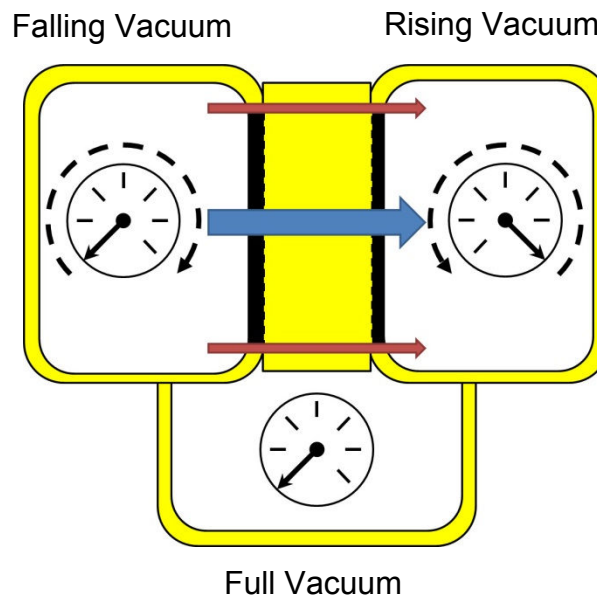


Figure D.2. Inter-chamber leak test setup for air-channel bridging.

E) Procedure for Initial Moisture Conditioning Trial

The initial trial moisture conditioning trial was based on a method developed by James Kay of the UBC Composites Group (Hsiao et al., 2011). This trial was used to determine the necessary number of days for moisture conditioning. Data from the initial trial also provides a way of calculating the moisture content and diffusion coefficient of the laminate. The procedure of the initial test is as follows:

1. Prepare two air-tight chambers, one with a relative humidity of 0 %RH, and the other with a greater relative humidity.
2. Prepare a 2- $\frac{1}{4}$ " x 2- $\frac{1}{4}$ " 4 ply test laminate and obtain its initial weight.
3. Place the test laminate into a 0 %RH conditioning chamber.
4. Periodically measure the weight of the test laminate as it loses moisture. When the weight of the test laminate stops changing, record the new weight as the laminate's dry weight. Initial moisture content of the prepreg as removed from the freezer is not 0 wt.% (Hsiao et al., 2011).
5. Take the 0 %RH conditioned test laminate and condition it at 75 %RH. If the weight change can be measured continuously in this step (i.e. weight gain per time) the data can be used to calculate the prepreg diffusion coefficient (see diffusion coefficient calculation Step 1).
6. Periodically measure the weight of the test laminate as it gains moisture. When the weight of the test laminate stops changing, record the new weight as the laminate's moist weight. The amount of time it takes for the weight change to stabilize is set as the duration time for moisture

conditioning. In this study, the duration for moisture conditioning was five days.

In order to calculate the moisture content of the conditioned test laminate:

1. Subtract the test laminate's dry weight from its moist weight. The difference is the weight of the absorbed moisture.
2. Divide the weight of the absorbed moisture by the laminate's dry weight, and then multiply by 100. The result is the laminate's moisture content as a weight percent when conditioned 75 %RH.
3. Initial moisture content of the test laminate as removed from the freezer can also be calculated by recalculating the weight of the moisture (the numerator in the fraction).

In order to calculate the diffusion coefficient of the prepreg:

1. Prepare a 0 %RH conditioned laminate and condition it to 75 %RH. Measure the weight gain until the weight change stabilizes and the laminate reaches equilibrium with its environment. In this study, this was performed using an analytical balance (Denver Instrument, Model No. P-214) that could continuously record weight data and export the results to a text file. This step can be performed during Step 5 in the initial test when determining the duration of moisture conditioning.
2. From the recorded weight gain data, calculate the changing moisture content of the test laminate throughout the entire conditioning period.

3. Plot the changing moisture content against square root time and obtain the slope of the linear portion of that curve.
4. The diffusion coefficient of the prepreg can then be calculated using the following Equation A10 (Naceri, 2009):

$$D(\text{cm}^2/\text{s}) = \pi \left(\frac{h}{4M_m} \right)^2 (\text{slope})^2 \quad \text{Equation A10}$$

In Equation A10, (h) is thickness in the direction of diffusion (or half the laminate thickness for diffusion from two sides) and (M_m) is the moisture content at saturation. For 5320/T650, the diffusion coefficient of water in uncured prepreg was calculated to be 2.45E-08 cm²/s.

F) Flow Calibration Calculation

Although the mass flow sensors were calibrated for air flow (reference gas), the actual gas flow measured was water vapour (actual gas). The measurements obtained during the test was calibrated by using a correlation factor which took into account the differences in density and specific heat between air and water vapour (Equation A11) (OMEGA, 2000).

$$K = \gamma C_p \quad (\text{Equation A11})$$

In Equation A11, (γ) is density in kg/m^3 , and (C_p) specific heat capacity in J/K . The correlation factor is the ratio of (K) for the reference and the actual gas. To calculate the actual flow rate of water vapour, the correlation factor was multiplied to the measured flow rate (Equation A12):

$$Q_{water\ vapour} = \left(\frac{K_{air}}{K_{water\ vapour}} \right) Q_{air} \quad (\text{Equation A12})$$

G) Vacuum Bagged Water Vapourization Leak Test

The vacuum bagged water vapourization leak test is very similar to the total system leak test (Appendix B), except there is only one test chamber. The procedure is as follows:

1. Apply vacuum to the vacuum bagged lay-up.
2. Once full vacuum has been achieved, disconnect the line from the vacuum pump and observe if vacuum drops in the vacuum bagged lay-up. If no leaks are present, full vacuum will be maintained in.